

**The Characteristic Function of the
Time-Integral of Geometric Brownian
Motion and its Application in Asian Option
Pricing**

Teun Wever
Student number: 4261097
Financial Engineering
Applied Mathematics
EEMCS, TU Delft
17-03-2023

1 Abstract

In this research a new method for pricing continuous Arithmetic averaged Asian options is proposed. The computation is based on Fourier-cosine expansion, namely the COS method. Therefore, we derive the characteristic function of Integrated Geometric Brownian Motion based on Bougerol's identity.

Extensive numerical error analysis on the CDF recovery of IGBM and the option prices is performed. Via numerical tests, the convergence of errors using our new method has been proved. We are able to price continuous Arithmetic averaged Asian options with a minimal error of order 10^{-2} , and a maximum precision of order 10^{-5} within seconds.

This research is performed as a masters' thesis for Financial Engineering within Applied Mathematics at the EEMCS faculty, TU Delft.

I would very much like to thank Dr. F. Fang and Dr. X. Shen for their contributions throughout this research and Dr. F. Fang for her guidance in particular. I would also like to thank Prof. Dr. A. Papantoleon and Prof. Dr. Ir C. Vuik for being part of the thesis committee.

Teun Wever, 10-03-2023.

Contents

1	Abstract	1
2	Introduction	4
3	Literature Summary	5
3.1	Integrated Geometric Brownian Motion	6
3.1.1	Squared Bessel Process	6
3.1.2	Scaling Property of IGBM	9
3.2	Distribution of A_t^ν	9
3.2.1	Bougerol's Identity	9
4	Bougerol's Identity Without Drift	13
4.1	Density Recovery via Fourier-Cosine Expansion	14
4.2	Characteristic Function	15
4.2.1	Characteristic Function of $X = \ln(Z^2)$	15
4.2.2	Comparison of the two Methods	17
4.2.3	Characteristic Function of $Y = \ln(\sinh^2(B_t))$	19
4.3	Numerical Implementation	22
4.3.1	Benchmark: Monte Carlo Simulation	23
4.4	CDF Error Analysis	23
4.4.1	Convergence of $g(\omega)$	24
4.4.2	Quadrature Points	26
4.4.3	Errors Analysis in the Tolerance Level	27
4.5	PDF Error Analysis	28
4.6	Conclusion	31
5	Bougerol's Identity With Drift	32
5.1	Characteristic Function	33
5.1.1	Arcsine Distribution	33
5.1.2	Distribution of $W = \ln(\phi^2(X, Y))$	37
5.2	Numerical Integration Errors	40
5.2.1	Change of Variables	40
5.2.2	Sensitivity to Parameters	41
5.3	Parameter Evaluation	42
5.4	Numerical Implementation	43
5.4.1	Parameter Choice	43
5.4.2	Truncation Range	44
5.4.3	Benchmark: Monte Carlo Simulation	45
5.5	Error Analysis	45
5.5.1	CDF Error Analysis	46
5.5.2	Analysis of $k(\omega)$	46
5.5.3	Quadrature Points for $l(\omega)$	47
5.5.4	Computation of $g(\omega)$	48
5.5.5	PDF Error Convergence	49
5.6	Conclusion	50
6	Pricing Continuous Asian Options	51
6.1	Financial Background	52
6.1.1	Asian Options	52
6.1.2	Black-Scholes	52
6.2	Continuous Geometric Averaged Asian Options	53
6.3	Continuous Arithmetic Averaged Asian Options	55
6.3.1	Option Pricing using Cosine Series Expansion	55
6.4	Errors and Computational Complexity	57

6.4.1	Errors	58
6.4.2	Computational Complexity	59
6.5	Option Pricing Results	59
6.5.1	Option Pricing with Zero Drift	59
6.5.2	Option Pricing with Drift	62
6.5.3	Convergence Experiments	65
6.6	Conclusion	69
7	Conclusion & Further Research	71

2 Introduction

Asian options, first introduced in 1987 by Banker's Trust Tokyo, are path dependent options, depending on the averaged value of the underlying over time. The average can either be Geometric or Arithmetic, yielding a different payoff function. The average can be calculated on a finite number of dates, leading to discrete Asian options, otherwise the option is continuous. Hence, these properties yield 4 types of Asian options. In this research, a fixed strike price K is used, and the options are European style.

We suppose that the stochastic process of the underlying follows a Geometric Brownian motion. For Geometric averaged Asian options, analytic solutions are available [11], for both discrete and continuously monitored times. In this research, we are interested with the Arithmetic averaged Asian options, which have fixed strike prices and are of European type. In particular, we focus on continuous Arithmetic averaged Asian options, whereby the stochastic process of the underlying is assumed to be a Geometric Brownian Motion. Under this assumption, for continuous Arithmetic options the underlying follows Integrated Geometric Brownian motion.

For Arithmetic averaged Asian options, no analytic solution is available. Thus, the option price has to be determined numerically. Different computational methods have been developed in literature. Monte Carlo simulation is used for the computation of these option prices [20]. In other numerical methods, a time discretization is needed, where after extrapolation techniques are used to convert a discrete Asian option price to the continuous time. Hsu [10], employs a Binomial Tree method is used for the computation and in [1]PDE methods are presented for computing the option price.

There are also methods based on Integrated Geometric Brownian Motion directly, without a time discretization. Donati-Martin [4] has found an expression for the Laplace transform of the option for a fixed strike price K . Furthermore, a triple integral expression and another Laplace transform were derived by Schröder [14]. In this research, we develop a new computational method for pricing continuous Arithmetic averaged Asian options, which is based directly on Integrated Geometric Brownian Motion as well.

The idea is to first derive and compute the characteristic function of the time-integral of Geometric Brownian Motion, and then apply the well-known COS method. The COS method is based on Fourier-Cosine expansion for recovering the characteristic function of the underlying, first introduced in [6]. In [19], the COS method is used for pricing discrete Arithmetic Asian options. The COS method gives exponential error convergence of the computation in the option price, which we will verify via error analysis.

As we stated above, we base our computation on Integrated Geometric Brownian Motion (IGBM). In [18], Yor has found the distribution of IGBM. Other expressions for the distributions of IGBM can be found in [5]. However, the characteristic function of IGBM has not been presented in this literature, which is what we need for our new pricing method.

To derive the characteristic function of IGBM, we use the famous identity introduced by Bougerol. Bougerol's identity shows a relation between two independent Brownian motions, in which a specific form of IGBM is used [17], based on Yor [18]. This identity has been extended by Alili and Gruet [17]. After some derivation, we are able to compute the characteristic function of IGBM, and apply this to the valuation of continuous Arithmetic averaged Asian options via the COS method. The derivation of the characteristic function of IGBM is the first contribution to the existing literature.

The setup in this research is as follows. In Section 3, we start with a general overview about IGBM and an introduction to the complete derivation of Bougerol's identity. In Section 4, we elaborate on the COS method in general, and then compute the characteristic function for IGBM, with a drift term equal to zero based on Bougerol's identity. The performance of the method be checked via error analysis on the recovered CDF. In Section 5, the characteristic function of IGBM is carefully derived, based on the extension of Bougerol's identity and an error analysis is conducted based on the CDF. In Section 6, we explain Asian option pricing in detail. Afterwards, the use of the COS method is presented for option pricing in general. As the second contribution to the literature, we insert the characteristic function of IGBM to the COS method to price continuous Arithmetic Asian options. The results are compared to reference prices.

3 Literature Summary

As stated in the introduction, the aim of our research is to price continuous Arithmetic averaged Asian options for Geometric Brownian motion using cosine series expansion, which is called the COS method, developed by Fang and Oosterlee [7]. In section 4.1 we will elaborate on the COS method in general. Using this method, we need to determine the characteristic function of our variable of interest.

In [19], the valuation of pricing Asian options has been done for discrete time intervals using the COS method. In this research we look for the pricing method of continuous Asian options. Asian options are path dependent options, depending on the evolution of the stochastic process of the underlying stock S_t . The option price depends on the average stock value of the underlying from $t = t_0$ until maturity time $t = T$, which for continuous time is given by

$$\frac{1}{T - t_0} \int_{t_0}^T S_u du, \quad (3.1)$$

and this is our variable of interest. In this research we set $t_0 = 0$. We assume that the underlying stock S_t is distributed as Geometric Brownian motion, hence the dynamics of S_t are given by

$$dS_t = \mu S_t + \sigma S_t dB_t, \quad (3.2)$$

where $\mu > 0$, which is denoted as the drift and $\sigma > 0$ is the volatility of the underlying stock. Furthermore B_t follows a standard Brownian motion. The value of the underlying S_t (with $t_0 = 0$) at maturity time T is given by

$$S_T = S_0 e^{(\mu - \frac{1}{2}\sigma^2)T + \sigma B_T}. \quad (3.3)$$

We will elaborate more on Asian options in general and Geometric Brownian motion in Section 6. In this section, we focus on a specific type of (3.1), where $\sigma = 2$, denoted by

$$A_t^\nu = \int_0^t e^{2(\nu s + B_s)} ds. \quad (3.4)$$

Once we have obtained the knowledge about the distribution of A_t^ν , we can extend it to derive to the distribution of (3.1).

First we show the relationship of A_t^ν with Bessel processes due to Lamperti's relation. Then we show how we can scale the distribution of A_t^ν to obtain the distribution for other parameter values than $\sigma = 2$ and different t and ν . Afterwards we introduce Bougerol's identity, which establishes the relation between two different distributions, where the term A_t^ν in appears. After some relatively simple computations, we can then derive the characteristic function of the \log of (A_t^ν), and using the scaling property of Brownian motion, we can then define the characteristic function of the \log of our variable of interest (3.1).

3.1 Integrated Geometric Brownian Motion

Expressions (3.1) and (3.5) are called integrated Geometric Brownian motion. This expression is used very often in mathematical finance. Marc Yor [18] has derived the distribution of IGBM as stated in (3.4), i.e.

$$A_t^\nu = \int_0^t e^{2(\nu s + B_s)} ds. \quad (3.5)$$

We start by summarizing the important steps in his derivation based on notes from Dufresne [5]. The key starting point is in the connection between Squared Bessel processes and integrated Geometric Brownian motion.

3.1.1 Squared Bessel Process

The Squared Bessel process can be seen as the squared Euclidean distance of multiple independent Brownian motions. Below is a more precise definition of this process.

Definition 3.1. Let $x, \delta \geq 0$. A squared Bessel process is the unique strong solution to the stochastic differential equation

$$Z_t = x + 2 \int_0^t \sqrt{Z_s} dB_s + \delta t, \quad (3.6)$$

where B_t denotes standard Brownian motion and x is the starting point of the process. The dimension of the process is given by δ . We denote this process by $Z_t \sim BESQ^\delta(x)$.

Note that (3.6) can also be given as:

$$dZ_t = 2\sqrt{Z_t} dB_t + \delta dt. \quad (3.7)$$

Now let $Y_t = \sqrt{Z_t}$. We apply Ito's formula for $g(t, Z_t) = \sqrt{Z_t}$ to compute the dynamics of Y_t :

$$\begin{aligned} dY_t &= \frac{\partial g}{\partial t} dt + \frac{\partial g}{\partial Z_t} dZ_t + \frac{1}{2} \frac{\partial^2 g}{\partial Z_t^2} (dZ_t)^2 \\ &= 0 + \frac{1}{2\sqrt{Z_t}} dZ_t + \frac{1}{2} \cdot \frac{1}{2} \cdot -\frac{1}{2} (Z_t)^{-\frac{3}{2}} (dZ_t)^2 \\ &= \frac{1}{2Y_t} (2Y_t dB_t + \delta dt) - \frac{1}{8} Y_t^{-3} (4Y_t^2 dt) \\ &= dB_t + \frac{(\delta - 1)}{2} \frac{1}{Y_t} dt, \end{aligned} \quad (3.8)$$

where we use that $dt dB_t = 0$. Based on the behaviour of $BESQ^\delta(x)$, we must have that $\delta \geq 2$ and, otherwise the point $Z_t = 0$ is reached and Ito's formula does not hold.

Definition 3.2. The strong solution to (3.8) is called a Bessel process starting at $x \geq 0$ with dimension $\delta \geq 2$, denoted by $Y_t \sim BES^\delta(x)$.

Note that we can write (3.8) also as

$$Y_t = x + B_t + \frac{(\delta - 1)}{2} \int_0^t \frac{ds}{Y_s}. \quad (3.9)$$

Now we use this result in Lamperti's proposition to clarify why Yor sets $\sigma = 2$, and thus the definition of A_t^ν . Lamperti has found the relationship between A_t^ν and Bessel processes. Here we state and prove Lamperti's proposition more precisely than in [5] to find out why A_t is defined as in (3.4).

Proposition 3.1. Let B_t be a standard Brownian motion and $\nu = \frac{\delta}{2} - 1 \geq 0$. There exists a $\rho \sim BES^\delta(1)$ such that

$$e^{\nu t + B_t} = \rho A_t^\nu, \quad (3.10)$$

with

$$A_t^\nu = \int_0^t e^{2(\nu s + B_s)} ds. \quad (3.11)$$

Proof. For $w > t$ we have $A_w^\nu = \int_0^w e^{2(\nu s + B_s)} ds = \int_0^t e^{2(\nu s + B_s)} ds + \int_t^w e^{2(\nu s + B_s)} ds > A_t^\nu$, hence A_t^ν is strictly increasing in t and $A_0^\nu = 0$. From [5] we conclude that A_t^ν is continuous. Since $\nu \geq 0$, we have that $\lim_{t \rightarrow \infty} A_t^\nu = \infty$. Hence we can define for any $u \geq 0$ the variable T_u such that

$$A_{T_u}^\nu = u. \quad (3.12)$$

Now let $F_t = e^{\nu t + B_t}$. Applying Ito's formula to $F_t = g(t, B_t)$, we find that the dynamics of F_t are given by

$$\begin{aligned} dF_t &= \frac{\partial g}{\partial t} dt + \frac{\partial g}{\partial B_t} (dB_t) + \frac{1}{2} \frac{\partial^2 g}{\partial B_t^2} (dB_t)^2 \\ &= \nu e^{\nu t + B_t} dt + e^{\nu t + B_t} dB_t + \frac{1}{2} e^{\nu t + B_t} (dB_t)^2 \\ &= \nu e^{\nu t + B_t} dt + e^{\nu t + B_t} dB_t + \frac{1}{2} e^{\nu t + B_t} dt \\ &= \left(\nu + \frac{1}{2}\right) e^{\nu t + B_t} dt + e^{\nu t + B_t} dB_t. \end{aligned} \quad (3.13)$$

Integration of (3.13) on both sides yields to

$$e^{\nu t + B_t} = 1 + \left(\nu + \frac{1}{2}\right) \int_0^t e^{\nu s + B_s} ds + M_t, \quad M_t = \int_0^t e^{\nu s + B_s} dB_s. \quad (3.14)$$

Lemma 3.1. The quadratic variation of M is given by $\langle M, M \rangle_t$, furthermore $\langle M, M \rangle_t = A_t^\nu$, $\langle M, M \rangle_\infty = \infty$ and $M_0 = 0$.

Proof. Clearly $M_0 = 0$. We use the result from page (3) in [5] regarding quadratic variation. Since $dM_t = e^{\nu t + B_t} dB_t$, we obtain that for M_t

$$\langle M, M \rangle_t = \int_0^t (e^{\nu s + B_s}) (e^{\nu s + B_s}) ds = \int_0^t e^{2(\nu s + B_s)} ds = A_t^\nu, \quad (3.15)$$

$$\langle M, M \rangle_\infty = \lim_{t \rightarrow \infty} \langle M, M \rangle_t = \lim_{t \rightarrow \infty} A_t^\nu = \infty. \quad (3.16)$$

□

Lemma 3.2. M is a continuous local Martingale.

Proof. 1. M_t is clearly F_t -measurable, and therefore M_t is adapted to the filtration $\{F_t\}$.

2. From (3.14) we see that

$$M_t = e^{\nu t + B_t} - 1 - \left(\nu + \frac{1}{2}\right) \int_0^t e^{\nu s + B_s} ds. \quad (3.17)$$

By the scaling property, which we show later in (3.32), we have that

$$\int_0^t e^{\nu s + B_s} ds = 4A_{\frac{1}{4}t}^{(2\nu)}, \quad (3.18)$$

which is continuous. M_t is thus a sum of continuous functions, and is therefore continuous.

Proposition 4.3(i) in [16] states that when an adapted process M_t is continuous and $M_0 = 0$, M_t is a local Martingale. □

Based on the two lemmas above, we use the result of Dambis, Dubins and Schwarz [13]. They state that when these two lemmas hold, M_t is a time-transformed Brownian motion and $M_t = \beta_{\langle M, M \rangle_t} = \beta_{A_t^\nu}$. Where β_t is a Brownian motion independent of B_t .

Equation (3.14) can now be written as

$$e^{\nu t + B_t} = 1 + \left(\nu + \frac{1}{2}\right) \int_0^t e^{\nu s + B_s} ds + \beta_{A_t^\nu}. \quad (3.19)$$

Replacing t by T_u we find that

$$\begin{aligned} e^{\nu T_u + B_{T_u}} &= 1 + \left(\nu + \frac{1}{2}\right) \int_0^{T_u} e^{\nu s + B_s} ds + \beta_{A_{T_u}^\nu} \\ &= 1 + \left(\nu + \frac{1}{2}\right) \int_0^{T_u} e^{\nu s + B_s} ds + \beta_u. \end{aligned} \quad (3.20)$$

Now we need the following computations. Differentiating both sides of (3.12) with respect to u results in:

$$\frac{dA_{T_u}^\nu}{du} = \frac{dA_{T_u}^\nu}{dT_u} \frac{dT_u}{du} = 1 \rightarrow \quad (3.21)$$

$$e^{2(\nu s + B_s)} \Big|_{s=T_u} \frac{dT_u}{du} = 1 \rightarrow \quad (3.22)$$

$$e^{2(\nu T_u + B_{T_u})} \frac{dT_u}{du} = 1 \leftrightarrow \quad (3.23)$$

$$e^{2(\nu T_u + B_{T_u})} dT_u = du \leftrightarrow \quad (3.24)$$

$$e^{\nu T_u + B_{T_u}} dT_u = \frac{du}{e^{\nu T_u + B_{T_u}}}. \quad (3.25)$$

As the next step, let $y = A_s^\nu$. Then by definition $s = T_y$ and

$$e^{\nu s + B_s} ds = e^{\nu T_y + B_{T_y}} dT_y. \quad (3.26)$$

Therefore, we obtain by (3.25) and (3.26):

$$\int_0^{T_u} e^{\nu s + B_s} ds = \int_0^{A_{T_u}^\nu} e^{\nu T_y + B_{T_y}} dT_y = \int_0^u e^{\nu T_y + B_{T_y}} dT_y = \int_0^u \frac{dy}{e^{\nu T_y + B_{T_y}}}. \quad (3.27)$$

Finally we define $\rho_u = \rho_{A_{T_u}^\nu} = e^{\nu T_u + B_{T_u}}$, and then we thus find by substituting (3.27) in (3.20):

$$\begin{aligned} \rho &= 1 + \left(\nu + \frac{1}{2}\right) \int_0^u \frac{dy}{\rho_y} + \beta_u \\ &= 1 + \frac{(\delta - 1)}{2} \int_0^u \frac{dy}{\rho_y} + \beta_u. \end{aligned} \quad (3.28)$$

Hence, $\rho_u = BES^{(\delta)}(1)$ and the proposition has been proved. \square

Remark 3.1. In the derivation by Lamperti, we must have that $\nu \geq 0$. Other proofs for the distribution of $A_{S_\lambda}^\nu$, however, have actually shown that it holds for have $\nu \in \mathbb{R}$.

In equation (3.25) it becomes clear why Yor sets $\sigma = 2$. One factor in the Taylor expansion of $e^{\nu t + B_t}$ can be replaced by $\int_0^u \frac{dy}{e^{\nu T_y + B_{T_y}}}$ based on the derivative $\frac{dT_u}{du}$, resulting in a Bessel process.

In the next steps towards the derivation of the density function of A_t^ν , the author starts by finding the joint law of $(e^{B_{S_\lambda}}, A_{S_\lambda})$, where S_λ is an exponential distribution. In one of the key steps involved, they use the fact that $\rho_x = e^{B_{T_x}} \sim BES^{(2)}(1)$ due to the result of Lamperti, for which the conditional expectation is known, i.e.

$$\mathbb{E} \left[e^{-v^2 \int_0^t \frac{ds}{\rho_s^2}} \Big| \rho_t = r \right] = \frac{I_{|v|} \left(\frac{rt}{x} \right)}{I_0 \left(\frac{rt}{x} \right)}. \quad (3.29)$$

And afterwards $e^{B_{S_\lambda}}$ is integrated out. For further reading we refer to Dufresne [5].

Now that we know why A_t^ν is defined this way, we show how we can determine the distribution for any (μ, σ, T) based on A_t^ν by the scaling property of Brownian motion.

3.1.2 Scaling Property of IGBM

We present how we can determine the distribution of Integrated Geometric Brownian motion for each value of (μ, σ, T) .

Let $B_t = B(t)$ be a standard Brownian motion. Recall that A_t^ν is defined as

$$A_t^\nu = \int_0^t e^{2(\nu s + B_s)} ds. \quad (3.30)$$

Let $u = \frac{4}{\sigma^2}s$, then $ds = \frac{\sigma^2}{4} du$. Furthermore, $B(s) = B(\frac{\sigma^2}{4}u) \stackrel{law}{=} \sqrt{\frac{\sigma^2}{4}}B(u) = \frac{\sigma}{2}B(u)$. It then follows that

$$\int_0^t e^{2(\nu s + B_s)} ds \stackrel{law}{=} \int_0^{\frac{4t}{\sigma^2}} e^{2(\nu \cdot \frac{\sigma^2}{4}u + \frac{\sigma}{2}B_u)} \cdot \frac{\sigma^2}{4} du \quad (3.31)$$

Now set $t = \frac{\sigma^2 T}{4}$ and $\nu = \frac{2\mu}{\sigma^2}$. Then

$$A_t^\nu = \int_0^t e^{2(\nu s + B_s)} ds = \int_0^{\frac{4t}{\sigma^2}} e^{2(\nu \cdot \frac{\sigma^2}{4}u + \frac{\sigma}{2}B_u)} \cdot \frac{\sigma^2}{4} du = \frac{\sigma^2}{4} \int_0^T e^{\mu u + \sigma B_u} du. \quad (3.32)$$

Looking at equation (3.1) and (3.3) and using (3.32), we can state that the following are the same in distribution:

$$\frac{1}{T} \int_0^T S_0 e^{(\mu - \frac{1}{2}\sigma^2)u + \sigma B_u} du \stackrel{law}{=} \frac{4S_0}{\sigma^2 T} A_t^\nu, \quad (3.33)$$

with

$$t = \frac{\sigma^2 T}{4}, \quad \nu = \frac{2(\mu - \frac{1}{2}\sigma^2)}{\sigma^2} = \frac{2\mu}{\sigma^2} - 1. \quad (3.34)$$

We can thus use any drift term μ , volatility σ and maturity time T using this scaling property and still use the useful results of the distribution of A_t^ν as defined in (3.5) by Marc Yor.

In the following subsection, we show how we can use Bougerol's identity to derive the distribution of A_t^ν .

3.2 Distribution of A_t^ν

In [18] and [5], several expressions for the distribution of A_t^ν are presented. All of the expressions are given by integrals or given by infinite series. For our research, we wish to recover the density of A_t^ν via cosine series expansion. Therefore, we need to derive the characteristic function of A_t^ν . To this end, we use Bougerol's identity, which appears a lot in different literature, mostly because of its simplicity.

3.2.1 Bougerol's Identity

Bougerol's identity establishes a relationship between two independent Brownian motions. In one of these, the term t is replaced by A_t^ν , of which we will make use to derive the characteristic function of A_t^ν . To be more specific, we will use this identity to derive the characteristic function of the *log* of A_t^ν .

Bougerol's identity holds for $\nu = 0$. Alili and Gruet [17] generalized Bougerol's identity for the case where $\nu \neq 0$, based on hyperbolic Brownian motion. A very short proof, only containing some key steps, for Bougerol's generalized identity can be found in [17], which also contains the following proposition.

Proposition 3.2. Let R_t be a 2-dimensional Bessel process with $R_0 = 0$. Let Ξ be an arcsine random variable and let $B_t^\nu = \nu t + B_t$. Further, we assume that B_t^ν , R_t and Ξ are independent. Then for a fixed t we have

$$\beta_{A_t^\nu} \stackrel{law}{=} (2\Xi - 1)\phi\left(B_t^\nu, \sqrt{R_t^2 + B_t^{\nu 2}}\right), \quad (3.35)$$

where $\phi(a, b)$ is given by

$$\phi(a, b) = \sqrt{2e^a \cosh(b) - e^{2a} - 1}, \quad b \geq |a|. \quad (3.36)$$

For $\nu = 0$ we recover Bougerol's identity:

$$\beta_{A_t} \stackrel{law}{=} \sinh(B_t). \quad (3.37)$$

Since the proof one can find in [17] is rather brief, below we provide a detailed proof.

Proof. Let β_t and B_t be independent Brownian motions and let W_t be another Brownian motion independent of B_t . Note that $\beta_{A_t} = \int_0^t e^{B_s} dW_s$ based on the result of Dambis, Dubins and Schwartz, but in this case we have $\nu = 0$. The time reversal of Brownian motion states that $\{B_t - B_{t-s}, 0 \leq s \leq t\} \stackrel{law}{=} \{B_s, 0 \leq s \leq t\}$. We obtain the following for a fixed $t \geq 0$:

$$\beta_{A_t} = \int_0^t e^{B_s} dW_s \stackrel{law}{=} \int_0^t e^{B_t - B_{t-s}} dW_s \quad (3.38)$$

$$= e^{B_t} \int_0^t e^{-B_{t-s}} dW_s \stackrel{law}{=} e^{B_t} \int_0^t e^{-B_s} dW_s, \quad (3.39)$$

where in (3.39) we used that the paths of B_{t-s} and B_s are the same for $0 \leq s \leq t$, only with opposite starting point and end point. Now define

$$X_t = e^{B_t} \int_0^t e^{-B_s} dW_s. \quad (3.40)$$

Applying Ito's lemma to $X_t = f(x, y) = e^x y = e^{B_t} \int_0^t e^{-B_s} dW_s$ results in the following dynamics for X_t :

$$\begin{aligned} dX_t &= df(x, y) = \frac{df}{dx}(dx) + \frac{1}{2} \frac{d^2 f}{dx^2}(dx)^2 + \frac{df}{dy}(dy) + \frac{1}{2} \frac{d^2 f}{dy^2}(dy)^2 + \frac{d^2 f}{dx dy}(dx)(dy) \\ &= e^{B_t} \int_0^t e^{-B_s} dW_s (dB_t) + \frac{1}{2} e^{B_t} \int_0^t e^{-B_s} dW_s (dB_t)^2 \\ &\quad + e^{B_t} d \left(\int_0^t e^{-B_s} dW_s \right) + 0 + e^{B_t} (dB_t) \left(d \int_0^t e^{-B_s} dW_s \right) \\ &= X_t dB_t + \frac{1}{2} X_t dt + e^{B_t} (e^{-B_t} dW_t) + 0 + e^{B_t} (dB_t) (e^{-B_t} dW_t) \\ &= X_t dB_t + \frac{1}{2} X_t dt + dW_t \\ &= \frac{1}{2} X_t dt + \sqrt{1 + X_t^2} \left(\frac{X_t}{\sqrt{1 + X_t^2}} dB_t + \frac{1}{\sqrt{1 + X_t^2}} dW_t \right) \\ &= \frac{1}{2} X_t dt + \sqrt{1 + X_t^2} dZ_t, \end{aligned} \quad (3.41)$$

where by independence of W_t and B_t we have $dW_t dB_t = 0$. We use the result of Dambis, Dubins and Schwarz again [5]. Let

$$dZ_t = \frac{X_t}{\sqrt{1 + X_t^2}} dB_t + \frac{1}{\sqrt{1 + X_t^2}} dW_t, \quad (3.42)$$

then

$$Z_t = \int_0^t \frac{X_s}{\sqrt{1 + X_s^2}} dB_s + \int_0^t \frac{1}{\sqrt{1 + X_s^2}} dW_s. \quad (3.43)$$

Clearly $Z_0 = 0$. In [9], Hariya and Matsumura state that Z_t is continuous. Note that X_t is an adapted process to the filtration $\{F_t\}$. Therefore Z_t is also adapted to the filtration $\{F_t, t \geq 0\}$. When an adapted stochastic process Z_t is continuous and $Z_0 = 0$, it is a local Martingale. The

quadratic variation of Z_t is given by

$$\begin{aligned}
\langle Z, Z \rangle_t &= \left\langle \int_0^t \frac{X_s}{\sqrt{1+X_s^2}} dB_s, \int_0^t \frac{X_s}{\sqrt{1+X_s^2}} dB_s \right\rangle \\
&+ \left\langle \int_0^t \frac{1}{\sqrt{1+X_s^2}} dW_s, \int_0^t \frac{1}{\sqrt{1+X_s^2}} dW_s \right\rangle \\
&+ 2 \left\langle \int_0^t \frac{X_s}{\sqrt{1+X_s^2}} dB_s, \int_0^t \frac{1}{\sqrt{1+X_s^2}} dW_s \right\rangle \\
&= \int_0^t \frac{X_s^2}{1+X_s^2} ds + \int_0^t \frac{1}{X_s^2+1} ds \\
&= \int_0^t 1 ds \\
&= t,
\end{aligned} \tag{3.44}$$

and

$$\langle Z, Z \rangle_\infty = \lim_{t \rightarrow \infty} \langle Z, Z \rangle_t = \lim_{t \rightarrow \infty} t = \infty. \tag{3.45}$$

We can conclude that Z_t is a Brownian motion, and $Z_t = \gamma_{\langle Z, Z \rangle_t} = \gamma_t$, where γ_t is a Brownian motion dependent on W_t and B_t . Hence, we can write (3.41) as

$$dX_t = \frac{1}{2} X_t dt + \sqrt{1+X_t^2} d\gamma_t. \tag{3.46}$$

On the other hand, we define another process $Q_t = \sinh(B_t)$, where B_t is the same Brownian motion as in (3.38). Applying Ito's lemma to $g(t, B_t) = Q_t$, we find that the dynamics of Q_t are given by

$$\begin{aligned}
dQ_t &= \frac{\partial g}{\partial t} dt + \frac{\partial g}{\partial B_t} (dB_t) + \frac{1}{2} \frac{\partial^2 g}{\partial B_t^2} (dB_t)^2 \\
&= \cosh(B_t) dB_t + \frac{1}{2} \sinh(B_t) (dB_t)^2 \\
&= \sqrt{1+\sinh^2(B_t)} dB_t + \frac{1}{2} \sinh(B_t) dt \\
&= \sqrt{1+Q_t^2} dB_t + \frac{1}{2} Q_t dt.
\end{aligned} \tag{3.47}$$

When we compare the stochastic differential equation (3.46) for X_t and (3.47) for Q_t , we see that they have the same coefficients. Now we use the fact that when two stochastic processes have the same Lipschitz coefficients, then they are the same in same law. Thus what is left to prove is that $f(x) = \frac{1}{2}x$ and $g(x) = \sqrt{1+x^2}$ are indeed Lipschitz coefficients.

We use the fact that when the first derivative of f and g are bounded, we have that $f(x)$ and $g(x)$ are Lipschitz coefficients. This follows directly from the mean value theorem, i.e. $\exists c \in [a, b]$ such that

$$\frac{f(b) - f(a)}{b - a} = f'(c). \tag{3.48}$$

This implies with $|f'(c)| \leq M$ that

$$|f(b) - f(a)| = |f'(c)(b - a)| \leq |f'(c)| |b - a| \leq M |b - a|. \tag{3.49}$$

These first derivatives are given by:

$$0 < f'(x) = \frac{1}{2} < 1, \tag{3.50}$$

$$-1 < g'(x) = \frac{x}{\sqrt{1+x^2}} < 1. \tag{3.51}$$

We conclude that X_t and Q_t are the same in law, and therefore

$$\beta_{A_t} = \int_0^t e^{B_s} dW_s \stackrel{\text{law}}{=} X_t \stackrel{\text{law}}{=} Q_t = \sinh(B_t). \quad (3.52)$$

□

In the following sections it will be shown how Bougerol's (extended) identity can be used to recover the characteristic function of $\ln(A_t^\nu)$, which is the first contribution of this research to existing literature.

In the next section we focus on the distribution of A_t^ν , with $\nu = 0$. For simplicity, we drop ν in the notation for $\nu = 0$. We then demonstrate how we can recover the density and CDF of $\ln(A_t)$ by the COS method.

4 Bougerol's Identity Without Drift

In this section we aim to recover the density function and the CDF of $\ln(A_t)^\nu$ via the COS method with $\nu = 0$, which is the case when $\sigma = \sqrt{2\mu}$ based on the scaling property (3.32). Therefore, we need to recover the characteristic function of $\ln(A_t)$, the only input needed by the COS method.

In the section 3.2 Bougerol's identity without drift has been stated and proven, i.e.

$$\beta_{A_t} \stackrel{\text{law}}{=} \sinh(B_t), \quad (4.1)$$

which is the key result we will use in our derivation. Recall that β_t and B_t are two independent Brownian motions and A_t is given by

$$A_t = \int_0^t e^{2B_s} ds. \quad (4.2)$$

In this section we will compute the characteristic function of $\ln(A_t)$ based on this identity. We use the *log* of A_t because then we can split Bougerol's identity into a sum of independent random variables, which we will show in section 4.2.

First, we explain how to recover the density and the CDF based on Fourier Cosine Expansion and the characteristic function. After we have computed the characteristic function, we conduct a proper error analysis in the CDF and the PDF of $\ln(A_t)$ for various values of t and with respect to the number of quadrature points J for numerical integration, the number of cosine expansion terms N and the truncation range of the marginal distributions to verify the exponential convergence in the errors compared to Monte Carlo simulation.

4.1 Density Recovery via Fourier-Cosine Expansion

In this Section we show how to recover the density function of $\ln(A_t)$ by the COS method, following the derivation in [7]. Let $f_X(x)$ be the density function of $\ln(A_t)$. Its Fourier cosine expansion on an interval $[a, b]$ is given by:

$$f_X(x) = \sum_{k=0}^{\infty} {}'F_k \cos\left(k\pi \frac{x-a}{b-a}\right) = \frac{1}{2}F_0 + \sum_{k=1}^{\infty} F_k \cos\left(k\pi \frac{x-a}{b-a}\right), \quad (4.3)$$

where

$$F_k = \frac{2}{b-a} \int_a^b f(x) \cos\left(k\pi \frac{x-a}{b-a}\right) dx, \quad (4.4)$$

and the $'$ means that the first term is multiplied by $\frac{1}{2}$. To approximate F_k we have

$$\begin{aligned} F_k &= \frac{2}{b-a} \int_a^b f(x) \cos\left(k\pi \frac{x-a}{b-a}\right) dx \\ &\approx \frac{2}{b-a} \operatorname{Re} \left[\int_{-\infty}^{\infty} f(x) \exp\left(-i \frac{k\pi a}{b-a}\right) \exp\left(i \frac{k\pi x}{b-a}\right) dx \right] \\ &= \frac{2}{b-a} \operatorname{Re} \left[\exp\left(-i \frac{k\pi a}{b-a}\right) \int_{-\infty}^{\infty} f(x) \exp\left(i \frac{k\pi x}{b-a}\right) dx \right] \\ &= \frac{2}{b-a} \operatorname{Re} \left[\exp\left(-i \frac{k\pi a}{b-a}\right) \mathbb{E}[e^{i \frac{k\pi x}{b-a}}] \right] \\ &= \frac{2}{b-a} \operatorname{Re} \left[\exp\left(-i \frac{k\pi a}{b-a}\right) \Phi_X\left(\frac{k\pi}{b-a}\right) \right]. \end{aligned} \quad (4.5)$$

For the CDF, we simply insert the Fourier cosine expansion in the definition to yield:

$$\begin{aligned} F_X(x) &= \int_{-\infty}^x f_X(x) dx \\ &\approx \int_b^x f_X(x) dx \\ &= \int_b^x \sum_{k=0}^{\infty} F_k \cos\left(k\pi \frac{x-a}{b-a}\right) dx \\ &\approx \sum_{k=0}^{N-1} F_k \int_b^x \cos\left(k\pi \frac{x-a}{b-a}\right) dx \\ &= \sum_{k=0}^{N-1} F_k \int_b^x \cos\left(k\pi \frac{x-a}{b-a}\right) dx. \end{aligned} \quad (4.6)$$

And note that

$$\int_c^d \cos\left(k\pi \frac{y-a}{b-a}\right) dy = \begin{cases} \frac{b-a}{k\pi} \left[\sin\left(k\pi \frac{d-a}{b-a}\right) - \sin\left(k\pi \frac{c-a}{b-a}\right) \right], & k \neq 0 \\ d-c, & k = 0. \end{cases} \quad (4.7)$$

Hence, once the characteristic function is known, we can recover the density function and the CDF. In the next section we compute the characteristic function of $\ln(A_t)$.

4.2 Characteristic Function

In this Section we present how we can compute the characteristic function of $\ln(A_t^\nu)$. We start with some relatively simple computations, based on Bougerol's identity. This is done as follows:

$$\beta_{A_t} \stackrel{law}{=} \sinh(B_t) \leftrightarrow \quad (4.8)$$

$$\sqrt{A_t} \cdot Z \stackrel{law}{=} \sinh(B_t) \leftrightarrow \quad (4.9)$$

$$A_t \cdot Z^2 \stackrel{law}{=} \sinh^2(B_t) \leftrightarrow \quad (4.10)$$

$$\ln(A_t) + \ln(Z^2) \stackrel{law}{=} \ln(\sinh^2(B_t)), \quad (4.11)$$

where $Z \sim N(0, 1)$ and $B_t \sim N(0, t)$ is a Brownian motion, which is independent of the Brownian motion β_t . If two distributions are the same in law, then their characteristic functions are the same. Computing the characteristic function of both sides of (4.11), we obtain:

$$\begin{aligned} \Phi(\omega) &= \mathbb{E}[\exp(i\omega(\ln(A_t) + \ln(Z^2)))] \\ &= \mathbb{E} \exp(i\omega \ln(A_t)) \cdot \mathbb{E}[\exp(i\omega \ln(Z^2))] \\ &= \Phi_{\ln(A_t)}(\omega) \cdot \Phi_{\ln(Z^2)}(\omega) \\ &= \Phi_{\ln(\sinh^2(B_t))}(\omega). \end{aligned} \quad (4.12)$$

It then follows that

$$\Phi_{\ln(A_t)}(\omega) = \frac{\Phi_{\ln(\sinh^2(B_t))}(\omega)}{\Phi_{\ln(Z^2)}(\omega)}. \quad (4.13)$$

From equation (4.3) in Section 4.1, we see that we can recover the density of $X = \ln(A_t)$ via

$$\begin{aligned} f_X(x) &\approx \frac{1}{2}F_0 + \sum_{k=1}^{N-1} \frac{2}{b-a} \operatorname{Re} \left[\exp\left(-i \frac{k\pi a}{b-a}\right) \frac{\Phi_{\ln(\sinh^2(B_t))}\left(\frac{k\pi}{b-a}\right)}{\Phi_{\ln(Z^2)}\left(\frac{k\pi}{b-a}\right)} \right] \cos\left(k\pi \frac{x-a}{b-a}\right) \\ &= \frac{1}{2}F_0 + \sum_{k=1}^{N-1} \frac{2}{b-a} \operatorname{Re} \left[\exp\left(-i \frac{k\pi a}{b-a}\right) \frac{h(\omega)}{g(\omega)} \right] \cos\left(k\pi \frac{x-a}{b-a}\right), \end{aligned} \quad (4.14)$$

with

$$h(\omega) = \Phi_{\ln(\sinh^2(B_t))}(\omega), \quad (4.15)$$

$$g(\omega) = \Phi_{\ln(Z^2)}(\omega). \quad (4.16)$$

The computation of the density function of $\ln(A_t^\nu)$ comes down to computing two characteristic functions, $g(\omega)$ and $h(\omega)$. We will analyse these two characteristic functions separately. We start with $g(\omega)$ in the next subsection.

4.2.1 Characteristic Function of $X = \ln(Z^2)$

We can compute $g(\omega)$ in two ways, analytically and numerically. We start with the first.

4.2.1.1 Method 1

We compute $g(\omega)$ directly, using the closed form formula of $g(\omega)$ which involves a special function. Let $Z \sim N(0, 1)$, then

$$\begin{aligned} g(\omega) &= \Phi_{\ln(Z^2)}(\omega) = \mathbb{E}[\exp(i\omega \ln(Z^2))] = \frac{1}{\sqrt{2\pi}} \int_{-\infty}^{\infty} e^{i\omega \ln(x^2)} e^{-\frac{1}{2}x^2} dx \\ &= \frac{2}{\sqrt{2\pi}} \int_0^{\infty} e^{i\omega \ln(x^2)} e^{-\frac{1}{2}x^2} dx. \end{aligned} \quad (4.17)$$

Applying the change of variable by $y = \frac{1}{2}x^2$, we yield

$$\frac{dy}{dx} = x \rightarrow dx = \frac{dy}{x} = (2y)^{-\frac{1}{2}} dy.$$

If $x = 0 \rightarrow y = 0$ if $x \rightarrow \infty, y \rightarrow \infty$. It holds that

$$\begin{aligned}
\Phi(\omega) &= \frac{2}{\sqrt{2\pi}} \int_0^\infty e^{i\omega \ln(x^2)} e^{-\frac{1}{2}x^2} dx \\
&= \frac{2}{\sqrt{2\pi}} \int_0^\infty e^{i\omega \ln(2y)} e^{-y} (2y)^{-\frac{1}{2}} dy \\
&= \frac{2}{\sqrt{2\pi}} \int_0^\infty (2y)^{i\omega - \frac{1}{2}} e^{-y} dy \\
&= \frac{2}{\sqrt{2\pi}} 2^{i\omega - \frac{1}{2}} \int_0^\infty y^{i\omega - \frac{1}{2}} e^{-y} dy \\
&= \frac{1}{\sqrt{\pi}} 2^{i\omega} \Gamma(i\omega + \frac{1}{2}),
\end{aligned} \tag{4.18}$$

where $\Gamma(\cdot)$ denotes the Gamma function, i.e

$$\Gamma(z) = \int_0^\infty t^{z-1} e^{-t} dt, \quad \text{Re}(z) > 0. \tag{4.19}$$

We can use the readily available Gamma function, such as `scipy.gamma` in Python to compute $g(\omega)$. In the second method, we make use of numerical integration.

4.2.1.2 Method 2

To solve the integration defined in (4.17), we propose to use a numerical integration technique as second method. Before applying any numerical integration rule, we seek a sufficient integration range such that $\int_a^b f(x) dx \geq 1 - TOL$, where TOL is a tolerance level one can choose upfront. We can derive boundaries based on the given TOL as follows.

First we compute the density function of $X = \ln(Z^2)$. Note that if $Y = Z^2 \sim \chi_1^2$, the PDF of Y is then given by

$$f_Y(y) = \frac{1}{\sqrt{2\pi}} y^{-\frac{1}{2}} e^{-\frac{1}{2}y}, \quad y \in [0, \infty). \tag{4.20}$$

Since $g(y) = \ln(y)$ is strictly increasing for $y \in (0, \infty)$ and $P(Y = 0) = 0$, it follows that the PDF of $X = g(Y) = \ln(Y)$ is given by

$$\begin{aligned}
f_X(x) &= f_Y(g^{-1}(x)) \frac{dg^{-1}(x)}{dx} \\
&= \frac{1}{\sqrt{2\pi}} e^{-\frac{1}{2}e^x} e^{-\frac{1}{2}x} e^x \\
&= \frac{1}{\sqrt{2\pi}} e^{-\frac{1}{2}(e^x - x)}, \quad x \in (-\infty, \infty).
\end{aligned} \tag{4.21}$$

For the lower bound we seek an $a \in \mathbb{R}$ such that

$$\int_{-\infty}^a f(x) dx \leq \frac{1}{2} TOL. \tag{4.22}$$

Let $y = e^x$. Then $dx = \frac{1}{y} dy$, and it follows that

$$\begin{aligned}
\int_{-\infty}^a f(x) dx &= \int_{-\infty}^a \frac{1}{\sqrt{2\pi}} e^{-\frac{1}{2}e^x} e^{\frac{1}{2}x} dx \\
&= \int_0^{e^a} \frac{1}{\sqrt{2\pi}} e^{-\frac{1}{2}y} \sqrt{y} \frac{1}{y} dy \\
&= \int_0^{e^a} \frac{1}{\sqrt{2\pi}} e^{-\frac{1}{2}y} y^{-\frac{1}{2}} dy \\
&= \int_0^{\frac{1}{2}e^a} \frac{1}{\sqrt{\pi}} e^{-z} z^{-\frac{1}{2}} dz,
\end{aligned} \tag{4.23}$$

where in the last step the substitution $z = \frac{1}{2}y$ was used. Now let $u = \sqrt{z}$, then $\frac{1}{\sqrt{z}}dz = 2du$. We continue our computation as follows:

$$\begin{aligned}
\int_{-\infty}^a f(x)dx &= \int_0^{\frac{1}{2}e^a} \frac{1}{\sqrt{\pi}} e^{-z} z^{-\frac{1}{2}} dz \\
&= \int_0^{\sqrt{\frac{1}{2}e^a}} \frac{2}{\sqrt{\pi}} e^{-u^2} du \\
&= \frac{2}{\sqrt{\pi}} \sqrt{2\pi} \left[\Phi \left(\sqrt{\frac{1}{2}e^a} \right) - \Phi(0) \right] \\
&= 2\sqrt{2}\Phi \left(\sqrt{\frac{1}{2}e^a} \right) - \sqrt{2} \leq \frac{1}{2}TOL \leftrightarrow \\
\Phi \left(\sqrt{\frac{1}{2}e^a} \right) &\leq \frac{1}{\sqrt{32}}TOL + \frac{1}{2} \leftrightarrow \\
a &\leq \ln \left[2 \left(\Phi^{-1} \left(\frac{1}{\sqrt{32}}TOL + \frac{1}{2} \right) \right)^2 \right],
\end{aligned} \tag{4.24}$$

where $\Phi(\cdot)$ denotes the CDF of the standard normal distribution. For the upper bound we do the same integration steps, only the boundaries change as follows:

$$\int_b^{\infty} f(x)dx \stackrel{y=e^x}{=} \int_{e^b}^{\infty} g(y)dy \stackrel{z=\frac{1}{2}y}{=} \int_{\frac{1}{2}e^b}^{\infty} h(z)dz \stackrel{u=\sqrt{z}}{=} \int_{\sqrt{\frac{1}{2}e^b}}^{\infty} k(u)du = \frac{2}{\sqrt{\pi}} \int_{\sqrt{\frac{1}{2}e^b}}^{\infty} e^{-u^2} du. \tag{4.25}$$

Thus, for the upper bound we find that

$$\lim_{u \rightarrow \infty} \frac{2}{\sqrt{\pi}} \sqrt{2\pi} \left[\Phi(u) - \Phi \left(\sqrt{\frac{1}{2}e^b} \right) \right] = 2\sqrt{2} \left[1 - \Phi \left(\sqrt{\frac{1}{2}e^b} \right) \right] \leq \frac{1}{2}TOL \leftrightarrow \tag{4.26}$$

$$b \geq \ln \left[2 \left(\Phi^{-1} \left(1 - \frac{1}{\sqrt{32}}TOL \right) \right)^2 \right]. \tag{4.27}$$

Hence, we have

$$\Phi(\omega) = \int_a^b e^{i\omega x} \frac{1}{\sqrt{2\pi}} e^{-\frac{1}{2}e^x} e^{\frac{1}{2}x} dx \geq 1 - TOL, \tag{4.28}$$

where $[a, b]$ is given by

$$[a, b] = \left[\ln \left[2 \left(\Phi^{-1} \left(\frac{1}{\sqrt{32}}TOL + \frac{1}{2} \right) \right)^2 \right], \ln \left[2 \left(\Phi^{-1} \left(1 - \frac{1}{\sqrt{32}}TOL \right) \right)^2 \right] \right]. \tag{4.29}$$

Now that we have defined our truncation range for numerical integration, we choose Clenshaw-Curtis quadrature as integration technique. In the next subsection, we give a comparison between the two methods.

4.2.2 Comparison of the two Methods

We compare the approximation of $g(\omega)$ via the two methods above. Later we will evaluate them both more precisely in the total error of the CDF of $\ln(A_t)$, but it is good to already know in which cases differences occur. In the first method we use `scipy.gamma` in Python to compute $g(\omega)$. In the second, Clenshaw-Curtis quadrature is used to compute the characteristic function for $\omega = \frac{N\pi}{b-a}$, where $[a, b]$ is given in (4.29). Note that the computational complexity of the use of the Gamma function is less than Clenshaw-Curtis quadrature.

For Clenshaw-Curtis quadrature, we make use a DCT-1 type to compute the weights, which takes $O(J_g \log J_g)$ operations. Afterwards, a vector-vector multiplication is performed, hence the

operational complexity is $O(J_g \log(J_g) + J_g)$. We plot the magnitude of the approximation of $g(\omega)$, with $J_g = 500$ quadrature points.

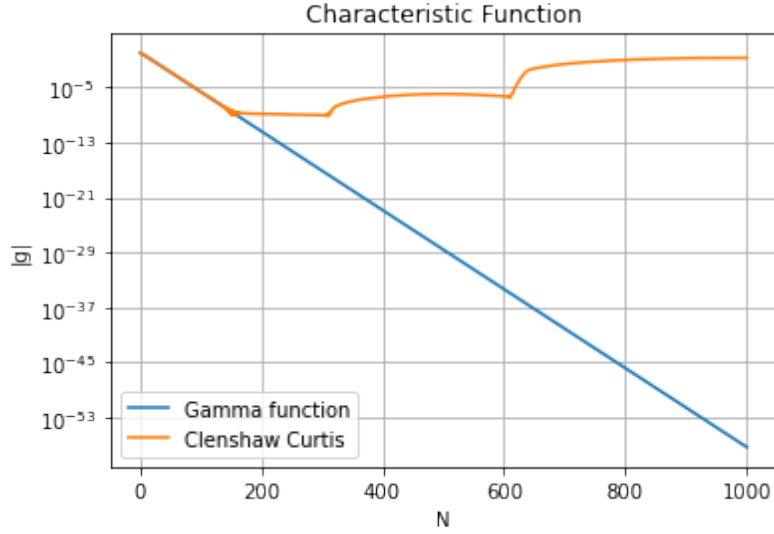


Figure 1: Absolute value of the characteristic function of $\ln(Z^2)$ using $J_g = 500$ quadrature points and the Gamma function.

The Gamma function decreases whereas the approximation using Clenshaw-Curtis quadrature increases in absolute value. We wish to seek the point where the difference occurs. In Figure 2 below, the absolute value of $g(\omega)$ plotted using both methods, again with $J = 500$, and using $TOL = 10^{-14}$ for numerical integration. Note that on the x -axis we use ω instead of N .

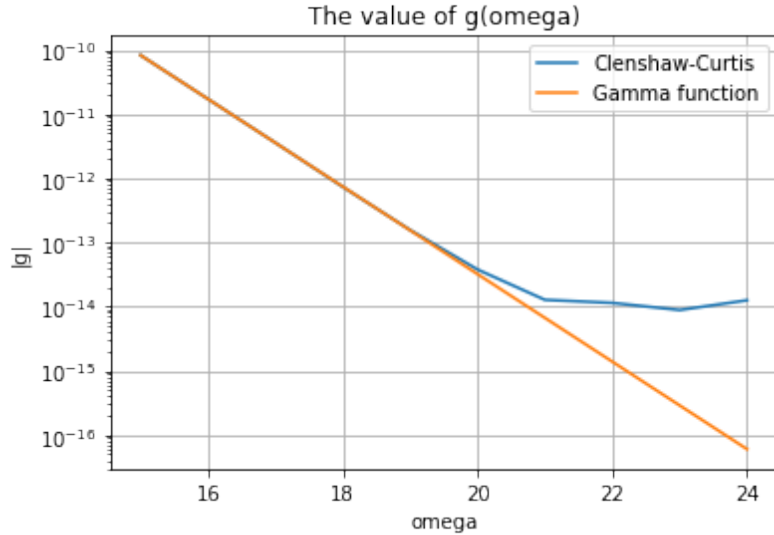


Figure 2: Absolute value of $g(\omega)$ using Clenshaw-Curtis quadrature and the Gamma function.

Based on Figure 2, we will compare $19 \leq \omega \leq 21$ in section 4.4.1. Note that $\omega = \frac{N\pi}{b-a}$, hence the truncation range $[a, b]$ determines the value of the number of cosine expansion terms N for each ω . In section 4.3, we will show that the truncation range is based on the parameter t . More details will be elaborated on the use of the Gamma function regarding N in that Section.

Lastly we will show the density function of $X = \ln(Z^2)$ in three different figures. We use the exact PDF found in (4.21), the COS method combined with the Gamma function and the COS

method combined with Clenshaw-Curtis quadrature using $N = 512$ quadrature points. For this plot, we set $[a_t, b_t]$ as in (4.62) with $t = 0.01$. For each other value of t , which will be noted below, the density recovery is still perfectly fine. It is important to state that we use the truncation range as in (4.62).

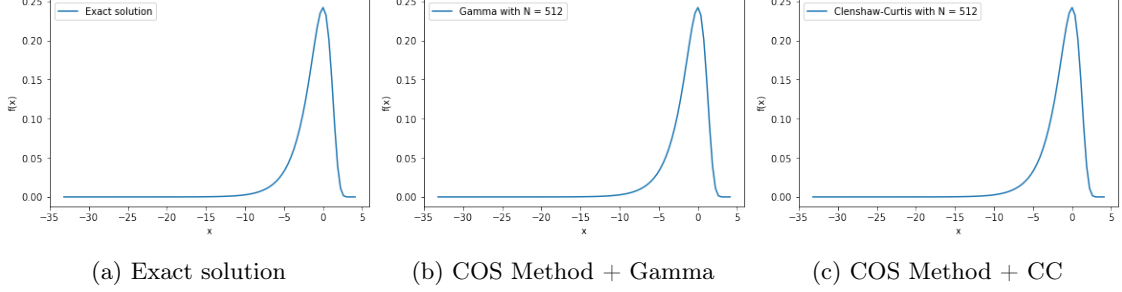


Figure 3: PDF of $X = \ln(Z^2)$.

Note that using both methods, we obtain a good recovery of the density function. In the next subsection, we will compute the characteristic function $h(\omega)$.

4.2.3 Characteristic Function of $Y = \ln(\sinh^2(B_t))$

We have determined the computation method of $g(\omega)$ in two ways. Next we compute $h(\omega)$.

Let B_t denote a standard Brownian motion. We have to solve

$$\begin{aligned} h(\omega) &= \Phi(\omega) = \mathbb{E} [\exp(i\omega \ln[\sinh^2(x)])] \\ &= \frac{1}{\sqrt{2\pi t}} \int_{-\infty}^{\infty} e^{i\omega \ln(\sinh^2(x))} e^{-\frac{1}{2t}x^2} dx. \end{aligned} \quad (4.30)$$

Just as in Method 2 in Section 4.2.1 we compute the density of $Y = \ln(\sinh^2(B_t))$. We have that $B_t \sim N(0, t)$. Let $X \sim N(0, t)$. Let $y = \ln[\sinh^2(x)]$, then

$$e^y = \sinh^2(x) \leftrightarrow \quad (4.31)$$

$$\pm \sqrt{e^y} = \sinh(x) \leftrightarrow \quad (4.32)$$

$$x_1 = \sinh^{-1}(\sqrt{e^y}) = \ln(\sqrt{e^y} + \sqrt{e^y + 1}), \quad x_1 > 0, \quad (4.33)$$

$$x_2 = \sinh^{-1}(-\sqrt{e^y}) = \ln(\sqrt{e^y + 1} - \sqrt{e^y}), \quad x_2 < 0, \quad (4.34)$$

$$\left| \frac{dx}{dy} \right| = \frac{1}{2} \sqrt{\frac{e^y}{e^y + 1}}, \quad x \in \{x_1, x_2\}. \quad (4.35)$$

Note that $f(x) = \ln[\sinh^2(x)]$ is strictly monotone and differentiable for $x \in (-\infty, 0)$ and $x \in (0, \infty)$, and $P(X = 0) = 0$. Therefore, we can state that for $Y = g(X) = \ln(\sinh^2(X))$ the PDF is given by

$$\begin{aligned} f_y(y) &= f_x(x_1(y)) \left| \frac{dx_1(y)}{dy} \right| + f_x(x_2(y)) \left| \frac{dx_2(y)}{dy} \right| \\ &= \frac{1}{2\sqrt{2\pi t}} \sqrt{\frac{e^y}{e^y + 1}} \left[e^{-\frac{1}{2t} [\ln(\sqrt{e^y} + \sqrt{e^y + 1})]^2} + e^{-\frac{1}{2t} [\ln(\sqrt{e^y + 1} - \sqrt{e^y})]^2} \right]. \end{aligned} \quad (4.36)$$

Therefore

$$h(\omega) = \frac{1}{2\sqrt{2\pi t}} \int_{-\infty}^{\infty} e^{i\omega y} \left[e^{-\frac{1}{2t} [\ln(\sqrt{e^y} + \sqrt{e^y + 1})]^2} + e^{-\frac{1}{2t} [\ln(\sqrt{e^y + 1} - \sqrt{e^y})]^2} \right] \sqrt{\frac{e^y}{e^y + 1}} dy. \quad (4.37)$$

This is quite a large expression and numerical integration would require a lot of computation. Analytic derivations for an upper bound such that $\int_b^\infty f_y(y) \leq \frac{1}{2}TOL$ did not yield to a closed form solution. Therefore, we wish to use another expression for the characteristic function of Y .

When we look at (4.30), we can also state that since

$$l(x) = \ln[(\sinh^2(x))e^{-\frac{1}{2}x^2}] = l(-x), \quad x \in \mathbb{R}, \quad (4.38)$$

it then follows that

$$\begin{aligned} h(\omega) &= \mathbb{E} [\exp(i\omega \ln[\sinh^2(x)])] \\ &= \frac{1}{\sqrt{2\pi t}} \int_{-\infty}^{\infty} e^{i\omega \ln[(\sinh^2(x))e^{-\frac{1}{2}x^2}]} dx \\ &= \frac{2}{\sqrt{2\pi t}} \int_0^{\infty} e^{i\omega \ln[(\sinh^2(x))e^{-\frac{1}{2}x^2}]} dx. \end{aligned} \quad (4.39)$$

Then for $x > 0$, $x = \sinh^{-1}(\sqrt{e^y}) = \ln(\sqrt{e^y} + \sqrt{e^y + 1})$ and $y = \ln[\sinh^2(x)] \in (-\infty, \infty)$, we compute the characteristic function as follows:

$$\begin{aligned} h(\omega) &= \mathbb{E} [\exp(i\omega \ln[\sinh^2(x)])] \\ &= \frac{2}{\sqrt{2\pi t}} \int_0^{\infty} e^{i\omega \ln[(\sinh^2(x))e^{-\frac{1}{2}x^2}]} dx \\ &= \frac{1}{\sqrt{2\pi t}} \int_{-\infty}^{\infty} e^{i\omega y} \exp\left[-\frac{1}{2t} \left[\ln\left(\sqrt{e^y} + \sqrt{e^y + 1}\right)\right]^2\right] \sqrt{\frac{e^y}{e^y + 1}} dy. \end{aligned} \quad (4.40)$$

We will solve expression (4.40) instead of (4.37) using numerical integration.

We seek a sufficient truncation range such that $h(\omega) \geq 1 - TOL$. Note that for large positive y :

$$0 < e^{i\omega y} \exp\left[-\frac{1}{2t} \left[\ln\left(\sqrt{e^y} + \sqrt{e^y + 1}\right)\right]^2\right] \sqrt{\frac{e^y}{e^y + 1}} \quad (4.41)$$

$$< \left| e^{i\omega y} \exp\left[-\frac{1}{2t} \left[\ln\left(\sqrt{e^y} + \sqrt{e^y + 1}\right)\right]^2\right] \sqrt{\frac{e^y}{e^y + 1}} \right| \quad (4.42)$$

$$\leq \exp\left[-\frac{1}{2t} \left[\ln\left(\sqrt{e^y} + \sqrt{e^y + 1}\right)\right]^2\right] \sqrt{\frac{e^y}{e^y + 1}} \quad (4.43)$$

$$< \exp\left[-\frac{1}{2t} \left[\ln\left(\sqrt{e^y} + \sqrt{e^y + 1}\right)\right]^2\right] \quad (4.44)$$

$$< \exp\left[-\frac{1}{2t} \left[\ln\left(2\sqrt{e^y}\right)\right]^2\right]. \quad (4.45)$$

Now we have for $d > 0$ that

$$\begin{aligned} \int_d^{\infty} \exp\left[-\frac{1}{2t} \left[\ln\left(2\sqrt{e^y}\right)\right]^2\right] dy &= \int_d^{\infty} \exp\left[-\frac{1}{2t} \left(\frac{1}{2}y + \ln(2)\right)^2\right] dy \\ &= \int_d^{\infty} \exp\left[-\frac{1}{2} \left(\frac{y + 2\ln(2)}{2\sqrt{t}}\right)^2\right] dy \\ &= 2\sqrt{2\pi t} \left[1 - \Phi\left(\frac{d + 2\ln(2)}{2\sqrt{t}}\right)\right]. \end{aligned} \quad (4.46)$$

Regarding the upper bound d , for the integration we obtain using (4.40):

$$\frac{1}{\sqrt{2\pi t}} \cdot 2\sqrt{2\pi t} \left[1 - \Phi\left(\frac{d + 2\ln(2)}{2\sqrt{t}}\right)\right] \leq \frac{1}{2} TOL \Leftrightarrow \quad (4.47)$$

$$\Phi\left(\frac{d + 2\ln(2)}{2\sqrt{t}}\right) \geq 1 - \frac{1}{4} TOL \Leftrightarrow \quad (4.48)$$

$$\frac{d + 2\ln(2)}{2\sqrt{t}} \geq \Phi^{-1}\left(1 - \frac{1}{4} TOL\right) \Leftrightarrow \quad (4.49)$$

$$d \geq 2\sqrt{t}\Phi^{-1}\left(1 - \frac{1}{4} TOL\right) - 2\ln(2). \quad (4.50)$$

Next we compute a lower bound c . Note that for large negative y the following holds:

$$0 < \exp \left[-\frac{1}{2t} \left[\ln \left(\sqrt{e^y} + \sqrt{e^y + 1} \right) \right]^2 \right] \sqrt{\frac{e^y}{e^y + 1}} < \sqrt{\frac{e^y}{e^y + 1}}. \quad (4.51)$$

Then we have the following for the lower bound $c < 0$:

$$\begin{aligned} \int_{-\infty}^c \sqrt{\frac{e^y}{e^y + 1}} dy &= 2 \ln \left(\sqrt{e^y} + \sqrt{e^y + 1} \right) \Big|_{-\infty}^c \\ &= 2 \ln \left(\sqrt{e^c} + \sqrt{e^c + 1} \right) \\ &= 2 \sinh^{-1}(\sqrt{e^c}) \leq \frac{1}{2} TOL. \end{aligned} \quad (4.52)$$

Therefore, for the lower bound c we find that

$$\frac{2}{\sqrt{2\pi t}} \sinh^{-1}(\sqrt{e^c}) \leq \frac{1}{2} TOL \Leftrightarrow \quad (4.53)$$

$$\sinh^{-1}(\sqrt{e^c}) \leq \frac{1}{4} \sqrt{2\pi t} TOL \Leftrightarrow \quad (4.54)$$

$$e^c \leq \sinh^2 \left(\frac{1}{4} \sqrt{2\pi t} TOL \right) \Leftrightarrow \quad (4.55)$$

$$c \leq \ln \left[\sinh^2 \left(\frac{1}{4} \sqrt{2\pi t} TOL \right) \right]. \quad (4.56)$$

Thus we choose

$$[c_t, d_t] = \left[\ln \left[\sinh^2 \left(\frac{1}{4} \sqrt{2\pi t} TOL \right) \right], 2\sqrt{t} \Phi^{-1} \left(1 - \frac{1}{4} TOL \right) - 2 \ln(2) \right] \quad (4.57)$$

as the interval for the numerical integration. Note that this range depends on t , and both c_t and d_t are increasing in t .

Just as for the numerical integration of $g(\omega)$, we will compute $h(\omega)$ using Clenshaw-Curtis quadrature. The computational complexity is $O(J_h \log(J_h) + J_h)$, for J_h quadrature points. We show the density of Y , using the exact PDF found in (4.36), and Clenshaw-Curtis quadrature using $N = 512$ cosine expansion terms with $J_h = 500$ quadrature points. Just as for $g(\omega)$, the used truncation range for the COS method, as well as interval for the plots, are defined by the truncation range as in (4.62).

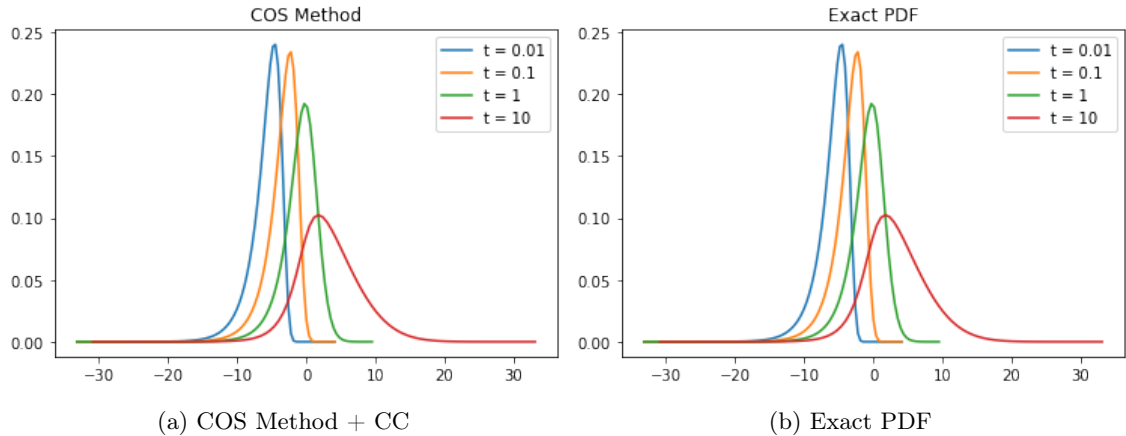


Figure 4: PDF of $Y = \ln(\sinh^2(B_t))$.

We have presented the computational methods for $g(\omega)$ and $h(\omega)$, which are the two elements to compute the characteristic function. In the next subsection we specify details of the numerical implementation.

4.3 Numerical Implementation

In Section 4.4 we conduct an error analysis of our method, where the computation of the CDF is used. First, we need a numerical implementation, which consists of three parts.

In our computation of the characteristic function of $\ln(A_t)$, the only parameter is t . We need to choose which values we will evaluate for the error analysis in Section 4.4.

The computation of the CDF and PDF of $\ln(A_t)$ is based on the characteristic function, for which we need the computation of $g(\omega)$, $h(\omega)$ and a truncation range. The truncation range will also be determined in this section.

Lastly, we need to define a benchmark for our computation. We will discuss all three components.

4.3.0.1 Choice of t

The final goal of this research is to efficiently price Asian options. We will look at a large variety of maturity times, also to get a good comparison for the numerical integration. By the scaling property of Brownian Motion described in Section 3.1.2, we have that $t = \frac{\sigma^2}{4}T$. Since $\sigma \in (0, 1]$, we will look at the values for $t \in [0.01, 0.1, 1, 10]$.

The last ingredient for the use of the COS method is the truncation range, which establish in the next subsection.

4.3.0.2 Choice of Truncation Range

The choice of integration range used for the density approximation for $\ln(A_t)$ is important for the efficiency of the method. An integration range too wide would require a lot of cosine expansion terms N . Making it too narrow, the error in the truncation range will dominate. Note that the density function of $\ln(A_t)$ is dependent on t , and we want to have a general integration range based on t . Since we cannot derive an analytic solution such that $\int_{a_t}^{b_t} f_{\ln(A_t)}(x)dx \geq 1 - TOL$, we define a rule of thumb below. The truncation ranges determined by

$$\int_a^b f_{\ln(Z^2)}(x)dx \geq 1 - TOL, \quad (4.58)$$

$$h(\omega) \geq 1 - TOL, \quad (4.59)$$

are equal to

$$[a, b] = \left[\ln \left[2 \left(\Phi^{-1} \left(\frac{1}{\sqrt{32}}TOL + \frac{1}{2} \right) \right)^2 \right], \ln \left[2 \left(\Phi^{-1} \left(1 - \frac{1}{\sqrt{32}}TOL \right) \right)^2 \right] \right], \quad (4.60)$$

$$[c_t, d_t] = \left[\ln \left[\sinh^2 \left(\frac{1}{4}\sqrt{2\pi t}TOL \right) \right], 2\sqrt{t}\Phi^{-1} \left(1 - \frac{1}{4}TOL \right) - 2\ln(2) \right]. \quad (4.61)$$

Based on (4.60) and (4.61), we set the overall truncation range as

$$[a_t, b_t] = [\min(a, c_t); \max(b, d_t)]. \quad (4.62)$$

For different values of t , the integration range is given below, with $TOL = 10^{-7}$. Note that this is a very wide truncation range. We come back to this in Section 5.2. In Table 1, the truncation ranges are shown for the different values of the parameter t .

	$h(\omega) \in [c_t, d_t]$	$[a_t, b_t]$
$t = 0.01$	$[-37.77; -0.30]$	$[-37.77; 4.11]$
$t = 0.1$	$[-35.47; 2.06]$	$[-35.47; 4.11]$
$t = 1$	$[-33.17; 9.52]$	$[-33.17; 9.52]$
$t = 10$	$[-30.87; 33.09]$	$[-30.87; 33.09]$

Table 1: Integration range $[a_t, b_t]$ based on $TOL = 10^{-7}$.

In Section 4.2.1 we concluded that differences in computing $g(\omega) = \ln(Z^2)$ occur around $19 \leq \omega \leq 21$, which is dependent on the truncation range. Using the truncation ranges in Table 1, we denote $N_t(\omega)$ as

$$N_t(\omega) = \frac{\omega(b_t - a_t)}{\pi}, \quad (4.63)$$

rounded to the lowest integer. This parameter $N_t(\omega)$ will also be used in the error analysis in Section 4.4.

In the next subsection we develop the benchmark method, which will be used to check the accuracy of our computation of the CDF of $\ln(A_t)$.

4.3.1 Benchmark: Monte Carlo Simulation

We have defined all the parameters for the COS method to compute the CDF of $\ln(A_t)$. We need a benchmark to check the accuracy of our method.

For the error analysis in the CDF and PDF of $\ln(A_t)$, we simulate $\ln(A_t)$ by Monte Carlo simulation. The Monte Carlo scheme for A_t is given by:

$$\begin{aligned} A_t &= \int_0^t e^{2B_s} ds \\ &= \sum_{i=0}^n e^{2B(t_{i+1})} (t_{i+1} - t_i) \\ &= \frac{t}{n} \sum_{i=0}^n e^{2B(t_{i+1})} \\ &= \frac{t}{n} \sum_{i=0}^n e^{2 \sum_{j=0}^i B(t_{j+1}) - B(j)} \\ &= \frac{t}{n} \sum_{i=0}^n e^{2 \sum_{j=0}^i \sqrt{\frac{t}{n}} Z_j}, \end{aligned} \quad (4.64)$$

where $Z_j \sim N(0, 1)$, $j \in \{0, \dots, n\}$. We set $n = 100$ time steps and simulate $m = 10^6$ Monte Carlo paths. Note that for each sample, we take the *log*-value. In Table 2 the integration ranges based on Monte Carlo simulation are given. Note that the density of $\ln(A_t)$ simulated by Monte Carlo simulation lies between the truncation ranges we chose for $f_X(x)$ and $f_Y(y)$.

	Monte Carlo	$[a_t, b_t]$
$t = 0.01$	$x \in [-5.18; -3.97]$	$[-37.77; 4.11]$
$t = 0.1$	$x \in [-3.78; -0.22]$	$[-35.47; 4.11]$
$t = 1$	$x \in [-3.24; 7.46]$	$[-33.17; 9.52]$
$t = 10$	$x \in [-3.71; 31.34]$	$[-30.87; 33.09]$

Table 2: Interval of $\ln(A_t)$ based on Monte Carlo simulation compared with the defined truncation range in (4.62).

To obtain the density function of $\ln(A_t)$ for our benchmark, we use a Kernel Density Estimation based on the m Monte Carlo simulations. To find a curve for the CDF of $\ln(A_t)$, we use `numpy.sort` and `numpy.arrange` in Python.

When we compare these intervals to the chosen integration ranges above, we see that we have a very wide integration range, especially for $x < 0$. We will elaborate more in detail in section 4.5. In the next section, our computation of the CDF will be compared to the Monte Carlo simulation.

4.4 CDF Error Analysis

In 4.6, we have shown how to recover the CDF via the COS method. We check our computation of the characteristic function of $\ln(A_t)$ via an error analysis in the CDF.

In Section 6.4 we will give a complete overview of all the errors involved in our method. In this section we conduct a numerical error analysis. Since we can easily extract data points from the CDF simulated by Monte Carlo, we will analyze the errors the CDF of $\ln(A_t)$. Later, we combine these results to see how the PDF errors converge using these values suggested by the CDF error analysis.

First we explore the difference in the use of the Gamma function and Clenshaw-Curtis quadrature for the computation of $g(\omega)$. Then we study the error convergence of the computation of $h(\omega)$ in both the COS expansion and the numerical integration: first we test the convergence in the COS method varying the number of cosine expansion terms, and setting very many quadrature points for $h(\omega)$; then, we check the error convergence by changing the number of quadrature points used for $h(\omega)$. Finally, we see how the level of tolerance TOL_h , which is used for the numerical integration of h , affects the results.

Using the Monte Carlo scheme above as benchmark, we compute the errors as follows. We compute $F(x)$ via the COS method and let $H(x)$ be our CDF obtained via Monte Carlo simulation. We compute $e_j = |F(x_j) - H(x_j)|, 1 \leq j \leq k$ as error using the COS method, and the total error in the $\|\cdot\|_1$ -norm and $\|\cdot\|_2$ -norm respectively are given by

$$\epsilon_1 = \max\{e_1, \dots, e_k\}, \quad (4.65)$$

$$\epsilon_2 = \sqrt{e_1^2 + \dots + e_k^2}. \quad (4.66)$$

We checked 10 testing points i.e. $k = 10$ for each value of t . We only use values that lie within the peak of the density function. In the next subsection, we analyse the computation of $g(\omega)$.

4.4.1 Convergence of $g(\omega)$

We start with the convergence analysis due the computation of $g(\omega)$. We look at the errors for various number of cosine terms N using the different methods described in Section 4.2.1. We let the integration range $[a_t, b_t]$ for the COS method still be based on $TOL = 10^{-7}$, since we have seen that this is indeed wide enough based on Monte Carlo simulation. To minimize errors, we integrate $g(\omega)$ and $h(\omega)$ over an interval where $TOL = 10^{-14}$ is used.

Setting the number of quadrature points very large, i.e. $J_h = 1500$, the overall error must be dominated by the number of cosine expansion terms. Note that such a number of quadrature points take a lot of computational time. For $h(\omega)$, we use Clenshaw-Curtis quadrature.

We compare the use of the Gamma function and Clenshaw-Curtis quadrature for $g(\omega)$. Setting also $J_g = 1500$, the results are presented in Table 3, whereby the errors are given in the $\|\cdot\|_2$ -norm. We simulated $m = 10^5$ Monte Carlo paths using $n = 100$ time steps. This may not be a sufficient number of simulations for $\ln(A_t)$. But for the purpose of this error analysis, it is sufficient enough to see convergence in N , and for the analysis in the number of quadrature points. When we price options for $\nu = 0$, we will use $4 \cdot 10^6$ simulations with a reducing variance method. We come back to this in Section 6.

Fourier Cosine Expansion + Gamma vs Clenshaw-Curtis ($g(\omega)$)									
N	$t = 0.01, \epsilon_2$		$t = 0.1, \epsilon_2$		$t = 1, \epsilon_2$		$t = 10, \epsilon_2$		
	Γ	CC	Γ	CC	Γ	CC	Γ	CC	
8	1.04	1.04	0.75	0.75	0.30	0.30	0.80	0.80	
16	0.91	0.91	0.47	0.47	0.072	0.072	0.019	0.019	
32	0.71	0.71	0.17	0.17	0.0063	0.0063	0.0046	0.0046	
64	0.37	0.37	0.020	0.020	0.0038	0.0038	0.0046	0.0046	
128	0.11	0.11	0.0036	0.0036	0.0038	0.0038	0.0046	0.0046	
256	0.0080	0.0080	0.0049	0.0049	0.0037	0.0037	0.0046	0.0046	
512	$5.32 \cdot 10^9$	0.13	$1.48 \cdot 10^{11}$	0.19	$4.17 \cdot 10^{11}$	6.09	349.76	1.74	

Table 3: Errors in the $\|\cdot\|_2$ -norm of the CDF for various number of cosine terms N using different computation methods for $g(\omega)$.

First we notice that we have convergence up to $N = 128$ for all t . Also note that the errors are the same for $N \leq 256$ for both methods. When $N = 256$, convergence does not hold for $t = 0.1$ compared to the Monte Carlo simulation, note that this may not very precise.

For $N = 512$, the Gamma function gives very large errors, due to the fast decay of the Gamma function in Python. The value becomes very low, and since it is in the denominator of our characteristic function, the value of the error becomes very large. For $N = 512$, also the error with Clenshaw-Curtis does not decrease. By the magnitude of this error, we can conclude that this is due to the error in the numerical integration in either $g(\omega)$ or $h(\omega)$.

To get a good understanding, we wish to look for the difference in the errors using Γ and CC for $19 \leq \omega \leq 21$. For these values, the values of the absolute value diverged in Figure 1. For each t , we look at the errors using this value. Where $N_t(\omega)$ is given by

$$N_t(\omega) = \frac{\omega(b_t - a_t)}{\pi}. \quad (4.67)$$

The results are shown in the small tables below. We include $N = 128$ and $N = 256$ for reference.

$t = 0.01$	$N = 128$	$\omega = 19, (N = 254)$	$N = 256$	$\omega = 20, (N = 266)$	$\omega = 21, (N = 279)$
Γ	0.11	0.0080	0.0080	0.0068	0.019
CC	0.11	0.0081	0.0080	0.0067	0.012

$t = 0.1$	$N = 128$	$\omega = 19, (N = 239)$	$\omega = 20, (N = 251)$	$N = 256$	$\omega = 21, (N = 264)$
Γ	0.0036	0.0035	0.0044	0.0049	0.0073
CC	0.0036	0.0035	0.0044	0.0049	0.0067

$t = 1$	$N = 128$	$N = 256$	$\omega = 19, (N = 258)$	$\omega = 20, (N = 271)$	$\omega = 21, (N = 285)$
Γ	0.0038	0.0037	0.0036	0.0028	0.0051
CC	0.0038	0.0037	0.0036	0.0028	0.0061

$t = 10$	$N = 128$	$N = 256$	$\omega = 19, (N = 381)$	$\omega = 20, (N = 407)$	$\omega = 21, (N = 427)$
Γ	0.0046	0.0046	0.0045	0.0056	0.0046
CC	0.0046	0.0046	0.0045	0.0056	0.0046

We can draw a good conclusion from these tables. We observe the following. Note that for $\omega \geq 21$, for each value of t the error increases for both methods.

For $t = 0.1$ and $t = 10$, the error for $\omega = 20$ is higher than for $\omega = 19$.

Up until $\omega = 19$, we see convergence in the errors for both methods, and the value is of the error is the same except for $t = 0.01$, the error using Γ is 0.0001 smaller. Hence for the maximum value of N for which we obtain convergence based on the 10^5 Monte Carlo simulations, we can conclude that use of the Gamma function is justified for this further error analysis. This decreases the computational complexity.

We plot the PDF of $\ln(A_t)$ using the Gamma function and $TOL = 10^{-14}$, with $J_h = 1500$. For $t = 0.01$ and $t = 10$, using the value of N for which $\omega = 20$, gave actually more oscillation than for $\omega = 19$. Hence we use the values of N for which $\omega = 19$. We set $N_{\max}(t) \in \{256, 239, 258, 381\}$. We obtain the following graphs if we recover the density via the COS method.

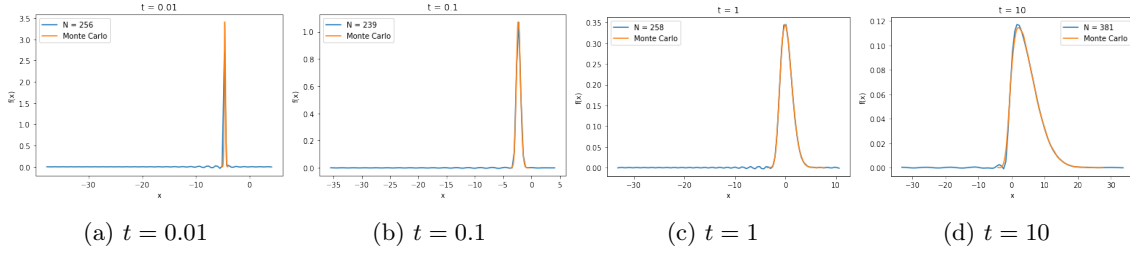


Figure 5: Density of $\ln(A_t)$ for various t via cosine series expansion.

Oscillation occurs in each density function, which means that errors occur in the computation of $h(\omega)$ or $g(\omega)$. When we plot the density function for $N_t \in \{256, 128, 128, 128\}$, we obtain less oscillation in the density function for $t > 0.01$, which will be shown in section 4.5 in Figure 9. Therefore, we will continue our error analysis therefore based on $N_t \in \{256, 128, 128, 128\}$.

In the following subsection, we aim to look at the convergence of errors based on the number of quadrature points used for $h(\omega)$.

4.4.2 Quadrature Points

In this subsection, we choose the Gamma function for the computation of $g(\omega)$. For $h(\omega)$, recall that we use Clenshaw-Curtis quadrature. To analyse the errors using a different number of quadrature points J_h for $h(\omega)$, we use the values for which convergence occurred in the previous analysis. Also setting $TOL = 10^{-14}$ for the computation of $h(\omega)$ to minimize the errors coming from the numerical integration.

We set $J_h \in \{100, 200, 300, 400, 500, 600, 700, 800, 900, 1000\}$. The $\|\cdot\|_2$ -norm is used to analyse error convergence. The benchmark method is the same Monte Carlo simulation as before.

We make use of 4 plots to verify the error convergence due to the quadrature points. On the y -axis, a log scale is used. The results are shown in Figure 6.

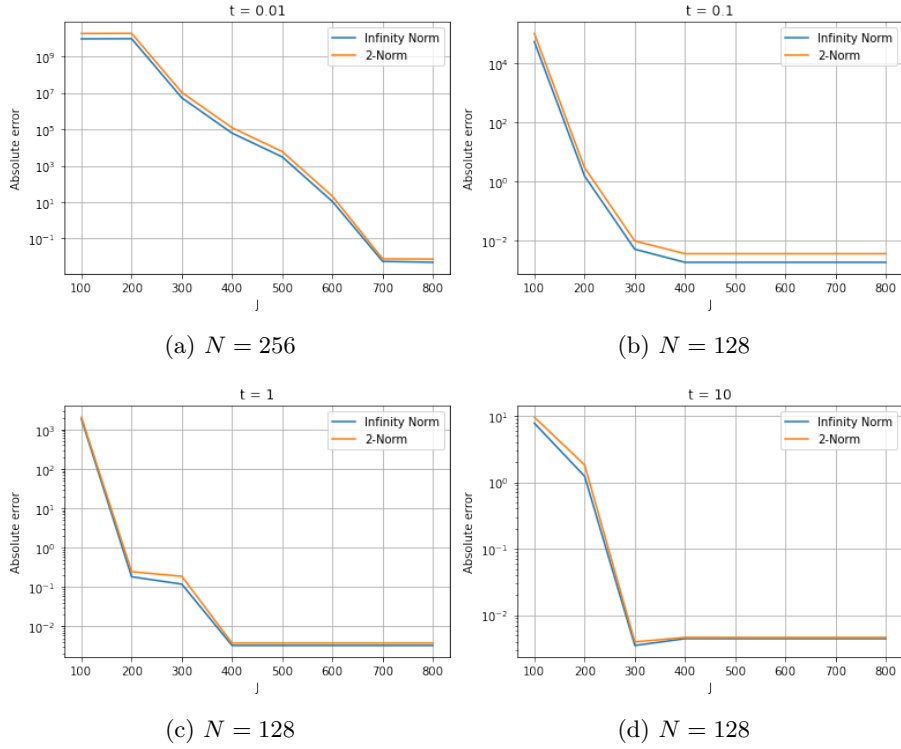


Figure 6: CDF errors for a different number of quadrature points J_h for Clenshaw-Curtis quadrature for $h(\omega)$.

For $t = 0.01$, 800 quadrature points are needed for the errors to stop converging. Based on Figure 6, we set $J_h = 800$ for each value of t . Lastly we look at the error convergence using different values for our tolerance level TOL_h for the numerical integration. Note that for the truncation range $[a_t, b_t]$ as in (4.62), we keep $TOL = 10^{-7}$.

4.4.3 Errors Analysis in the Tolerance Level

The third dimension for the error analysis is the tolerance level chosen for the numerical integration of h , which we will analyze in this Subsection.

We have a sufficient number of quadrature points for the Clenshaw-Curtis quadrature for $h(\omega)$ and have found $N_{\max}(t)$ such that the CDF errors converge compared to Monte Carlo simulation.

At last, we look at the error in the truncation range for computing $h(\omega)$. Note that the overall truncation range for the COS method does not change. Until now we have set $TOL_h = 10^{-14}$ for $h(\omega)$. Choosing the values based on the analysis above, we vary the tolerance level. Setting $J_h = 800$, $N_t \in \{256, 128, 128, 128\}$ and varying $TOL_h \in \{10^{-8}, 10^{-11}, 10^{-14}\}$.

Clenshaw-Curtis + Gamma and Fourier Cosine Expansion								
	$t = 0.01$		$t = 0.1$		$t = 1$		$t = 10$	
	ϵ_1	ϵ_2	ϵ_1	ϵ_2	ϵ_1	ϵ_2	ϵ_1	ϵ_2
$TOL_h = 10^{-8}$	1.65	3.22	0.0018	0.0037	0.0033	0.0038	0.0044	0.0046
$TOL_h = 10^{-11}$	0.0053	0.0068	0.0018	0.0035	0.0033	0.0038	0.0044	0.0046
$TOL_h = 10^{-14}$	0.0056	0.0080	0.0018	0.0035	0.0033	0.0038	0.0044	0.0046

Table 4: Errors in the CDF using different levels of tolerance.

We compare the results with Table 3. For $t \in \{0.1, 1, 10\}$, we see the same results when $TOL_h \geq 10^{-11}$. For $t = 0.01$, the error using $TOL_h = 10^{-11}$ is smaller than for $TOL_h = 10^{-14}$.

We come back to this in Section 5.2. Lastly, we show the exponential convergence using the values above in Figure 7 for a different number of cosine expansion terms N .

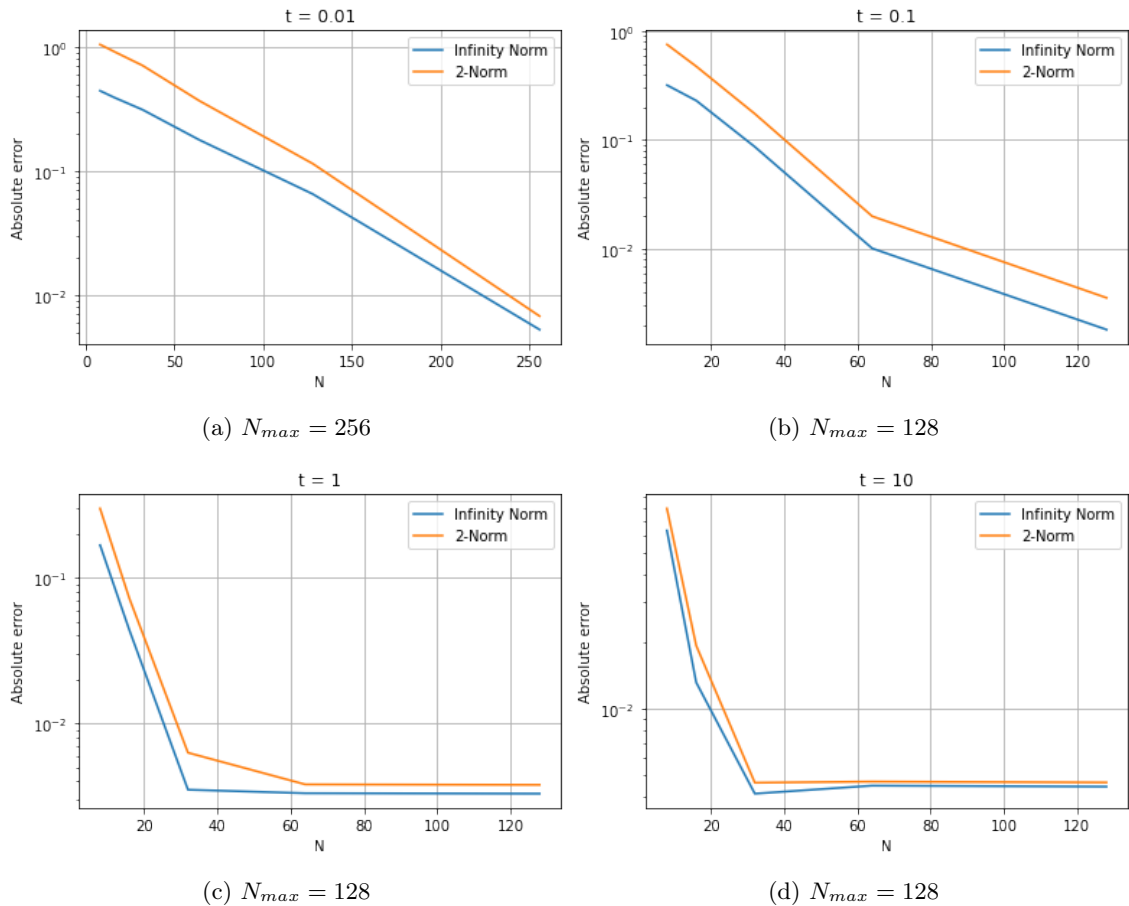


Figure 7: Exponential convergence shown in both norms for the CDF of $\ln(A_t)$.

Finally we combine these values and look at the the PDF of $\ln(A_t)$ in the next Subsection.

4.5 PDF Error Analysis

The error analysis for the CDF was performed with Monte Carlo simulation as benchmark, since we could easily contract data points from the Monte Carlo simulation. For the Probability Density Function we used Kernel Density Estimation, which makes this not possible.

We have concluded that the Gamma function works sufficiently well for the computation of $g(\omega)$ until the point that we observed convergence for both methods, and for $h(\omega)$ we use Clenshaw-Curtis quadrature. First, we show the PDF recovery using the COS method, afterwards we show convergence in N again and make a note on the truncation range.

4.5.0.1 PDF Recovery

We will use the obtained values from the previous sections and plot the PDF of $\ln(A_t)$ for each value of t , setting $J_h = 800$, $N_t \in \{256, 128, 128, 128\}$ and $TOL_h = 10^{-11}$.

The results are shown in Figure 8. Note that we truncate the integration range showed in the plot, but in fact the integration range $[a_t, b_t] = [\min(a, c_t), \max(b, d_t)]$ as in (4.62) is still used.

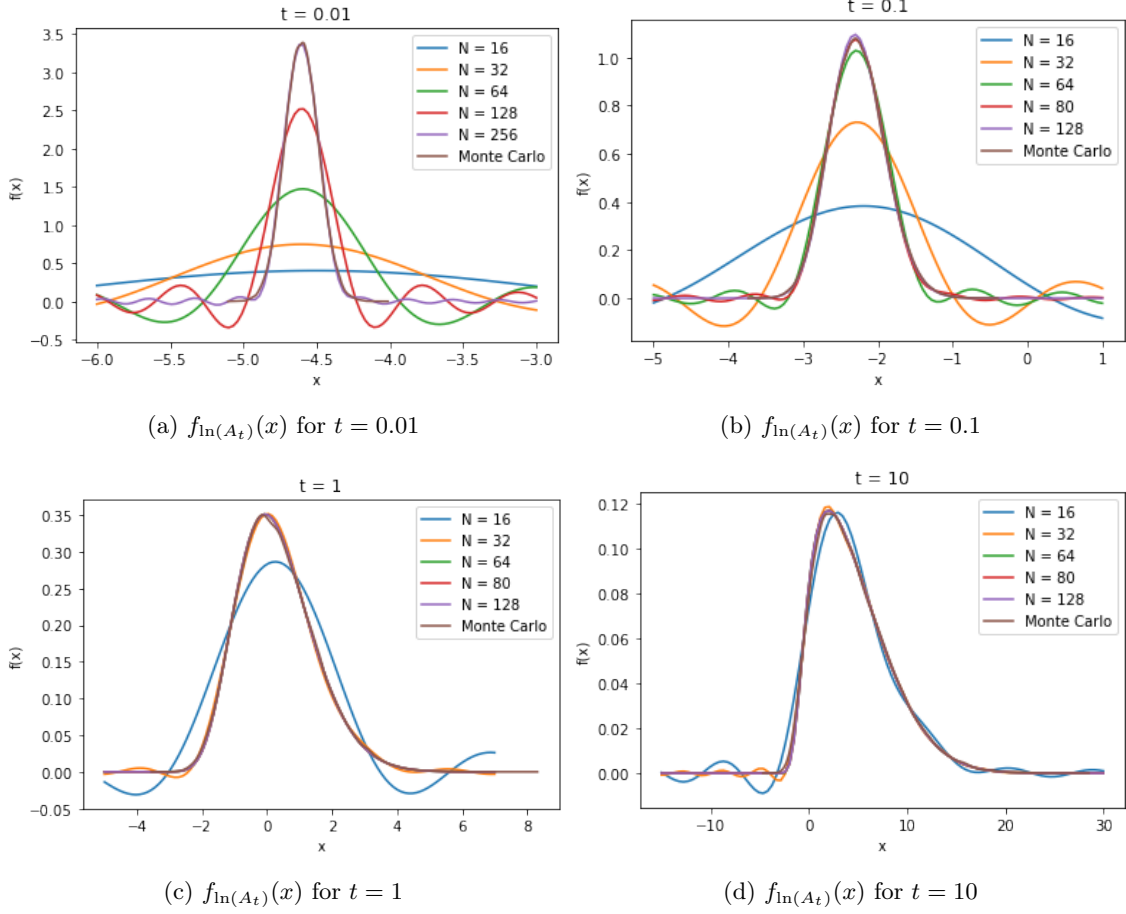


Figure 8: Density recovery by the COS method for different t for multiple cosine expansion terms N .

Here we set $m = 100$ steps in the density function. Note that for $t \in \{0.1, 1, 10\}$ we obtain no oscillation in the density function, opposed to $t = 0.01$. The peak in the density is too narrow to get a smooth result using the COS method combined with the proposed numerical integration.

In Section 4.2.1 and 4.2.3, we recovered the density functions of $X = \ln(Z)$, $Z \sim N(0, 1)$ and $Y = \ln(\sinh^2(B_t))$, where B_t is a standard Brownian motion, for $N = 512$ with the truncation range used for $\ln(A_t)$ as in (4.62). It is important to note that these recoveries were good compared to the exact solution of the PDF. Meanwhile in Table 3, we saw that taking $N = 512$ cosine expansion terms led to large errors in the CDF. It is important to note that for the density recovery of $\ln(A_t)$, which uses both characteristic functions, we have less accuracy than for the marginal distributions. We come back to this in section 5.2. Lastly, we show the convergence of errors in N of the PDF.

4.5.0.2 Convergence in N

To finalize the error analysis for the approximation of the distribution of $\ln(A_t)$, we show convergence in N in the two norms based for the PDF. The results are shown in Table 5. For $t = 0.01$, $N_{\max} = 256$. For $t \in \{0.1, 1, 10\}$, $N_{\max} = 128$.

Clenshaw Curtis + Gamma and Fourier Cosine Expansion								
	$t = 0.01$		$t = 0.1$		$t = 1$		$t = 10$	
N	ϵ_1	ϵ_2	ϵ_1	ϵ_2	ϵ_1	ϵ_2	ϵ_1	ϵ_2
40	2.42	3.45	0.25	0.43	0.0026	0.0049	0.0016	0.0022
60	2.01	3.01	0.084	0.17	0.00016	0.00027	0.0016	0.00024
80	1.62	2.56	0.022	0.040	$2.31 \cdot 10^{-5}$	$3.65 \cdot 10^{-5}$	$6.13 \cdot 10^{-3}$	$7.16 \cdot 10^{-5}$
100	1.26	2.07	0.0045	0.0098	$1.43 \cdot 10^{-6}$	$1.98 \cdot 10^{-6}$	$1.59 \cdot 10^{-5}$	$1.98 \cdot 10^{-5}$
120	0.95	1.59	0.00055	0.00012	$2.77 \cdot 10^{-7}$	$4.49 \cdot 10^{-7}$	$1.60 \cdot 10^{-6}$	$2.33 \cdot 10^{-6}$
160	0.49	0.87	-	-	-	-	-	-
200	0.22	0.41	-	-	-	-	-	-

Table 5: Convergence of errors based on $|N - N_{max}(t)|$ for the PDF of $\ln(A_t)$.

For $t = 0.01$, the errors are quite large compared to N_{max} , which is due to the large truncation range. In the next subsection, we comment on this truncation range. For $t > 0.01$, the difference in errors gets extremely small.

4.5.0.3 Truncation range

We plot the density functions for each t . The results are shown in Figure 9.

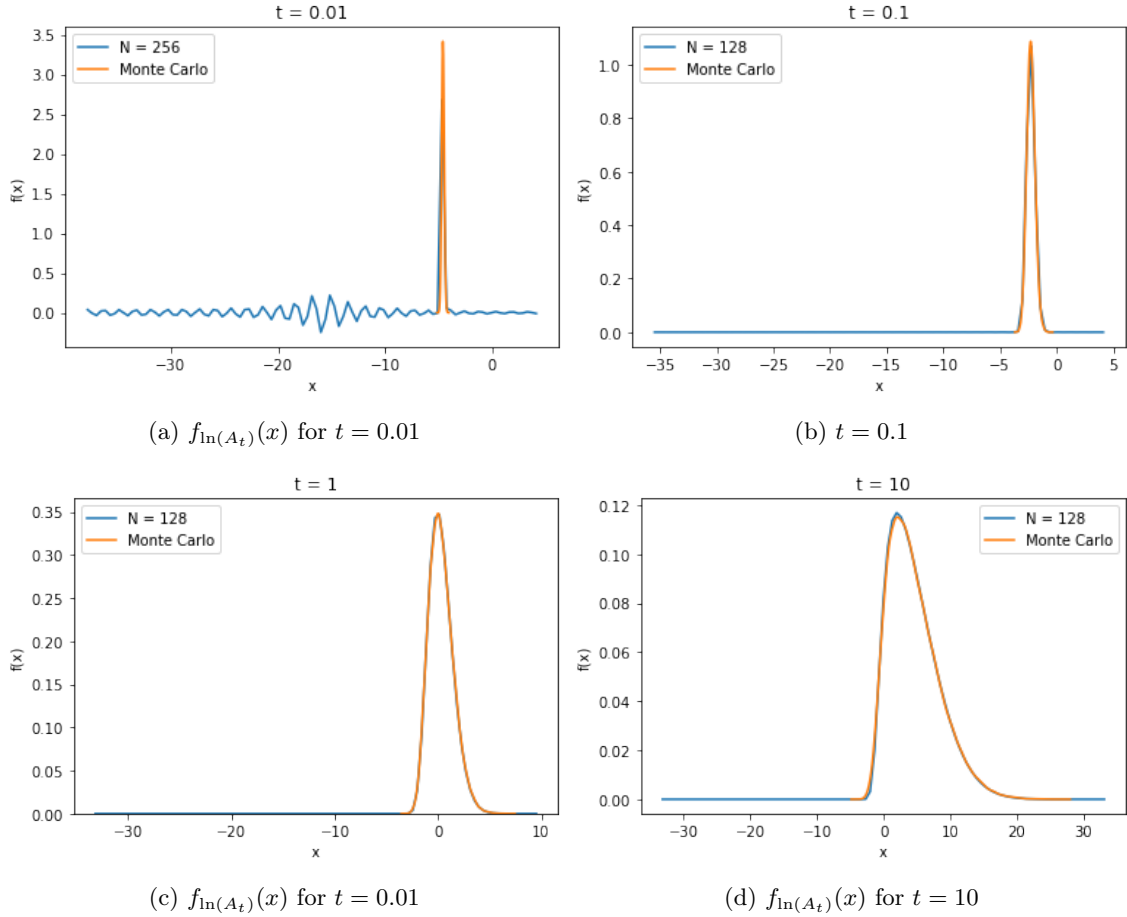


Figure 9: PDF of $\ln(A_t)$ compared to Monte Carlo Simulation.

In Figure 7(a) we see that a lot of oscillation occurs for $t = 0.01$ around $x = -15$. This makes

sense if we look at how we recover the density function using the COS method:

$$f_X(x) = \sum_{k=0}^{\infty} F_k \cos\left(k\pi \frac{x-a}{b-a}\right) = \frac{1}{2}F_0 + \sum_{k=1}^{\infty} F_k \cos\left(k\pi \frac{x-a}{b-a}\right). \quad (4.68)$$

The errors in the computation of F_k , i.e. in the computation of the characteristic function, are multiplied by $\cos(k\pi \frac{x-a}{b-a})$. When $\frac{x-a}{b-a} \approx \frac{1}{2}$, $F_k \cos(k\pi \frac{x-a}{b-a}) \approx F_k$. A large computational error thus leads to a large error in the density function in that region. Note that

$$\frac{x-a}{b-a} \approx \frac{1}{2} \rightarrow x \approx \frac{1}{2}(b+a), \quad (4.69)$$

which coincides with Figure 9a. Setting a lower truncation range, for $t = 0.01$, this oscillation would actually not vanish. We will encounter the same for $\nu = 0$. One could try to use extremely many cosine expansion terms.

In Figure 5a, using $TOL_h = 10^{-14}$ showed a better recovery of the density function for $t = 0.01$. This difference in tolerance level already makes a large impact on the total computation of the characteristic function of $\Phi_{\ln(A_t)}(\omega)$. We come back to this in Section 5.2.

The CDF and PDF recovery of $\ln(A_t)$ has been checked due to error convergence in three dimensions. We draw a conclusion from the results in this section.

4.6 Conclusion

In this section we have derived the characteristic function of $\ln(A_t)$ based on Bougerol's identity. The CF was separable as a ratio of two characteristic functions which have been analysed separately. For $g(\omega)$ two computational methods were compared.

After truncating both functions correctly, via the COS method the density and CDF of $\ln(A_t)$ were recovered. As a rule of thumb for the truncation range, we used the minimum and maximum of the two truncation ranges for the lower bound and upper bound respectively of the marginal distributions. We obtained correct density recovery for the marginal distributions using this truncation range. It is very important to state that when we divide the two characteristic functions to obtain the CF of $\ln(A_t)$, computational errors do occur for small t . We come back to this in section 5.2.

First we showed that the use of the Gamma function gave the same errors with respect to Clenshaw-Curtis quadrature for the N for which convergence occurred, therefore we could continue the error analysis using the Gamma function for the computation of $g(\omega)$.

Based on Monte Carlo simulation, we performed an error analysis on the CDF based on number of quadrature points J_h , number of cosine expansion terms N and tolerance level TOL_h for x values that lie within the peak of the density.

Using optimal parameters based on this analysis, exponential convergence has been observed for each value of t for the CDF as well as the PDF. The obtained results are sufficient, but only for $t = 0.01$ we could not get rid of oscillation in the density function. Hence for $t = 0.01$, numerical errors occur in the computation of the characteristic function.

In the next section, we use the extension of Bougerol's identity with drift term $\nu \neq 0$ to compute the characteristic function of $\ln(A_t^\nu)$.

5 Bougerol's Identity With Drift

Just as in the previous section, we aim to recover the density of $\ln(A_t^\nu)$, now with $\nu \neq 0$, using cosine series expansion. We use the extended identity of Bougerol, developed by Alili and Gruet [17]. Recall that they state that the following identity holds:

$$\beta_{A_t^\nu} \stackrel{law}{=} (2\xi - 1)\phi\left(B_t^\nu, \sqrt{R_t^2 + (B_t^\nu)^2}\right), \quad (5.1)$$

where

- β_t follows a Brownian motion.
- $\xi \sim \text{Arcsine}(0, 1)$.
- R_t is a squared Bessel process starting at zero, which means that $R_t = \sqrt{W_1(t)^2 + W_2(t)^2}$, where $W_1(t)$ and $W_2(t)$ are independent Brownian motions starting at zero. Then

$$R_t^2 = W_1(t)^2 + W_2(t)^2 \stackrel{law}{=} (\sqrt{t}Z_1)^2 + (\sqrt{t}Z_2)^2 = t \cdot (Z_1^2 + Z_2^2) \sim t \cdot \chi^2, \quad (5.2)$$

which is the constant t times a Chi-squared distribution with two degrees of freedom. Furthermore $Z_1, Z_2 \sim N(0, 1)$ and $Z_1 \perp Z_2$.

- $B_t^\nu = \nu t + B_t$, where B_t is a Brownian motion. Hence $B_t^\nu \sim N(\nu t, t)$ and $\nu \in \mathbb{R}$.
- $\phi(a, b) = \sqrt{2e^a \cosh(b) - e^{2a} - 1}$, for $b \geq |a|$.
- ξ, R_t and B_t^ν are all independent random variables.

We start by deriving the characteristic function of $\ln(A_t^\nu)$. Afterwards we compute the CDF and PDF using cosine series expansion and perform convergence analysis on the CDF and PDF of $\ln(A_t^\nu)$ compared with Monte Carlo simulation for different values of (ν, T) . A parameter study will also be conducted.

5.1 Characteristic Function

Just as in Section 4.3, we compute the characteristic function of $\ln(A_t^\nu)$, now based on Bougerol's extended identity. The computation of the characteristic function of $\ln(A_t^\nu)$, with $\nu \neq 0$, is done as follows. By independence of Ξ , R_t and B_t^ν we have that

$$\beta_{A_t^\nu} \stackrel{\text{law}}{=} (2\Xi - 1)\phi\left(B_t^\nu, \sqrt{R_t^2 + (B_t^\nu)^2}\right) \leftrightarrow \quad (5.3)$$

$$\sqrt{A_t^\nu} \cdot Z \stackrel{\text{law}}{=} (2\Xi - 1)\phi\left(B_t^\nu, \sqrt{R_t^2 + (B_t^\nu)^2}\right) \leftrightarrow \quad (5.4)$$

$$A_t^\nu \cdot Z^2 \stackrel{\text{law}}{=} (2\Xi - 1)^2 \phi^2\left(B_t^\nu, \sqrt{R_t^2 + (B_t^\nu)^2}\right) \leftrightarrow \quad (5.5)$$

$$\ln(A_t^\nu) + \ln(Z^2) \stackrel{\text{law}}{=} \ln((2\Xi - 1)^2) + \ln\left(\phi^2\left(B_t^\nu, \sqrt{R_t^2 + (B_t^\nu)^2}\right)\right), \quad (5.6)$$

where $Z \sim N(0, 1)$. If two random variables are the same in law, then their characteristic function is the same. On the left side of (5.6) we have by independence of random variables:

$$\begin{aligned} \Phi(\omega) &= \mathbb{E}\left[\exp(i\omega(\ln(A_t^\nu) + \ln(Z^2)))\right] \\ &= \mathbb{E}\left[\exp(i\omega \ln(A_t^\nu)) \cdot \exp(i\omega \ln(Z^2))\right] \\ &= \mathbb{E}\left[\exp(i\omega \ln(A_t^\nu))\right] \cdot \mathbb{E}\left[\exp(i\omega \ln(Z^2))\right] \\ &= \Phi_{\ln(A_t^\nu)}(\omega) \cdot \Phi_{\ln(Z^2)}(\omega). \end{aligned} \quad (5.7)$$

And on the right side of (5.6) we find:

$$\begin{aligned} \Phi(\omega) &= \mathbb{E}\left[\exp\left(i\omega\left(\ln((2\Xi - 1)^2) + \ln\left(\phi^2\left(B_t^\nu, \sqrt{R_t^2 + (B_t^\nu)^2}\right)\right)\right)\right)\right] \\ &= \mathbb{E}\left[\exp(i\omega \ln((2\Xi - 1)^2))\right] \cdot \mathbb{E}\left[\exp(i\omega \ln\left[\phi^2\left(B_t^\nu, \sqrt{R_t^2 + (B_t^\nu)^2}\right)\right])\right] \\ &= \Phi_{\ln((2\Xi - 1)^2)}(\omega) \cdot \Phi_{\ln(\phi^2)}(\omega). \end{aligned} \quad (5.8)$$

Hence for the characteristic function of $\ln(A_t^\nu)$ we obtain the following formula:

$$\Phi_{\ln(A_t^\nu)}(\omega) = \frac{\Phi_{\ln((2\Xi - 1)^2)}(\omega) \cdot \Phi_{\ln(\phi^2)}(\omega)}{\Phi_{\ln(Z^2)}(\omega)} = \frac{k(\omega)l(\omega)}{g(\omega)}. \quad (5.9)$$

Opposed to Section 4.3, the characteristic function of $\ln(A_t^\nu)$ is now a combination of three characteristic functions. Each characteristic function will be evaluated separately again. The denominator in equation (5.9) has already been discussed in the previous chapter. The characteristic function $g(\omega)$ was computed by the Gamma function and by Clenshaw-Curtis quadrature.

For the computation of $k(\omega)$ two different quadrature rules will be compared, i.e. Clenshaw-Curtis quadrature and Chebyshev-Gauss quadrature. The first one is known to be more stable for oscillating functions, whereas Chebyshev-Gauss quadrature has a lower operational complexity. Lastly, the characteristic function $l(\omega)$ will be computed using Clenshaw-Curtis quadrature.

We start with the computation of $k(\omega)$ in the next subsection.

5.1.1 Arcsine Distribution

We start with the distribution of $\Xi \sim \text{Arcsine}(0, 1)$. We will use two different methods to compute the characteristic function of $k(\omega) = \Phi_{\ln(2\Xi - 1)^2}(\omega)$, each with a different numerical integration method.

5.1.1.1 Method 1

Let $\Xi \sim \text{Arcsine}(0, 1)$, then $2\Xi - 1 \sim \text{Arcsine}(-1, 1)$ and $(2\Xi - 1)^2 \sim \text{Arcsine}(0, 1) \stackrel{\text{law}}{=} \Xi$. First we compute the PDF of $Z = \ln(\Xi)$ based on the PDF of Ξ , which is given by

$$f_\Xi(\xi) = \frac{1}{\pi\sqrt{\xi(1-\xi)}}, \quad \xi \in [0, 1]. \quad (5.10)$$

Let $Z = g(\Xi) = \ln(\Xi)$. Then $Z \in (-\infty, 0)$ and since $g(\xi) = \ln(\xi)$ is strictly increasing for $\xi \in (0, 1]$ and $P(\Xi = 0) = 0$, the PDF of Z is given by

$$\begin{aligned} f_Z(z) &= f_\Xi(g^{-1}(z)) \frac{dg^{-1}(z)}{dz} \\ &= \frac{1}{\pi \sqrt{e^z(1-e^z)}} \cdot \frac{de^z}{dz} \\ &= \frac{e^z}{\pi \sqrt{e^z(1-e^z)}}, \quad z \in (-\infty, 0]. \end{aligned} \quad (5.11)$$

The characteristic function $k(\omega)$ is thus given by

$$k(\omega) = \int_{-\infty}^0 e^{i\omega z} \frac{e^z}{\pi \sqrt{e^z(1-e^z)}} dz \quad (5.12)$$

We seek for a truncation range $[a, 0]$ such that $\int_a^0 f(z) \geq 1 - TOL_k$. Note that for negative a :

$$0 < \int_{-\infty}^a \frac{e^z}{\pi \sqrt{e^z(1-e^z)}} = \frac{2}{\pi} \arcsin(\sqrt{e^z}) \Big|_{-\infty}^a = \frac{2}{\pi} \arcsin(\sqrt{e^a}). \quad (5.13)$$

In order to obtain that

$$\int_{-\infty}^a \frac{e^z}{\pi \sqrt{e^z(1-e^z)}} < \frac{1}{2} TOL_k, \quad (5.14)$$

we must have for the lower bound a that

$$\int_{-\infty}^a \frac{e^z}{\pi \sqrt{e^z(1-e^z)}} \leq \frac{1}{2} TOL_k \leftrightarrow \quad (5.15)$$

$$\frac{2}{\pi} \arcsin(\sqrt{e^a}) \leq \frac{1}{2} TOL_k \leftrightarrow \quad (5.16)$$

$$\sqrt{e^a} \leq \sin\left(\frac{1}{4} \pi TOL_k\right) \leftrightarrow \quad (5.17)$$

$$a \leq \ln\left(\sin^2\left(\frac{1}{4} \pi TOL_k\right)\right). \quad (5.18)$$

We also determine an upper bound which we have to use for numerical integration later to avoid numerical issues. For $b < 0$ we compute:

$$0 < \int_b^0 \frac{e^z}{\pi \sqrt{e^z(1-e^z)}} = \frac{2}{\pi} \arcsin(\sqrt{e^z}) \Big|_b^0 = \frac{2}{\pi} \left(\frac{\pi}{2} - \arcsin(\sqrt{e^b})\right) \leq \frac{1}{2} TOL_k. \quad (5.19)$$

Solving this equation for b gives us

$$1 - \frac{2}{\pi} \arcsin(\sqrt{e^b}) \leq \frac{1}{2} TOL_k \leftrightarrow \quad (5.20)$$

$$\arcsin(\sqrt{e^b}) \geq \frac{\pi}{2} - \frac{\pi}{4} TOL_k \leftrightarrow \quad (5.21)$$

$$\sqrt{e^b} \geq \sin\left(\frac{\pi}{2} - \frac{\pi}{4} TOL_k\right) \leftrightarrow \quad (5.22)$$

$$b \geq \ln\left(\sin^2\left(\frac{\pi}{2} - \frac{\pi}{4} TOL_k\right)\right). \quad (5.23)$$

Hence we use

$$[a, b] = \left[\ln\left(\sin^2\left(\frac{1}{4} \pi TOL_k\right)\right), \ln\left(\sin^2\left(\frac{1}{2} \pi - \frac{1}{4} \pi TOL_k\right)\right) \right] \quad (5.24)$$

as truncation range to compute $k(\omega)$ with Clenshaw-Curtis quadrature. The operational complexity of Clenshaw-Curtis quadrature is $O(J \log(J))$ for J quadrature points.

Note that we have $z < 0$ and as $z \uparrow 0$, $f_Z(z) \rightarrow \infty$. This will lead to numerical errors in the computation of the characteristic function, which will be magnified by multiplying and dividing by $l(\omega)$ and $g(\omega)$. We will come back to this in Section 5.2.

To handle this issue, we need to perform a change of variable. Note that the two boundaries a and b are both smaller than zero. We wish to scale z to the *log* domain, but we need first we mirror the density of Z in $y = 0$. Then the following holds for $Z = \ln(U)$:

$$\int_a^b f_Z(z) dz = \int_{-b}^{-a} f_Z(-z) dz = \int_{\ln(-b)}^{\ln(-a)} f_Z(-e^u) e^u du \geq 1 - \text{TOL}_k. \quad (5.25)$$

The new boundaries for the numerical integration of $k(\omega)$ are thus given by:

$$[a_1, b_1] = \left[\ln \left[-\ln \left(\sin^2 \left(\frac{1}{4} \pi \text{TOL}_k \right) \right) \right], \ln \left[-\ln \left(\sin^2 \left(\frac{1}{2} \pi - \frac{1}{4} \pi \text{TOL}_k \right) \right) \right] \right]. \quad (5.26)$$

The density functions of Z and U are shown in Figure 10 using $[a, b]$ and $[a_1, b_1]$ with $\text{TOL} = 10^{-7}$, which is the minimal level of tolerance for which the computation of the boundaries is possible. For the density of $Z = \ln(\Xi)$, we use a *log*-scale on the y -axis.

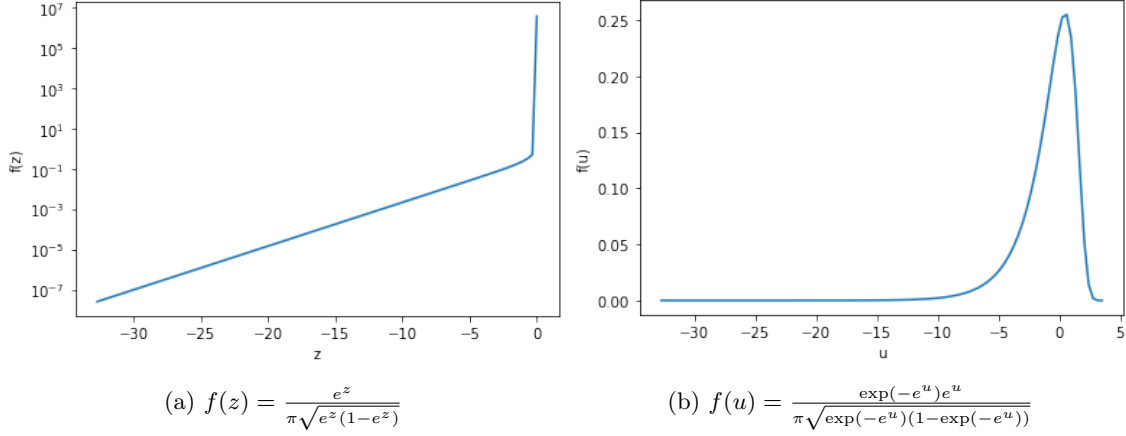


Figure 10: Exact PDF

The characteristic function we compute using Clenshaw-Curtis quadrature is thus given by

$$k(\omega) = \int_{a_1}^{b_1} e^{-i\omega e^u} f(u) du, \quad (5.27)$$

with $f(u)$ given as in Figure 10b and $[a_1, b_1]$ as in (5.26). In the second method, we will use a different quadrature rule, for which no boundaries have to be computed.

5.1.1.2 Method 2

In this method, we make use of Chebyshev-Gauss quadrature. For the computation of $k(\omega)$ using this numerical integration method, we use a different variation of the Arcsine distribution. As we already stated, if $\Xi \sim \text{Arcsine}(0, 1)$, then $2\Xi - 1 \sim \text{Arcsine}(-1, 1)$. Instead of using the distribution of the *log* of Ξ , we can also use the distribution of $Z = (2\Xi - 1) \sim \text{Arcsine}(-1, 1)$. The PDF of Z is given by:

$$f(z) = \frac{1}{\pi \sqrt{(z+1)(1-z)}}, \quad z \in [-1, 1]. \quad (5.28)$$

Then we compute the characteristic function directly:

$$\begin{aligned}
k(\omega) &= \mathbb{E}[\exp(i\omega \ln(z^2))] \\
&= \int_{-1}^1 e^{i\omega \ln(z^2)} \frac{1}{\pi \sqrt{(z+1)(1-z)}} dz \\
&= \int_{-1}^1 e^{i\omega \ln(z^2)} \frac{1}{\pi \sqrt{1-z^2}} dz.
\end{aligned} \tag{5.29}$$

This is exactly the type of integral computed with Chebyshev-Gauss quadrature, which evaluates integrals of the form

$$\int_{-1}^1 \frac{f(x)}{\sqrt{1-x^2}} dx. \tag{5.30}$$

Therefore the characteristic function can also be computed as

$$\begin{aligned}
\Phi_{\ln(2\xi-1)^2}(\omega) &= \int_{-1}^1 e^{i\omega \ln(z^2)} \frac{1}{\pi \sqrt{1-z^2}} \\
&= \frac{f(z)}{\sqrt{1-z^2}} \\
&= \sum_{j=1}^n w_j f(z_j)
\end{aligned} \tag{5.31}$$

where

$$w_j = \frac{\pi}{n}, \tag{5.32}$$

$$z_j = \cos\left(\frac{2j-1}{2n}\pi\right), \tag{5.33}$$

$$f(z_j) = e^{i\omega \ln(z_j^2)}. \tag{5.34}$$

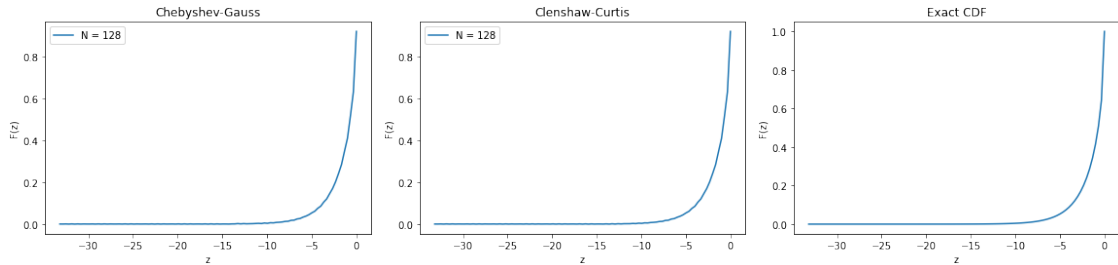
Using a vector-vector multiplication for the computation of $k(\omega)$, the operational complexity using Chebyshev-Gauss quadrature is $O(n)$, which is less than using Clenshaw-Curtis quadrature.

Note that we do not need to perform a change of variable using Chebyshev-Gauss quadrature. Even though $\frac{1}{\sqrt{1-z^2}} \rightarrow \infty$ as $|z| \rightarrow 1$, this expression is not used in the calculation of $k(\omega)$.

We show the CDF recovery using cosine series expansion using both integration methods, and compare it with the exact CDF. Note that the CDF of Z is given by

$$F(z) = \int_{-\infty}^z f_Z(u) du = \int_{-\infty}^z \frac{e^u}{\pi \sqrt{e^u(1-e^u)}} du = \frac{2}{\pi} \arcsin(\sqrt{e^u}) \Big|_{-\infty}^z = \frac{2}{\pi} \arcsin(\sqrt{e^z}). \tag{5.35}$$

For Clenshaw-Curtis quadrature, no change of variable is performed here, which is important to note as we come back to this in section 5.2. We set $J_k = 1500$ quadrature points and $m = 100$ different points on the z -axis. We use the truncation range $[a, b] = [-33, 0]$, with $N = 128$ cosine expansion terms. The results are shown in Figure 11.



(a) $F(z)$ using Chebyshev-Gauss (b) $F(z)$ using Clenshaw-Curtis (c) $F(z)$ exact

Figure 11: CDF recovery of $Z = \ln(\Xi)$, $\Xi \sim \text{Arcsine}(0, 1)$, using $N = 128$ cosine terms.

We will analyse the difference between the two numerical integration methods for the CDF recovery of $\ln(A_t^\nu)$ in section 5.5 via an error analysis.

Two of the three characteristic functions for the computation of $\Phi_{\ln(A_t^\nu)}(\omega)$ have been discussed. Lastly, we need to determine the characteristic function $l(\omega)$ as in (5.9).

5.1.2 Distribution of $W = \ln(\phi^2(X, Y))$

In this section we compute the third characteristic function. Recall that the characteristic function of $\ln(A_t^\nu)$ is given by

$$\Phi_{\ln(A_t^\nu)}(\omega) = \frac{\Phi_{\ln((2E-1)^2)}(\omega) \cdot \Phi_{\ln(\phi^2)}(\omega)}{\Phi_{\ln(Z^2)}(\omega)} = \frac{k(\omega)l(\omega)}{g(\omega)}. \quad (5.36)$$

What is left is to determine the characteristic function $l(\omega)$ of $W = g(X, Y) = \ln(\phi^2(X, Y))$, with

$$\phi(a, b) = \sqrt{2e^a \cosh(b) - e^{2a} - 1}, \quad b \geq |a|. \quad (5.37)$$

Note that

- $X = B_t^\nu \sim N(\nu t, t)$, which PDF is given by $f(x) = \frac{1}{\sqrt{2\pi t}} e^{-\frac{1}{2}\left(\frac{x-\nu t}{\sqrt{t}}\right)^2}$, $x \in (-\infty, \infty)$.
- $Y = R_t^2 \sim t \cdot \chi_2^2$, which PDF is given by $f(y) = \frac{1}{2t} e^{-\frac{y}{2t}}$, $y \in [0, \infty)$.

For the characteristic function $l(\omega)$ of W we find that

$$\begin{aligned} \Phi_W(\omega) &= \mathbb{E} \left[\exp(i\omega \ln \left[\phi^2 \left(B_t^\nu, \sqrt{R_t^2 + (B_t^\nu)^2} \right) \right]) \right] \\ &= \mathbb{E} \left[\exp(i\omega \ln \left[\phi^2 \left(x, \sqrt{y + x^2} \right) \right]) \right] \\ &= \mathbb{E} \left[\exp(i\omega \ln \left(2e^x \cosh(\sqrt{y + x^2}) - e^{2x} - 1 \right)) \right] \\ &= \int_{-\infty}^{\infty} \int_0^{\infty} \exp \left[i\omega \ln \left(2e^x \cosh(\sqrt{y + x^2}) - e^{2x} - 1 \right) \right] \\ &\quad \cdot \frac{1}{2t} e^{-\frac{y}{2t}} \cdot \frac{1}{\sqrt{2\pi t}} e^{-\frac{1}{2}\left(\frac{x-\nu t}{\sqrt{t}}\right)^2} dy dx. \end{aligned} \quad (5.38)$$

We need to truncate both integrals properly for the numerical computation. Note that by independence of X and Y , we have that for

$$0 < \frac{1}{2t} e^{-\frac{y}{2t}} \cdot \frac{1}{\sqrt{2\pi t}} e^{-\frac{1}{2}\left(\frac{x-\nu t}{\sqrt{t}}\right)^2}, \quad (5.39)$$

$$\int \int \frac{1}{2t} e^{-\frac{y}{2t}} \cdot \frac{1}{\sqrt{2\pi t}} e^{-\frac{1}{2}\left(\frac{x-\nu t}{\sqrt{t}}\right)^2} dy dx = \int \frac{1}{\sqrt{2\pi t}} e^{-\frac{1}{2}\left(\frac{x-\nu t}{\sqrt{t}}\right)^2} dx \cdot \int \frac{1}{2t} e^{-\frac{y}{2t}} dy. \quad (5.40)$$

For $Y \sim t \cdot \chi_2^2$, we seek boundaries such that $\int_a^b f(y) dy \geq 1 - TOL_y$. For the upper bound we have that:

$$\int_b^{\infty} \frac{1}{2t} e^{-\frac{y}{2t}} dy = -e^{-\frac{y}{2t}} \Big|_b^{\infty} = e^{-\frac{b}{2t}} \leq \frac{1}{2} TOL_y \leftrightarrow \quad (5.41)$$

$$-\frac{b}{2t} < \ln\left(\frac{1}{2} TOL_y\right) \leftrightarrow \quad (5.42)$$

$$b \geq -2t \ln\left(\frac{1}{2} TOL_y\right). \quad (5.43)$$

Since numerical integration at $y = 0$ can give rise to problems, we also seek for a proper lower bound:

$$\int_0^a \frac{1}{2t} e^{-\frac{y}{2t}} dy = -e^{-\frac{y}{2t}} \Big|_0^a = 1 - e^{-\frac{a}{2t}} \leq \frac{1}{2} TOL_y \leftrightarrow \quad (5.44)$$

$$-\frac{a}{2t} \geq \ln\left(1 - \frac{1}{2}TOL_y\right) \leftrightarrow \quad (5.45)$$

$$a \leq -2t \ln\left(1 - \frac{1}{2}TOL_y\right). \quad (5.46)$$

Hence, we choose the following truncation range for y :

$$[y_{\min}(t), y_{\max}(t)] = \left[-2t \ln\left(1 - \frac{1}{2}TOL_y\right), -2t \ln\left(\frac{1}{2}TOL_y\right)\right]. \quad (5.47)$$

Lastly we need a truncation range for X . The Brownian motion with drift B_t^ν is normally distributed with mean νt and variance t . Hence we seek for the correct truncation range for the lower bound the following:

$$\int_{-\infty}^a \frac{1}{\sqrt{2\pi t}} e^{-\frac{1}{2}\left(\frac{x-\nu t}{\sqrt{t}}\right)^2} dx \leq \frac{1}{2}TOL_x \leftrightarrow \quad (5.48)$$

$$\Phi\left(\frac{a - \nu t}{\sqrt{t}}\right) \leq \frac{1}{2}TOL_x \leftrightarrow \quad (5.49)$$

$$a \leq \nu t + \sqrt{t}\Phi^{-1}\left(\frac{1}{2}TOL_x\right). \quad (5.50)$$

And for the upper bound we have:

$$\int_b^{\infty} \frac{1}{\sqrt{2\pi t}} e^{-\frac{1}{2}\left(\frac{x-\nu t}{\sqrt{t}}\right)^2} dx \leq \frac{1}{2}TOL_x \leftrightarrow \quad (5.51)$$

$$1 - \Phi\left(\frac{b - \nu t}{\sqrt{t}}\right) \leq \frac{1}{2}TOL_x \leftrightarrow \quad (5.52)$$

$$\Phi\left(\frac{b - \nu t}{\sqrt{t}}\right) > 1 - \frac{1}{2}TOL_x \leftrightarrow \quad (5.53)$$

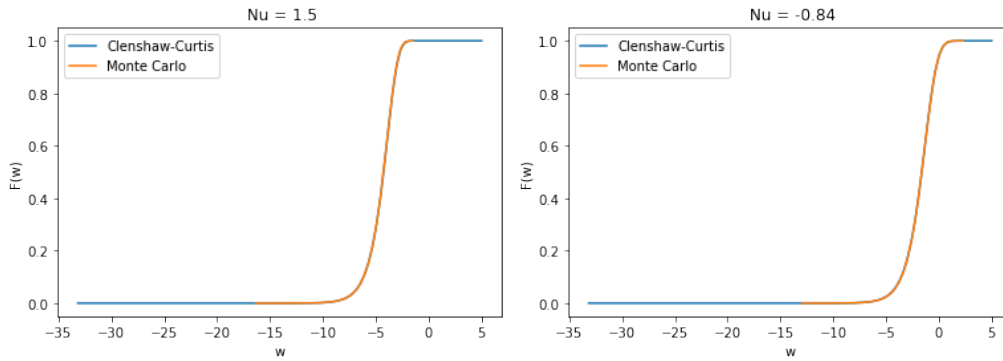
$$b \geq \nu t + \sqrt{t}\Phi^{-1}\left(1 - \frac{1}{2}TOL_x\right), \quad (5.54)$$

which gives us the following truncation range for X :

$$[x_{\min}(t), x_{\max}(t)] = \left[\nu t + \sqrt{t}\Phi^{-1}\left(\frac{1}{2}TOL_x\right), \nu t + \sqrt{t}\Phi^{-1}\left(1 - \frac{1}{2}TOL_x\right)\right]. \quad (5.55)$$

We use 2-dimensional Clenshaw-Curtis quadrature to compute $l(\omega) = \Phi_W(\omega)$, which takes $O(J \log(J))$ operations for each variable. The total operational complexity is therefore $O(2J \log(J))$.

In Figure 12, the CDF recovery via cosine series expansion is shown. We set $T = 1$, use $J_l = 500$ quadrature points and use $N = 512$ cosine expansion terms. We set $\mu = 0.05$ and vary $\sigma \in \{0.2, 0.8\}$, which results in $\nu \in \{1.5, -0.84\}$. We set the truncation as $[-33, 6]$ and compare the CDF recovery with Monte Carlo simulation.



(a) $F(w)$ for $T = 1$, $\nu > 0$.

(b) $F(w)$ for $T = 1$, $\nu < 0$.

Figure 12: CDF recovery of $W = \ln(\phi^2(X, Y))$ compared with Monte Carlo simulation.

We observe that we can recovery the CDF properly using the proposed numerical integration method However, as for the Arcsine distribution, we encountered numerical issues using this proposed integration method for the CDF and PDF recovery of $\ln(A_t^\nu)$, which will be shown in Section 5.2.

The problem can be observed if we focus on Y : when we take $T = 1$ (often seen for Asian option pricing) and $\sigma \in [0.05, 1]$, the value of t becomes very small, since $t = \frac{\sigma^2}{4}T$ by the scaling property in (3.32). Looking at the density function of Y , one can immediately see that the value of $f_Y(y) = e^{-\frac{y}{2t}}$ gets very close to zero very fast. To encounter this issue, we perform a change of variable again to increase in the width of the density of Y by setting $z = \ln(y)$, and the characteristic function of W is then given by

$$\Phi_W(\omega) = \int_{-\infty}^{\infty} \int_{-\infty}^{\infty} \exp \left[i\omega \ln \left[2e^x \cosh \left(\sqrt{e^z + x^2} \right) - e^{2x} - 1 \right] \right] \frac{1}{2t} e^{-\frac{1}{2t}e^z} e^z f_X(x) dz dx. \quad (5.56)$$

The only thing left is to change the boundaries for the numerical integration. We seek $[z_1, z_2]$ such that $\int_{z_1}^{z_2} \frac{1}{2t} e^{-\frac{1}{2}e^z} e^z dz \geq 1 - \text{TOL}_y$. To solve this equation, we can use the boundaries computed in equation (5.47), by deriving for $y_{\min}(t), y_{\max}(t) > 0$:

$$\int_{y_{\min}(t)}^{y_{\max}(t)} f_Y(y) dy = \int_{\ln(y_{\min}(t))}^{\ln(y_{\max}(t))} f_Y(e^z) e^z dz = \int_{z_1(t)}^{z_2(t)} f_{\ln(Y)}(z) dz \geq 1 - \text{TOL}_y. \quad (5.57)$$

Hence, the boundaries for the numerical integration after a change of variable for the computation of Y are given by

$$[z_1(t), z_2(t)] = \left[\ln \left(-2t \ln \left(1 - \frac{1}{2} \text{TOL}_y \right) \right), \ln \left(-2t \ln \left(\frac{1}{2} \text{TOL}_y \right) \right) \right]. \quad (5.58)$$

In Figure 13 the density function of Y are shown, with and without change of variable for $(\sigma, T) = (0.2, 1)$, with $\text{TOL}_y = 10^{-12}$, which is the minimal level of tolerance possible to avoid a computation of $\ln(0)$ in Python, where the functions are plotted on their truncation ranges as in (5.47) and (5.58). In Figure 13a it is shown a *log*-scale to show the rapid decay, which of course results in a straight line.

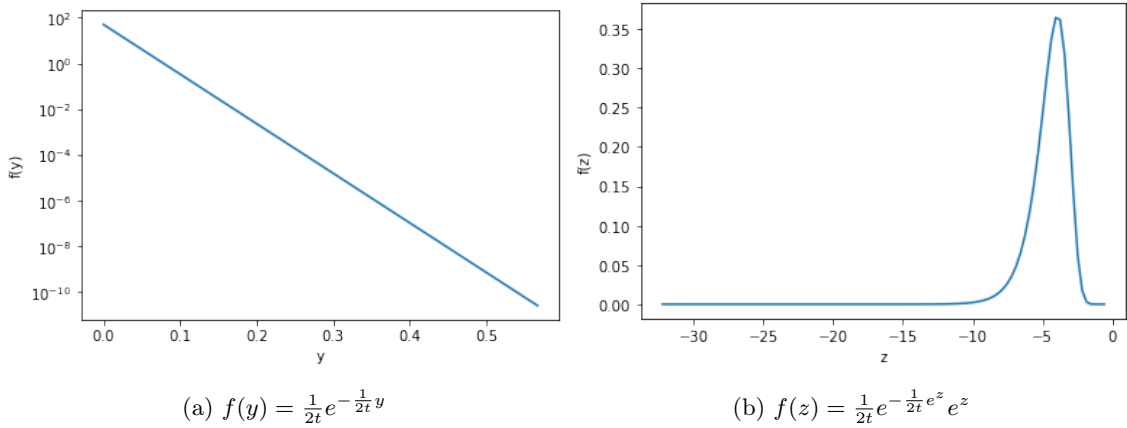


Figure 13: Exact PDF

Remark 5.1. In earlier experiments, to decrease the rapid decay of Y , we inserted the variable t within the exponent, leading to

$$\Phi_W(\omega) = \int_{-\infty}^{\infty} \int_0^{\infty} \exp \left[i\omega \ln \left[2e^x \cosh \left(\sqrt{ty + x^2} \right) - e^{2x} - 1 \right] \right] \frac{1}{2} e^{-\frac{1}{2}y} f_X(x) dy dx, \quad (5.59)$$

which was already a good adjustment. But taking the change of variable $y = \ln(z)$, we get better results.

Remark 5.2. The distribution of $X = B_t^\nu$ has a variance \sqrt{t} . Hence, the peak of the density around $x = \nu t$ is very narrow. We performed a change of variable with $X = N(\nu t, t) \stackrel{law}{=} \frac{1}{a}\sqrt{t}N(a\nu\sqrt{t}, a^2)$ to increase the variance (with $a \in \mathbb{N}$), leading to

$$\Phi_W(\omega) = \int_{-\infty}^{\infty} \int_0^{\infty} \exp \left[i\omega \ln \left[2e^{\sqrt{t}x} \cosh \left(\sqrt{ty + \frac{t}{a^2}x^2} \right) - e^{2\sqrt{t}x} - 1 \right] \right] \frac{1}{2} e^{-\frac{1}{2}y} \frac{1}{\sqrt{2\pi}} e^{-\frac{1}{2}\left(\frac{x-\nu\sqrt{t}}{\sqrt{a}}\right)^2} dy dx, \quad (5.60)$$

which led to better results for the recovery of the density function. But after the change of variable for Y and the Arcsine distribution to the *log* domain, this did not lead to better results either. Also changing X to the *log* domain did not lead to better results. We will see that for certain small values of $\sigma^2 T = 4t$, the oscillation in the density function does not vanish, just as for $\nu = 0$.

In the next subsection, we show the importance of these changes of variables.

5.2 Numerical Integration Errors

We have determined how we compute each characteristic function. We then only need to establish the truncation range for the COS method, which will be done in Section 5.4.2 to compute the characteristic function of $\ln(A_t^\nu)$.

Before we continue our computation, we first elaborate on the importance of the numerical integration and the behaviour of our computation based on certain parameter settings. Since we compute the characteristic function of $\ln(A_t^\nu)$ via computation via multiple different characteristic functions, the computation is very sensitive to errors in each characteristic function.

5.2.1 Change of Variables

In Figure 3c we recovered the PDF of $\ln(Z^2)$ properly using cosine series expansion. In Figure 11c we have shown the CDF recovery of the Arcsine distribution, and in Figure 12 the CDF recovery of W was shown, using no change of variable. We conclude from this that each characteristic function is computed properly in the sense for its own CDF or PDF recovery. We did not show this, but also for each CF, $|\Phi(\cdot)| \leq 1$ was satisfied. The errors in the coefficients seem to be small enough using the numerical integration we proposed.

But combining all three characteristic function for the characteristic function of $\ln(A_t^\nu)$ leads to large numerical errors. Note that for the computation of $\Phi_{\ln(A_t^\nu)}(\omega)$, the characteristic function of $X = \ln(Z^2)$, $Z \sim N(0, 1)$ is in the denominator, of which the absolute value becomes very small. This means that the errors in the nominator are being magnified, which has a large effect on the overall error of the computation of the characteristic function of $\ln(A_t^\nu)$.

For example, when we look at $\nu = 0$, we observed in section 4.3, due to the decay of the Gamma function, errors would become extremely large in the computation for $\Phi_{\ln(A_t)}(\omega)$. We used a wide truncation range, therefore the numerical errors would appear after larger values of N using Γ . In the next section we will use a different truncation, which is a new defined truncation range based on [6] and [7] (5.71), which also works for $\nu = 0$ for option pricing. But using the Gamma function becomes inefficient for large values of N , as we have seen that Gamma becomes very small after $N = \frac{19(b-a)}{\omega}$. We will verify this in section 5.5.4.

Now we go back to $\nu \neq 0$, to show the importance of the change of variables made. This is especially important for small values of t (due to the χ_2^2 distribution), which are used in Asian option pricing. We plot the CDF of $\ln(A_t^\nu)$ for $T = 1$ using the integration methods with and without change of variable to the *log* domain. We use Clenshaw-Curtis quadrature with $J = 1000$ for each distribution. We set $(\mu, \sigma, T) = (0.05, 0.4, 1)$ and use $N = 128$ cosine expansion terms. The truncation range is set as in (5.71).

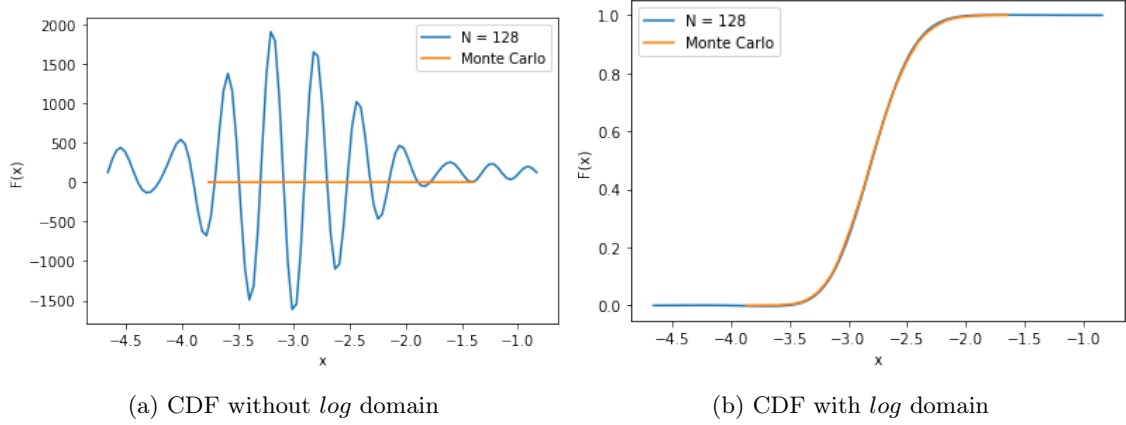


Figure 14: Difference in CDF recovery due to change of variables

It is observed that making no use of change of variable, the values of $F(x)$ get extremely large and small.

It can actually be shown that the change of variable for Y is the most important, but also applying a change of variable to the Arcsine distribution led to better results option pricing.

In the next subsection, we also make a note on the sensitivity of parameters, due to the fact that we use multiple separate characteristic functions in our computation.

5.2.2 Sensitivity to Parameters

We focus now on $\nu = 0$. Our computation is very sensitive to the parameters due to our division of two characteristic functions, which we will show by counterexamples. We show here by example the sensitivity of the level of tolerance used and number of quadrature points. Intuition would be that an increase in TOL for numerical integration should lead to an increase in the errors and an increase in quadrature points should lead to a decrease in errors. We show by counterexample that this does not hold. We use as benchmark that

$$|\Phi_{\ln(A_t^r)}(\omega)| = \left| \frac{h(\omega)}{g(\omega)} \right| \leq 1. \quad (5.61)$$

We use the numerical integration technique proposed as in Section 4.3 for $t = 0.01$. In Figure 15a the parameters are set as $(J_h, J_g, TOL_h, TOL_g) = (1000, 1000, 15, 15)$. Then we reduce the number of quadrature points for $g(\omega)$ using Clenshaw-Curtis quadrature. We see an increase of accuracy around $\omega = 20$ and a decrease of accuracy around $\omega = 70$. In Figure 15c, the tolerance level of h is increased from 10^{-15} to 10^{-9} . As $h(\omega)$ is in the nominator, this should lead to a large increase in errors in the characteristic function, but the values have actually improved. This can be concluded since the absolute value of the characteristic function does not get greater than 1 for a larger number of ω .

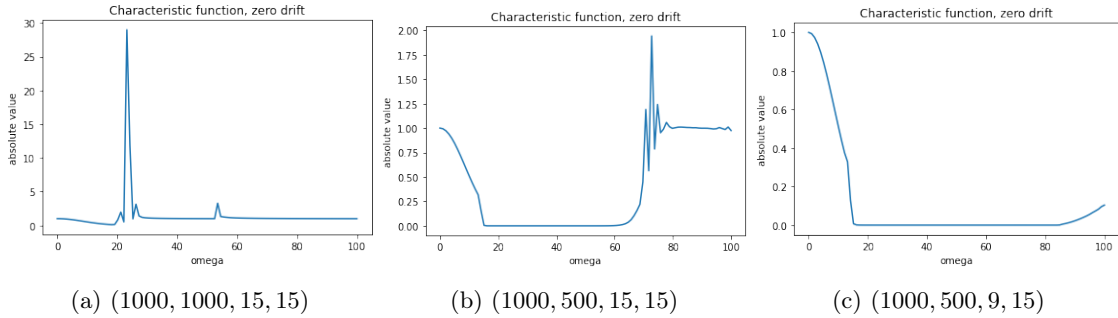


Figure 15: $|\Phi(\cdot)|$ due to tolerance levels and quadrature points.

That is why for the computation of the characteristic function of $\ln(A_t^\nu)$ using our method based on Bougerol's identity, every parameter regarding the numerical integration should be evaluated. For $\nu = 0$ we have done this in the previous section for $h(\omega)$. For $\nu \neq 0$ we will do this via error analysis again. The tolerance levels for the separate characteristic functions will be analyzed in Section 6, when we price Asian options.

In Section 5.3 we first elaborate more on the different parameters appearing in A_t^ν .

5.3 Parameter Evaluation

In order to have a good analysis of the density function and CDF of $\ln(A_t^\nu)$ we need to comprehend the behaviour depending on different parameter values. Recall that T is the maturity time, μ is the risk-free rate and σ is the volatility. By the scaling property, which is shown in Section 3.1.2, ν and t are given by

$$\nu = \nu(\mu, \sigma) = \frac{2\mu}{\sigma^2} - 1 \quad (5.62)$$

$$t = t(\sigma, T) = \frac{\sigma^2}{4}T. \quad (5.63)$$

Recall that our variable of interest A_t^ν is given by

$$A_t^\nu = \int_0^t e^{2\nu s + B_s} ds = \int_0^t f(s) ds. \quad (5.64)$$

Since Brownian motion is continuous, we have that $f(s) = e^{2(\nu s + B_s)}$ is continuous, therefore we can state the following:

$$\frac{d}{dt} A_t^\nu = \frac{d}{dt} \int_0^t e^{2(\nu s + B_s)} ds = e^{2(\nu t + B_t)}. \quad (5.65)$$

The change in distribution of A_t^ν and therefore $\ln(A_t^\nu)$ regarding t is very large. Also regarding the change of time, the parameter ν is of great importance. Especially when $\nu > 0$, from (5.64) and (5.65) we can immediately see that the values of A_t^ν become very large as t increases.

To really appreciate every parameter in $\ln(A_t^\nu)$, we state the following. Since $x \rightarrow \ln(x)$ is strictly increasing for $x > 0$:

- $\ln(A_t^\nu)$ is strictly increasing in t , and therefore in T . Note that for Asian option pricing, T is given in years.
- $\ln(A_t^\nu)$ is strictly increasing in ν , and therefore in μ . Note that μ only determines the mean of the normal distribution X in $W = \ln(\phi^2(X, Y))$.
- The difficulty lies in the volatility σ . Clearly ν is decreasing in σ , whereas t is increasing in σ . We make three plots of the value of $\ln(A_t^\nu)$. We set $\mu = 0.05$ and simulate the value of $\ln(A_t^\nu)$ using Monte Carlo simulation for different maturity times, $T \in \{1, 10, 100\}$. We compute the value of $\ln(A_t^\nu)$ for 30 values of the volatility between $[0.1, \dots, 1]$. If $\sigma > 0.32$, then $\nu < 0$. The results are shown in the Figure 16.

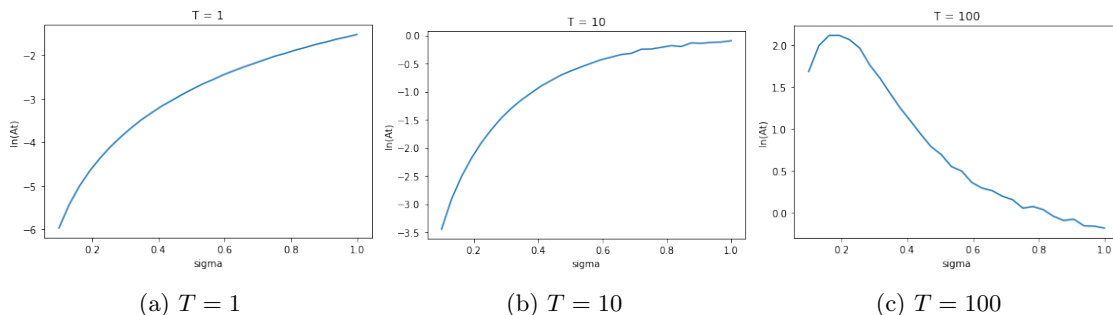


Figure 16: Increase and decrease of $\ln(A_t)$ with respect to σ for various T .

Note that ν is decreasing in each subplot of Figure 16, but in Figure 16a and 16b the value of $\ln(A_t^\nu)$ is still increasing due to the increase of t . On the other hand, in Figure 16c we see that for $T = 100$, when σ gets larger and ν becomes negative, the value of $\ln(A_t)$ decreases, even though t increases.

We examine the three components of which the distribution of $\ln(A_t^\nu)$ consists based on Bougerol's extended identity. Note that $Z = \ln(\Xi)$, $\Xi \sim \text{Arcsine}(0, 1)$ and $X = \ln(Z^2)$, with $Z \sim N(0, 1)$, both do not rely on μ, σ or T . Therefore, we analyze the distribution of $W = \ln(\phi^2(X, Y))$ as in section 5.1, still with $T \in \{1, 10, 100\}$. Since $\ln(A_t^\nu)$ is strictly increasing in μ , we set $\mu = 0.05$ as in Figure 16, and will only observe the changes in σ (therefore ν) and T .

We recover the density of $W = \ln(\phi^2(X, Y))$ via the COS method, applying no change of variable is performed. We use a 2-dimensional Clenshaw-Curtis quadrature, with $N = 512$ cosine expansion terms and $J_W = 500$ quadrature points, and set a wide truncation range. In Figure 17 the PDF of W for $\sigma \in \{0.2, 0.4, 0.6, 0.8\}$ and $T \in \{1, 10, 100\}$ are shown.

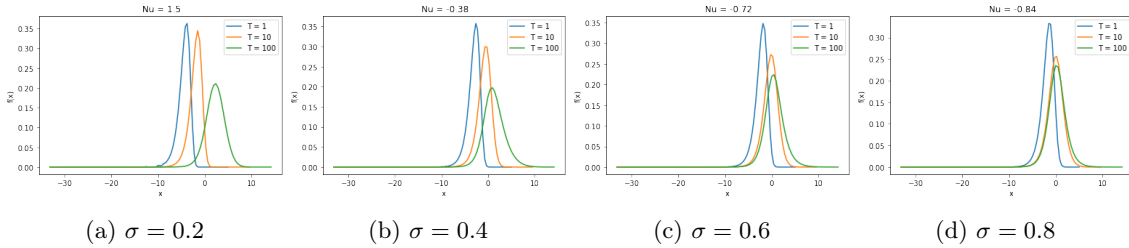


Figure 17: Density of W for various volatility values for multiple maturity times T via cosine series expansion.

We observe indeed the same behaviour as in Figure 16. For $T \in \{1, 10\}$, a decrease in ν leads to a wider peak in the density due to the change in time obtained by the change in σ , whereas for $T = 100$, the peak gets narrower as σ increases.

In the following subsection, we specify details regarding the numerical implementation.

5.4 Numerical Implementation

In this Section we choose which parameter values we wish to evaluate in the error analysis. Also, a new sufficient truncation range for the COS method will be determined. We start with the parameters based on the parameter study we have given.

5.4.1 Parameter Choice

We have a wide set of parameters we can choose from to perform an error analysis. Above we see that the relationship between σ and T defines the distribution of $\ln(A_t^\nu)$. In [8], it is stated that the most important parameter for the pricing of continuous Asian options is $\sigma^2 T = 4t$. As $\sigma^2 T \rightarrow 0$, Laplace transforms and other numerical methods do not converge. We obtain the same problems as $\sigma^2 T$ decreases using cosine series expansion. Therefore, we base our error analysis on this parameter.

We evaluate $\sigma^2 T \in \{0.05, 0.1, 0.5\}$, as large values lead to less computational complications and the interest lies for smaller values of $\sigma^2 T$. In the next Section, when we price Asian options, we will evaluate more values of $\sigma^2 T$. We set $\mu = 0.01$, which coincides with an average of the currently used yearly risk free rates by different banks. We also fix $T = 1$, opposed to the previous section, where different values of the parameter T (actually t , but there is a linear relationship due to the scaling property) were evaluated. The values of σ then become $\sigma \approx (0.21, 0.32, 0.70)$, which are reasonable values to evaluate. In [3], $\sigma \in \{0.8, 0.9, 1\}$ are even used, but these are not very commonly observed in the market. We will however use them as reference prices for the variable $\sigma^2 T$ in the next section. Note that setting T this small, the sign of ν is no longer of great importance. Since we choose the risk free rate to be of current annual value, the sign of ν will always be negative in our error analysis in Section 5.5. But as we said earlier, this defines the

mean of the normal distribution in W , which is yet multiplied by t . Since our aim is Asian option pricing, this is a good choice as the parameter setting for the error analysis.

For our derivation of the CDF and PDF of the distribution of $\ln(A_t^\nu)$ based on cosine series expansion, the two elements are the numerical integration technique and the truncation range. The numerical integration has been discussed and improved by a change of variable, now we need to set a proper truncation range for the COS method.

5.4.2 Truncation Range

In section 4.3, we proposed a truncation range based on the minima and maxima of the separate distributions. We chose a very wide truncation range in that section and could therefore make use of the Γ function for $N_t \in \{256, 128, 128, 128\}$.

For $\nu \neq 0$ we use a different truncation range, which is based on [6] and [7]. A proper truncation range for the COS method is given by:

$$[a, b] = \left[c_1 - L\sqrt{c_2 + \sqrt{c_4 + \sqrt{c_6}}}, \quad c_1 + L\sqrt{c_2 + \sqrt{c_4 + \sqrt{c_6}}} \right], \quad (5.66)$$

where $c_i, i \leq 1 \leq 6$ are the cumulants of the underlying distribution, and $L \in [6, 12]$ ($L \in \mathbb{N}$). It is also used with $c_6 = 0$, or $c_4 = c_6 = 0$. The use of these cumulants is determined by how fat the tails of the underlying distribution are. We stated already that we cannot determine the moments of $\ln(A_t)$, but we can use the moments of A_t^ν .

If $h(x)$ is the density function of A_t^ν , then a proper truncation range for $\ln(A_t^\nu)$ based on the moments of A_t^ν can be computed by:

$$\int_a^b h(x)dx = \int_{\ln(a)}^{\ln(b)} h(e^u)e^u du = \int_{\ln(a)}^{\ln(b)} h_{\ln(A_t^\nu)}(u)dx \geq 1 - \text{TOL}_{A_t^\nu} \quad (5.67)$$

We can compute $[a, b]$ for A_t^ν , and scale back to $[\ln(a), \ln(b)]$. The cumulants of A_t^ν are determined by the moments, which are given by [18]

$$\mathbb{E}[(A_t^\nu)^n] = 2^{-2n} n! \sum_{j=0}^n c_{j,n}^{(\nu)} \exp((2j^2 + 2j\nu)t), \quad (5.68)$$

where $c_{j,n}^{(\nu)}$ is given by

$$c_{j,n}^{(\nu)} = \left[\prod_{k=0, k \neq j}^n \frac{(\frac{\nu}{2} + j)^2}{2} - \frac{(\frac{\nu}{2} + k)^2}{2} \right]^{-1}. \quad (5.69)$$

Since $A_t^\nu > 0$, no problems occur for computing the upper bound $\ln(b)$. But even setting $c_4 = c_6 = 0$, computations of a for $\sigma \geq 0.2$ lead to $a < 0$ (of course also depending on T). We need a rule of thumb for the lower bound. First we estimate the expectation of $\ln(A_t^\nu)$ by

$$\mathbb{E}[\ln(A_t^\nu)] \approx \ln(\mathbb{E}[A_t^\nu]). \quad (5.70)$$

Note that the left side is always smaller by Jensen's inequality. Even though the right tale is fatter than the left tail, the distribution of $\ln(A_t^\nu)$ is close to symmetric, especially for small values of $\sigma^2 T$. Therefore we set as new rule of thumb for the truncation range $[A, B]$ for the COS method:

$$[A, B] = [\ln(\mathbb{E}[A_t^\nu]) - |\ln(\mathbb{E}[A_t^\nu]) - \ln(b)|, \ln(b)], \quad (5.71)$$

with b as in (5.66). We have done numerical testing on the option pricing using various values of L , and the use of c_4 and c_6 . Note that taking c_6 (and c_4) into account would require more cosine terms N . The use of c_6 is mostly preferable for fat-tailed distributions. It appeared that overall a good choice for the truncation range is set with $L = 8$, $c_6 = 0$, which is what we will use for our error analysis. We will come back to the truncation range in Section 6.

In the next Subsection we establish the benchmark for the error analysis, which is conducted in Section 5.5.

5.4.3 Benchmark: Monte Carlo Simulation

Just as in the previous chapter, the benchmark we use for the computation of the CDF and PDF of $\ln(A_t^\nu)$ is Monte Carlo simulation. The Monte Carlo scheme for A_t^ν with drift term is given by the following:

$$\begin{aligned}
A_t^\nu &= \int_0^t e^{2(\nu s + B_s)} ds \\
&= \sum_{i=0}^n e^{2(\nu t_{i+1} + B(t_{i+1}))} (t_{i+1} - t_i) \\
&= \frac{t}{n} \sum_{i=0}^n e^{2(\nu t_{i+1} + B(t_{i+1}))} \\
&= \frac{t}{n} \sum_{i=0}^n e^{2(\nu \frac{t}{n}(i+1) + \sum_{j=0}^i B(t_{j+1}) - B(j))} \\
&= \frac{t}{n} \sum_{i=0}^n e^{2(\nu \frac{t}{n}(i+1) + \sum_{j=0}^i \sqrt{\frac{t}{n}} Z_j)},
\end{aligned} \tag{5.72}$$

where $Z_j \sim N(0, 1)$, $j \in \{0, \dots, n\}$. Again, we take the log of our Monte Carlo simulation. For the error analysis in the following sections, we use $m = 10^6$ Monte Carlo simulations.

5.5 Error Analysis

In Section 6.4 we give a full overview of all the error sources and their contribution of the total error in our method. In this section we perform a numerical error analysis for our computation of the characteristic function of $\ln(A_t^\nu)$ for $\sigma^2 T \in \{0.05, 0.1, 0.5\}$. Recall that we have

$$\Phi_{\ln(A_t^\nu)}(\omega) = \frac{\Phi_{\ln((2\Xi-1)^2)}(\omega) \cdot \Phi_{\phi^2}(\omega)}{\Phi_{\ln(Z^2)}(\omega)} = \frac{k(\omega)l(\omega)}{g(\omega)}. \tag{5.73}$$

Each characteristic function is computed numerically.

For the computation of $g(\omega)$ we saw that for $\nu = 0$, we obtained no difference in errors in the CDF of $\ln(A_t)$ for

$$N_t \leq \frac{\omega_{\max}(b_t - a_t)}{\pi} = \frac{19(b_t - a_t)}{\pi}, \tag{5.74}$$

using the Gamma function and Clenshaw-Curtis quadrature. Note that the truncation range is now very small, since we are examining the error behaviour for difficult cases, i.e. with very small values of t . The use of the Gamma function will therefore lose its purpose, which we will confirm by numerical experiments. Furthermore, $k(\omega)$ will be computed with two different quadrature rules, i.e. Clenshaw-Curtis quadrature and Chebyshev-Gauss quadrature. For the computation of $l(\omega)$, Clenshaw-Curtis quadrature will be used.

For various cosine expansion terms N , we measure the error convergence using the $\|\cdot\|_2$ -norm. For option pricing in Section 6, we aim to have the computational time as low as possible. Therefore, we need to minimize each number of quadrature point $J \in \{J_g, J_k, J_l\}$. Therefore, convergence tests due to the number of quadrature points for the computation of each characteristic function will be done. Furthermore, the computational complexity of Chebyshev-Gauss quadrature is lower than for Clenshaw-Curtis, hence we make a good comparison between these as well.

Note that we have 4 different levels of tolerance: TOL_g , TOL_k (with Clenshaw-Curtis quadrature), TOL_x and TOL_y for $W = \ln(\phi(X, Y))$. Numerical experiments have shown that the following values lead to good results, hence we start with the following: $TOL_g = 10^{-9}$, $TOL_k = 10^{-7}$ (which is the minimal value for which the computation is possible), $TOL_x = 10^{-15}$, $TOL_y = 10^{-12}$. But as we stated in Section 5.2, this needs to be evaluated properly. We will analyse the different values of TOL in Section 6 with reference prices.

In this error analysis, we will thus look at the following for three different values of $\sigma^2 T$:

- For the computation of $g(\omega)$ we use Clenshaw-Curtis quadrature and seek for the the minimal number of quadrature points, and compare its performance with the use of the Gamma function.
- For the computation of $k(\omega)$ we compare Chebyshev-Gauss quadrature and Clenshaw-Curtis quadrature, varying the number of quadrature points for each integration technique.
- For the computation of $l(\omega)$, we use Clenshaw-Curtis quadrature and vary the number of quadrature points.

We start by using many quadrature points to suppress the error coming from the numerical integration technique, and test the error convergence regarding the number of cosine expansion terms N . We will then continue with a fixed N for after which no convergence is observed (within $N = 2^d, d \in \mathbb{N}$), and analyse the error convergence using different number of quadrature points for each method. We will mostly use plots on a *log* scale for the error convergence to ensure a clear observation of the behaviour of the error.

5.5.1 CDF Error Analysis

In Section 4.4, we based our error analysis on the CDF compared with Monte Carlo simulation. For $\nu \neq 0$, we do the same. We use points $x_j, 0 \leq j \leq 10$, to evaluate the errors in $F(x_j)$. Note that we only use x -values which lie within the range of the peak of the density and use $\|\cdot\|_2$ -norm for measurement of the errors. For the Monte Carlo simulation, 10^6 paths are used. We start with the characteristic function of $k(\omega)$.

5.5.2 Analysis of $k(\omega)$

5.5.2.1 Convergence in N

First we look the values of the errors using both methods for $k(\omega)$. Setting $J = 1000$ for each integration method, we vary the number of cosine expansion terms N and look at the error convergence regarding N . The errors are computed in the $\|\cdot\|_2$ -norm. The levels of tolerance are set as we stated earlier. The results are shown in Table 6.

Fourier Cosine Expansion + CC (2x) + Chebyshev-Gauss vs CC						
	$\sigma^2 T = 0.05, \epsilon_2$		$\sigma^2 T = 0.1, \epsilon_2$		$\sigma^2 T = 0.5, \epsilon_2$	
N	<i>Cheb - Gauss</i>	CC	<i>Cheb - Gauss</i>	CC	<i>Cheb - Gauss</i>	CC
4	$1.127 \cdot 10^{-1}$	$1.121 \cdot 10^{-1}$	$9.697 \cdot 10^{-2}$	$9.510 \cdot 10^{-2}$	$6.470 \cdot 10^{-2}$	$6.341 \cdot 10^{-2}$
8	$1.266 \cdot 10^{-1}$	$9.274 \cdot 10^{-3}$	$9.778 \cdot 10^{-3}$	$8.638 \cdot 10^{-3}$	$6.502 \cdot 10^{-3}$	$5.703 \cdot 10^{-3}$
16	$8.631 \cdot 10^{-3}$	$8.472 \cdot 10^{-3}$	$4.630 \cdot 10^{-3}$	$4.627 \cdot 10^{-3}$	$5.626 \cdot 10^{-3}$	$3.989 \cdot 10^{-3}$
32	$7.905 \cdot 10^{-3}$	$8.464 \cdot 10^{-3}$	$6.752 \cdot 10^{-3}$	$4.627 \cdot 10^{-3}$	$5.626 \cdot 10^{-3}$	$3.989 \cdot 10^{-3}$
64	$7.896 \cdot 10^{-3}$	$8.464 \cdot 10^{-3}$	$6.752 \cdot 10^{-3}$	$4.627 \cdot 10^{-3}$	$5.626 \cdot 10^{-3}$	$3.989 \cdot 10^{-3}$
128	$7.896 \cdot 10^{-3}$	$8.464 \cdot 10^{-3}$	$6.752 \cdot 10^{-3}$	$4.627 \cdot 10^{-3}$	$5.626 \cdot 10^{-3}$	$3.989 \cdot 10^{-3}$
256	$7.896 \cdot 10^{-3}$	$8.464 \cdot 10^{-3}$	$6.752 \cdot 10^{-3}$	$4.627 \cdot 10^{-3}$	$5.626 \cdot 10^{-3}$	$3.989 \cdot 10^{-3}$

Table 6: $\|\cdot\|_2$ errors for the CDF of $\ln(A_t^\nu)$ based on two integration methods for $k(\omega)$.

As expected, we have very fast error convergence regarding the number of cosine expansion terms N . Important to note is that this is due to the number of Monte Carlo paths simulated. The precision for 10^6 simulated paths might not be precise enough. In the PDF error analysis, further in this section, this is confirmed. For option pricing in Section 6, therefore we will make use of an Antithetic Variate method, and perform 10^6 simulations to reach a better level of accuracy. However, the magnitude of the error is very low.

Also is observed that as $\sigma^2 T$ increases, the error increases as well. Hence, we confirm that using our method, the computation of $\Phi_{\ln(A_t^\nu)}(\omega)$ is less accurate as $\sigma^2 T$ decreases.

Only for $\sigma^2 T = 0.05$, using Chebyshev-Gauss quadrature leads to a lower error in the CDF approximation. The maximum difference in error between the two methods however is $2.125 \cdot 10^{-3}$.

5.5.2.2 Convergence in J_k

Now we look at the error convergence in J_k , to minimize the number of quadrature points for option pricing in Section 6. We do this via two figures, each with three subfigures for different values of $\sigma^2 T$. Still setting $N_J = N_l = 1000$, we vary the number of quadrature points $J_k \in [100, \dots, 1000]$. We use $N = 64$ cosine expansion terms. The results are shown via *log* scale on the y -axis in Figures 18 and 19.

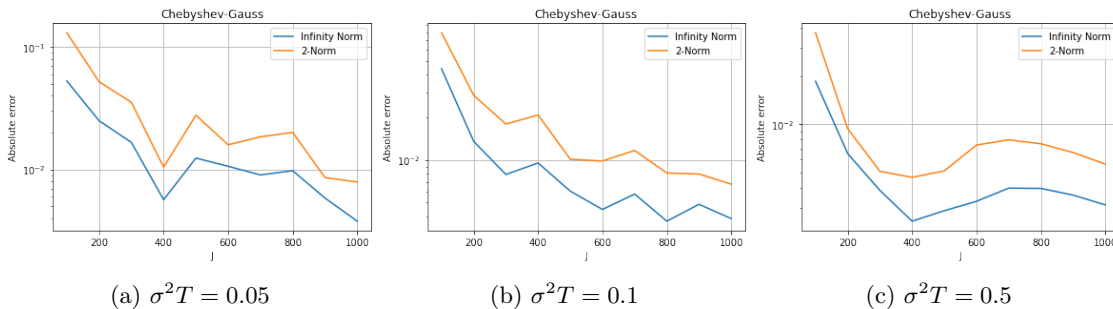


Figure 18: CDF error convergence due to J_k using Chebyshev-Gauss quadrature.

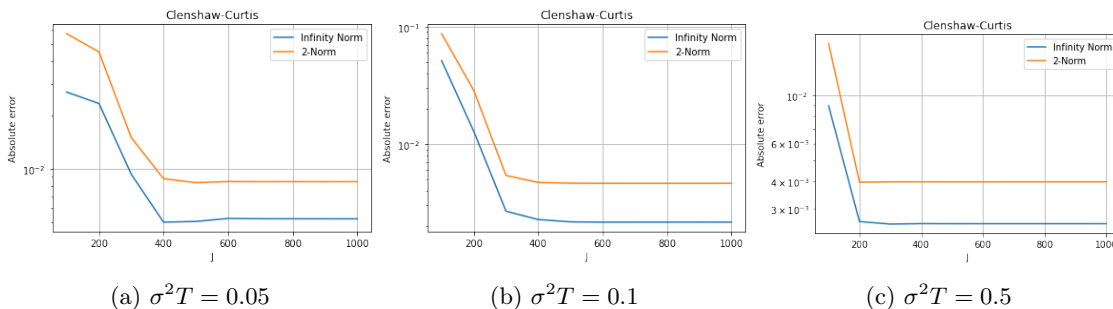


Figure 19: CDF error convergence due to J_k using Clenshaw-Curtis quadrature.

First we look at Figure 18. Chebyshev-Gauss quadrature does not have a good convergence of errors for different values of quadrature points. $J_k = 1000$ returns the lowest error in the first two cases, but convergence might not have even stopped there. It is not a very stable method for computing $k(\omega)$. In Section 6 we will see how the errors will behave with respect to the computational time as well. But looking at Clenshaw-Curtis quadrature, we can conclude we only need $J_k = \max\{500, 400, 400\} = 500$. In combination with the fact that in two of the three values for $\sigma^2 T$ the errors were lower using Clenshaw-Curtis quadrature, it seems like a more preferable method for the computation of $k(\omega)$. We continue our error analysis based on Clenshaw-Curtis quadrature for $k(\omega)$.

5.5.3 Quadrature Points for $l(\omega)$

In this subsection, we analyze the error convergence due to the computation of $g(\omega)$ and $l(\omega)$.

We start with the characteristic function of W . We use the results from the last Subsection and continue with Clenshaw-Curtis quadrature for each distribution. We look for the minimal number of quadrature points J_l first, based on a *log*-scaled plot as well. Setting $N = 64$, $J_k = 500$ and $J_g = 1000$, we assess the convergence using $J_\epsilon \in [100, \dots, 1000]$ with step sizes of 100. The results are presented in Figure 20.

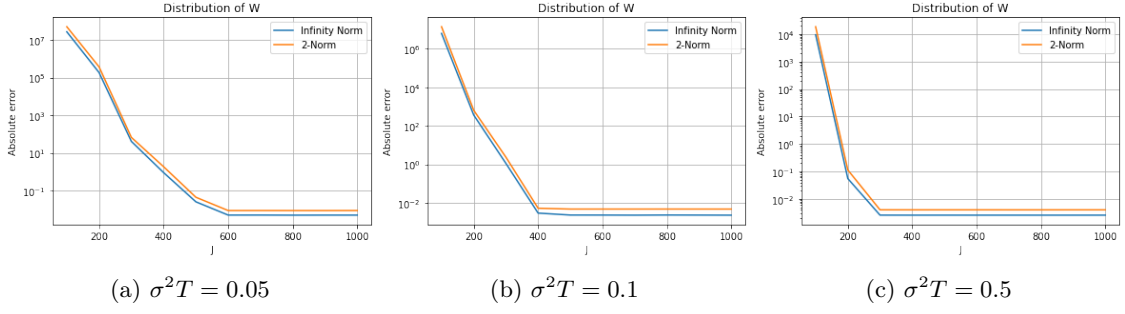


Figure 20: CDF error convergence due to J_l using Clenshaw-Curtis quadrature.

We see quick and decreasing error convergence just as in Figure 19. For $\sigma^2 T = 0.05$, we need 600 quadrature points to reach the same level of accuracy. For larger values only $J_l = 400$ is necessary. We will thus set $J_l = 600$ from now on. At last, we analyze the convergence of errors regarding the computation of $g(\omega)$.

5.5.4 Computation of $g(\omega)$

We observe the convergence of errors due to the computation of $g(\omega)$ in this subsection, using two computational methods.

The characteristic function of $X = \ln(Z^2)$ is computed in two ways, which is the denominator in our computation of $\Phi_{\ln(A_t^v)}(\omega)$. We perform 10^6 Monte Carlo simulations for each value of $\sigma^2 T$ to generate a reference value, and we compare Clenshaw-Curtis quadrature and $\Gamma(i\omega + \frac{1}{2})$ for the computation of $g(\omega)$.

First we use Clenshaw-Curtis quadrature and check the error convergence for $N = 64$ by varying the number of quadrature points. We set $J_l = 600$, $J_k = 500$. The tolerance levels are still as we set above. The results are shown in Figure 21.

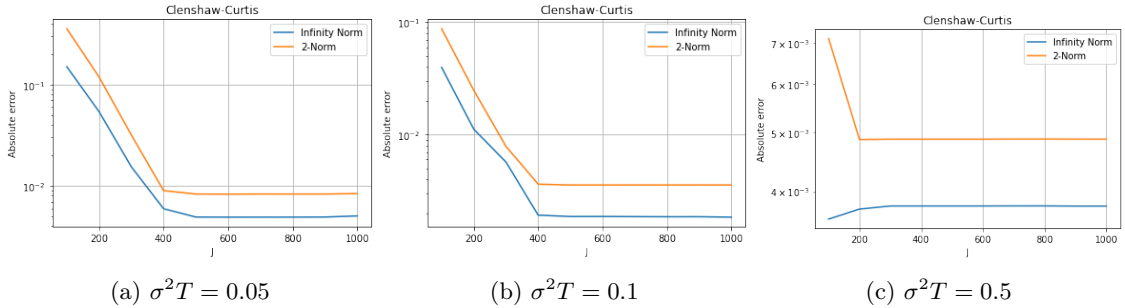


Figure 21: CDF error convergence due to J_g using Clenshaw-Curtis quadrature.

We see that convergence in the error stops after $J_g = 500$ for each value of $\sigma^2 T$. We have now reduced every number of quadrature points for all numerical integration methods.

Lastly, we need to verify whether the Gamma function is beneficial or not. We have shrunken the truncation range now drastically and have a different calculation of $\Phi_{\ln(A_t^v)}(\omega)$ than in Section 4.3, based on Bougerol's extended identity. Hence, we need to verify the use of Γ again. We will use $\sigma^2 T = 0.1$ for this experiment. We set $(J_l, J_k, J_g) = (600, 500, 500)$. The results are shown in Table 7.

N	CC	Γ
8	$8.555 \cdot 10^{-3}$	$8.554 \cdot 10^{-3}$
16	$3.558 \cdot 10^{-3}$	$5.830 \cdot 10^{-2}$
32	$3.558 \cdot 10^{-3}$	$2.461 \cdot 10^{14}$
64	$3.558 \cdot 10^{-3}$	$1.018 \cdot 10^{45}$

Table 7: CDF errors due to two methods for $g(\omega)$.

Due to the rapid decay of the Gamma function in Python, the errors get extremely large, as expected. It is confirmed that the use of the Gamma function for the computation of $g(\omega)$ is not suitable due for the computation of $g(\omega)$ with the new defined truncation range. This means we continue with Clenshaw-Curtis quadrature for $g(\omega)$ as well.

We combine the results we have obtained in the CDF error analysis, to look at the error convergence of the PDF of $\ln(A_t^i)$.

5.5.5 PDF Error Convergence

To finalize the error analysis, we use the PDF recovery via the COS method in this section. We look at the convergence regarding the number of cosine expansion terms N .

First we plot the PDF using $N = 256$ and $(J_l, J_k, J_g) = (600, 500, 500)$ using Clenshaw-Curtis quadrature for each method. We set $\mu = 0.01$ and $T = 1$. The truncation range is as in (5.71) with $c_6 = 0$, $L = 8$. The results are shown in Figure 22.

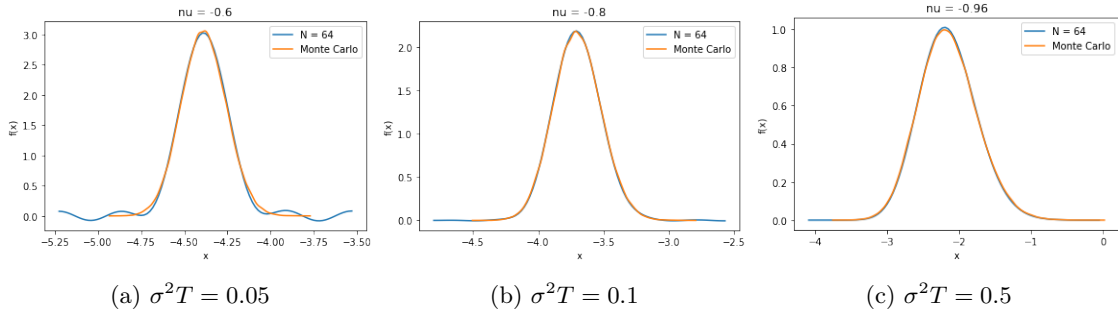


Figure 22: PDF recovery for various values of $\sigma^2 T$.

The truncation range is well defined on the left side tail. For $\sigma^2 T > 0.5$ we might need to increase the parameter L . Note that oscillation occurs for $\sigma^2 T = 0.05$, even using $N = 256$ cosine expansion terms.

Lastly we show the convergence of errors of the PDF for multiple cosine expansion terms N compared with $N = 256$. We use the \log_{10} of the $\|\cdot\|_2$ -norm error to make the distinction clearer for very small errors. For the computation of $k(\omega)$, both Clenshaw-Curtis quadrature and Chebyshev-Gauss quadrature are used. The results are shown in Table 8.

Fourier Cosine Expansion + CC (2x) + Chebyshev-Gauss vs CC						
	$\sigma^2T = 0.05, \epsilon_2$		$\sigma^2T = 0.1, \epsilon_2$		$\sigma^2T = 0.5, \epsilon_2$	
N	<i>Cheb - Gauss</i>	CC	<i>Cheb - Gauss</i>	CC	<i>Cheb - Gauss</i>	CC
4	0.247	0.429	0.239	0.242	0.125	0.121
8	-0.292	-0.314	-0.508	-0.502	-0.596	-0.609
16	-7.130	-6.940	-7.127	-6.696	-6.740	-6.708
32	-11.084	-10.594	-11.911	-11.441	-11.688	-11.459
64	-11.122	-10.589	-12.004	-11.460	-11.842	-11.519
128	-11.141	-10.597	-12.004	-11.575	-12.074	-11.544

Table 8: \log_{10} of $\|\cdot\|_2$ errors for the PDF of $\ln(A_t^\nu)$ compared with $N = 256$.

For each parameter value of σ^2T , there is still a decrease in error for up to $N = 128$, with a clear exponential convergence. But it is also verified, that after $N = 32$, the differences in error are very small. Which confirms that for the CDF analysis, the convergence did not stop, but converged up to the point of the accuracy of Monte Carlo simulation for $N > 16$. We can already see that the option pricing will not need a lot of computational time to reach a good level of accuracy.

Chebyshev-Gauss quadrature shows slightly faster error convergence speed for $N \geq 16$. But for both integration methods for $k(\omega)$, it seems that $N = 16$ cosine expansion terms already leads to incredibly small errors compared to $N = 256$. We will further analyse this by pricing the options. We finalize this section with a conclusion, including all the information we have developed this section.

5.6 Conclusion

In this section we have explained in detail how to compute the characteristic function of $\ln(A_t^\nu)$ with drift term $\nu \neq 0$, based on the extension of Bougerol's identity. The computation is a product and division of three independent characteristic functions.

We computed each characteristic function separately via numerical integration. For the Arcsine distribution, two numerical methods were proposed. We checked the numerical results via either CDF or PDF recovery, compared with the exact formula for the Arcsine distribution, and with Monte Carlo simulation for $W = \ln(\phi(X, Y))$. The results showed a good recovery for each distribution. However, combining the characteristic functions led to numerical issues. For Clenshaw-Curtis quadrature of $Y \sim \chi_2^2$ and $Z = \ln(\Xi)$, $\Xi \sim \text{Arcsine}(0, 1)$, a change of variable had to be made to the *log* domain. Afterwards, the CF of $\ln(A_t^\nu)$ can be computed properly.

We gave an overview of how the distribution relies on (μ, σ, T) and how the computation of $\Phi_{\ln(A_t^\nu)}(\omega)$ is very sensitive to the level of tolerance used, as well as the number of quadrature points used for numerical integration. These can be counter intuitive.

Extensive error analysis with Monte Carlo simulation as benchmark has been done based on the number of quadrature points in the numerical integration, after we defined a new truncation range for the COS method.

Numerical tests evidenced a good convergence of errors. Already after $N = 32$ cosine expansion terms, the same level of accuracy as the MC benchmark is achieved. However, in the PDF analysis it was confirmed that convergence did not actually stop, and the exponential convergence was showed. By comparing two numerical integration methods for $k(\omega)$, We concluded that Clenshaw-Curtis quadrature leads to smaller errors in the CDF recovery except for $\sigma^2T = 0.05$.

In the next section we will price Asian options using our method of cosine series expansion via Bougerol's identity based on the derived characteristic function in this section.

6 Pricing Continuous Asian Options

In Sections 4 and 5, the characteristic function of $\ln(A_t^\nu)$ based on Bougerol's identity for $\nu = 0$ and $\nu \neq 0$ has been computed. Afterwards we have derived the PDF and CDF of $\ln(A_t^\nu)$ and studied the behaviour of the distribution of $\ln(A_t^\nu)$ with respect to different parameter values. In this section we aim to price Asian options using the derived densities in Sections 4 and 5.

We start with some financial background on options and Asian options in general. Then we lie the focus on continuous Asian options. First we discuss the Geometric averaged option based on Geometric Brownian motion, for which we can derive an analytic solution.

Then, we show how we can price options using the COS method and apply this the option pricing for Arithmetic averaged Asian options.

Afterwards, we will give an overview of the errors occurring in our method, and their contribution to our method regarding option pricing. The computational complexity of our new developed method will also be explained.

At the end of this section, we perform multiple convergence experiments for the option prices both in the number of quadrature points for different methods J , as for the number of cosine expansion terms N . As benchmark for the option pricing, several prices from the literature will be used. The computational time will also be computed, which we aim to have as low as possible.

In Section 6.1, the financial background on Asian options will be given.

6.1 Financial Background

In this section we explain more on Asian option pricing in general. Throughout this research, we have used Geometric Brownian motion as stochastic process of the underlying. We will elaborate on this as well.

6.1.1 Asian Options

An option is a contract which gives the buyer of the contract the right to buy or sell the underlying asset for a strike price K at some points $t = T$. The strike price can be a floating strike price depending on the underlying. In this research we focus on a fixed strike price. T is known as the maturity time, or expiration time of the option. In our case the underlying is a stock which follows a Geometric Brownian motion. There are two types of options. *Call* options give the right to buy the asset. *Put* options give the right to sell the underlying asset.

As stated earlier, in this research we look at Asian options. Asian options are Exotic options which are path dependent options, meaning they rely on the behaviour of the underlying S_t for $0 \leq t \leq T$ instead of only the value of the underlying at time T . Asian options are determined by the averaged price of the underlying until maturity time T . They were first introduced in 1987 by Banker's Trust Tokyo used for crude oil contracts, which is where the name comes from.

There are 4 types of Asian options, which can be divided into two categories: continuous Asian options and discrete Asian options, which on their turn can be divided into two categories: Geometric averaged or Arithmetic averaged.

As the name suggests, discrete Asian options are based on fixed time points of the value of the underlying $0 = t_0 < t_1 < \dots < t_{n-1} < t_n = T$ (t_0 does not necessarily need to be zero, but for simplicity we set $t_0 = 0$). For the pricing of Geometric discrete Asian options, analytic solutions are available when the underlying follows a Geometric Brownian motion as is shown in [20]. In [19], the COS method is used to compute discrete Arithmetic averaged Asian options. The characteristic function is there by recursion computed for each point in time. For a continuous time average, we have derived the characteristic function based on Bougerol's identity.

We focus on continuous Asian options. The payoff functions for a call option for continuous Geometric averaged - and Arithmetic averaged Asian options respectively are given by

$$H_G(T, S) = \left[e^{\frac{1}{T} \int_0^T \log(S_u) du} - K \right]^+, \quad (6.1)$$

$$H_A(T, S) = \left[\frac{1}{T} \int_0^T S_u du - K \right]^+, \quad (6.2)$$

where $[x]^+ = \max\{0, x\}$. Note that for discrete Asian options, the difference is a replacement in the payoff function:

$$\frac{1}{T} \int_0^T S_u du \rightarrow \frac{1}{N+1} \sum_{i=0}^N S_i. \quad (6.3)$$

For the Geometric average, analytic solutions can be found when the underlying follows a Geometric Brownian motion, which is shown in Section 6.2. For continuous Arithmetic Asian options, no analytic solution has been found, which makes this topic challenging.

First we explain the meaning of Geometric Brownian motion in more detail.

6.1.2 Black-Scholes

As stated in the Introduction and Section 3, we will compute the price of Asian options where the underlying follows a Geometric Brownian motion. This is used in the Black-Scholes framework.

Let W_t be a standard Brownian motion. For a risk-free asset and a risky asset, the dynamics are respectively given by

$$dM_t = rM_t dt, \quad (6.4)$$

$$dS_t = \mu S_t dt + \sigma S_t dW_t^{\mathbb{P}}, \quad (6.5)$$

where, r is the risk-free rate and μ and σ are deterministic values denoted by the drift and volatility. M_t can be seen as a bank account. \mathbb{P} denotes the real-world measure and M_t and S_t are the prices of the risk-free and risky assets respectively. Equation (6.5) is called geometric Brownian motion. It then follows that under a different measure, the risk-neutral measure \mathbb{Q} , the dynamics for S_t are given by

$$dS_t = \left(r - \frac{1}{2}\sigma^2\right)S_t dt + \sigma S_t dW_t^{\mathbb{Q}}. \quad (6.6)$$

We have notated $\mu = r$ in the previous Sections. The solution of (6.6) at time $t = T$ is given by

$$S_T = S_0 e^{(\mu - \frac{1}{2}\sigma^2)T + \sigma W_T}, \quad (6.7)$$

as we already stated in Section 3.

In the next Subsection, we focus on the Geometric averaged Asian option, for which we can derive an analytic solution.

6.2 Continuous Geometric Averaged Asian Options

In this section we show how we can derive an analytic solution for Geometric averaged options where the underlying follows a Geometric Brownian motion. We focus on a *call* option here. For a *put* option, the computation is similar.

Recall that the payoff function for the Geometric average is given by

$$H_G(T, S) = \left[e^{\frac{1}{T} \int_0^T \log(S_u) du} - K \right]^+. \quad (6.8)$$

By the Feynman-Kac theorem [12], the value of the option at time $t = t_0$ is denoted by

$$\begin{aligned} V(t_0, S) &= \mathbb{E}^{\mathbb{Q}}[H(T, S) | F_{t_0}] \\ &= \mathbb{E}^{\mathbb{Q}} \left[\left(e^{\frac{1}{T} \int_0^T \log(S_u) du} - K \right)^+ | F_{t_0} \right] \\ &= \mathbb{E}^{\mathbb{Q}}[(e^y - K)^+ | F_{t_0}], \end{aligned} \quad (6.9)$$

with

$$y = \frac{1}{T} \int_0^T \log(S_u) du. \quad (6.10)$$

We set $t_0 = 0$ and make the following computation. Let W_t follow a standard Brownian motion. Using (6.7), computation of y yields to:

$$\begin{aligned} y &= \frac{1}{T} \int_0^T \log(S_u) du \\ &= \frac{1}{T} \int_0^T \left[\log(S_0) + \left(\mu - \frac{1}{2}\sigma^2\right)u + \sigma W_u \right] du \\ &= \log(S_0) + \frac{1}{2}(\mu - \frac{1}{2}\sigma^2)T + \frac{1}{T} \int_0^T \sigma W_u du \\ &= \log(S_0) + \frac{1}{2}(\mu - \frac{1}{2}\sigma^2)T + \frac{\sigma}{T} \int_0^T W_u du. \end{aligned} \quad (6.11)$$

By Ito's formula for $g(u, W_u) = uW_u$, we obtain that

$$d(uW_u) = W_u du + u dW_u \leftrightarrow \quad (6.12)$$

$$\int_0^T d(uW_u) = \int_0^T W_u du + \int_0^T u dW_u \leftrightarrow \quad (6.13)$$

$$TW_T = \int_0^T W_u du + \int_0^T u dW_u. \quad (6.14)$$

Therefore, we can write

$$\begin{aligned}
\int_0^T W_u du &= TW_T - \int_0^T u dW_u \\
&= T \int_0^T dW_u - \int_0^T u dW_u \\
&= \int_0^T (T - u) dW_u,
\end{aligned} \tag{6.15}$$

which is a Gaussian random variable. Since $f(u) = T - u$ is deterministic and $\int_0^T (f(u))^2 du < \infty$, the expectation and variance of (6.15) are given by

$$\mathbb{E} \left[\int_0^T (T - u) dW_u \right] = 0, \tag{6.16}$$

$$\text{Var} \left[\int_0^T (T - u) dW_u \right] = \mathbb{E} \left[\left(\int_0^T (T - u) dW_u \right)^2 \right] = \int_0^T (T - u)^2 du = \frac{1}{3}T^3. \tag{6.17}$$

Hence,

$$\int_0^T W_u du \sim N\left(0, \frac{1}{3}T^3\right). \tag{6.18}$$

We can conclude that e^y is lognormally distributed, where y is distributed as

$$y \sim N\left(\log(S_0) + \frac{1}{2}(\mu - \frac{1}{2}\sigma^2)T, \frac{\sigma^2}{3}T\right). \tag{6.19}$$

Since $e^{\frac{1}{T} \int_0^T \log(s_u) du}$ is lognormally distributed, we can compute an analytic solution for the option price at time $t_0 = 0$ as follows. Let $Z \sim N(0, 1)$. The price at $t_0 = 0$ is then

$$\begin{aligned}
V(t_0, S) &= \mathbb{E}^{\mathbb{Q}}[(e^y - K)^+ | F_0] \\
&= e^{-rT} \mathbb{E} \left[S_0 e^{\sqrt{\frac{1}{3}\sigma^2 T} z + \frac{1}{2}(r - \frac{1}{2}\sigma^2)T} - K \right]^+.
\end{aligned} \tag{6.20}$$

Solving

$$S_0 e^{\sqrt{\frac{1}{3}\sigma^2 T} z + \frac{1}{2}(r - \frac{1}{2}\sigma^2)T} - K \geq 0 \tag{6.21}$$

leads to

$$z \geq -\frac{\log\left(\frac{S_0}{K}\right) + \frac{1}{2}(r - \frac{1}{2}\sigma^2)T}{\sqrt{\frac{1}{3}\sigma^2 T}} = -d_2. \tag{6.22}$$

Now we set

$$\begin{aligned}
d_1 &= d_2 + \sqrt{\frac{1}{3}\sigma^2 T} \\
&= \frac{\log\left(\frac{K}{S_0}\right) - \frac{1}{2}(r - \frac{1}{2}\sigma^2)T + \frac{1}{3}\sigma^2 T}{\sqrt{\frac{1}{3}\sigma^2 T}},
\end{aligned} \tag{6.23}$$

the value of the option in (6.20) then becomes

$$\begin{aligned}
V(t_0, S) &= e^{-rT} \mathbb{E} \left[S_0 e^{\sqrt{\frac{1}{3}\sigma^2 T} z + \frac{1}{2}(r - \frac{1}{2}\sigma^2)T} - K \right]^+ \\
&= e^{-rT} \int_{-d_2}^{\infty} \frac{1}{\sqrt{2\pi}} \left(S_0 e^{\sqrt{\frac{1}{3}\sigma^2 T} z + \frac{1}{2}(r - \frac{1}{2}\sigma^2)T} - K \right) e^{-\frac{1}{2}z^2} dz \\
&= e^{-rT} \int_{-\infty}^{d_2} \frac{1}{\sqrt{2\pi}} \left(S_0 e^{-\sqrt{\frac{1}{3}\sigma^2 T} z + \frac{1}{2}(r - \frac{1}{2}\sigma^2)T} - K \right) e^{-\frac{1}{2}z^2} dz \\
&= -K e^{-rT} \Phi(d_2) + e^{-rT} e^{\frac{1}{2}(r - \frac{1}{2}\sigma^2)T} S_0 \int_{-\infty}^{d_2} \frac{1}{\sqrt{2\pi}} e^{-\sqrt{\frac{1}{3}\sigma^2 T} z} e^{-\frac{1}{2}z^2} dz.
\end{aligned} \tag{6.24}$$

Setting $y = z + \sqrt{\frac{1}{3}\sigma^2 T}$, we obtain

$$\begin{aligned} \int_{-\infty}^{d_2} \frac{1}{\sqrt{2\pi}} e^{-\sqrt{\frac{1}{3}\sigma^2 T}z} e^{-\frac{1}{2}z^2} dz &= \int_{-\infty}^{d_1} \frac{1}{\sqrt{2\pi}} e^{-\sqrt{\frac{1}{3}\sigma^2 T}(y-\sqrt{\frac{1}{3}\sigma^2 T})} e^{-\frac{1}{2}(y-\sqrt{\frac{1}{3}\sigma^2 T})^2} dy \\ &= \int_{-\infty}^{d_1} \frac{1}{\sqrt{2\pi}} e^{-\frac{1}{2}y^2} e^{\frac{1}{6}\sigma^2 T} dy = e^{\frac{1}{6}\sigma^2 T} \Phi(d_1). \end{aligned} \quad (6.25)$$

Thus the option price at $t_0 = 0$ is given by

$$V(t_0, S) = e^{-rT} e^{\frac{1}{2}(r-\frac{1}{2}\sigma^2)T} e^{\frac{1}{6}\sigma^2 T} S_0 \Phi(d_1) - K e^{-rT} \Phi(d_2). \quad (6.26)$$

As we stated earlier, the challenge lies indeed in pricing Asian options with Arithmetic mean. We show how we can price these options using the COS method in the next subsection based on Bougerol's extended identity and the distribution of A_t^ν .

6.3 Continuous Arithmetic Averaged Asian Options

Now we continue with the Arithmetic average, for which we need our derivations based on Bougerol's (extended) identity. For this type of option, there are no analytic solutions available. Different computational methods have been developed to price this type of option [3]:

1. Monte Carlo simulation
2. Binomial Tree method
3. Convolution method
4. PDE methods
5. Direct integration

The accuracy of these numerical methods, compared to each other, is of order 10^{-4} . The Binomial Tree method is known to be sufficient for large volatility values. We use therefore the Binomial Tree method from Hsu [10] as benchmark for high volatilities.

In our research, the option pricing is based on the distribution of A_t^ν . Several expressions for the Arithmetic Averaged Asian option price were given used based on A_t^ν . Donati-Martin [4] found an expression for the Laplace transform of the option price for a fixed strike price K :

$$\int_0^\infty e^{-\lambda t} \mathbb{E}[A_t^\nu - K]^+ dt = \frac{(2K)^{1-\beta} \Gamma(\alpha + 1)}{2\lambda(\beta - 1)\Gamma(\alpha + \beta + 1)} F_1(\beta - 1, \alpha + \beta + 1, -\frac{1}{2K}), \quad (6.27)$$

with

$$\gamma = \sqrt{2\lambda + \nu^2}, \quad \alpha = \frac{\gamma + \nu}{2}, \quad \beta = \frac{\gamma - \nu}{2}. \quad (6.28)$$

where F_1 denotes the hypergeometric function. Schröder [14] has found another expression for the Laplace transform, and also an explicit triple integral expression.

In this research, we use the COS method in combination with the distribution of A_t^ν , which is a new approach to the pricing of Arithmetic Averaged Asian options. In the next subsection we first explain how to compute the option using the distribution of A_t^ν via the COS method based on the derivations in [6].

6.3.1 Option Pricing using Cosine Series Expansion

In this subsection we show how to compute the option values for Arithmetic averaged options using the COS method, following [7]. Here is where we need the derived densities in sections 4 and 5. At the end, we also make an adjustment on the truncation range, which is shifted compared to the truncation range for the density function of $\ln(A_t^\nu)$. We start with some computation, based on the Feynman-Kac theorem [12].

Recall that the payoff functions of an Asian option with Arithmetic mean for a *call* and *put* option respectively are given by

$$H_{call}(T, y) = \left[\frac{1}{T} \int_0^T S_u du - K \right]^+ = [X_T - K]^+, \quad (6.29)$$

$$H_{put}(T, y) = \left[K - \frac{1}{T} \int_0^T S_u du \right]^+ = [K - X_T]^+. \quad (6.30)$$

where S_t follows a Geometric Brownian motion and K is the fixed strike price. We denoted our variable of interest as

$$X_t = \frac{1}{t} \int_0^t S_u du, \quad (6.31)$$

with $x = X_0 = 0$ and $y = X_T$. Therefore the price for a *call* option based on (6.7) and (6.9) is given by

$$V(t_0, x) = e^{-rT} \mathbb{E}^{\mathbb{Q}}[H(T, y) | F_{t_0}] = e^{-rT} \int_{\mathbb{R}} V(T, y) f_X(y) dy. \quad (6.32)$$

Now we use the cosine series expansion for the density of X_t as in (4.3). After some computation, and interchanging integral and summation, we can conclude that the option price is given by

$$V(t_0, x) = e^{-r(T-t_0)} \sum_{k=0}^{N-1} \frac{2}{b-a} \operatorname{Re} \left[\phi_X \left(\frac{k\pi}{b-a} \right) \exp \left(-ik\pi \frac{a}{b-a} \right) \right] \cdot H_k, \quad (6.33)$$

where

$$H_k = \int_a^b V(T, y) \cos \left(k\pi \frac{y-a}{b-a} \right) dy, \quad (6.34)$$

which is shown in [7]. We apply a change of variable and set $Y_t = \ln \left(\frac{X_t}{K} \right)$. The payoff function for (6.29) for a *call* option can than be written as

$$\begin{aligned} H(T, y) &= \left[\frac{1}{T} \int_0^T S_u du - K \right]^+ \\ &= [X_T - K]^+ \\ &= \left[K \left(\frac{X_T}{K} - 1 \right) \right]^+ \\ &= [K(e^y - 1)]^+. \end{aligned} \quad (6.35)$$

Lastly, the coefficients H_k in (6.34) can be computed analytically as in [7], which are given by

$$\begin{aligned} \chi_k(c, d) &= \int_c^d e^y \cos \left(k\pi \frac{y-a}{b-a} \right) dy \\ &= \frac{1}{1 + \left(\frac{k\pi}{b-a} \right)^2} \left[\cos \left(k\pi \frac{d-a}{b-a} \right) e^d - \cos \left(k\pi \frac{c-a}{b-a} \right) e^c \right. \\ &\quad \left. + \frac{k\pi}{b-a} \sin \left(k\pi \frac{d-a}{b-a} \right) e^d - \frac{k\pi}{b-a} \sin \left(k\pi \frac{c-a}{b-a} \right) e^c \right] \\ \psi_k(c, d) &= \int_c^d \cos \left(k\pi \frac{y-a}{b-a} \right) dy \\ &= \begin{cases} \frac{b-a}{k\pi} \left[\sin \left(k\pi \frac{d-a}{b-a} \right) - \sin \left(k\pi \frac{c-a}{b-a} \right) \right], & k \neq 0 \\ d - c, & k = 0. \end{cases} \end{aligned} \quad (6.36)$$

What we need to price the option is thus the characteristic function of $Y_T = \ln\left(\frac{X_T}{K}\right)$. Note that S_t follows a Geometric Brownian motion, therefore using (6.7) we find that

$$X_t = \frac{1}{t} \int_0^t S_u du = \frac{S_0}{t} \int_0^t e^{(\mu - \frac{1}{2}\sigma^2)s + \sigma B_s} ds \quad (6.37)$$

and

$$Y_T = \ln \left[\frac{S_0}{KT} \int_0^T e^{(\mu - \frac{1}{2}\sigma^2)s + \sigma B_s} ds \right]. \quad (6.38)$$

Now we use the scaling property of IGBM shown in equation (3.32) in section 3.1.2. The following are the same in law:

$$Y_T \stackrel{law}{=} \ln \left(\frac{4S_0}{\sigma^2 KT} A_t^\nu \right) = \ln \left(\frac{S_0}{Kt} A_t^\nu \right), \quad (6.39)$$

with

$$t = \frac{\sigma^2 T}{4}, \quad \nu = \frac{2\mu}{\sigma^2} - 1. \quad (6.40)$$

Then the characteristic function of Y_T can be computed as:

$$\mathbb{E} [e^{i\omega Y_T}] = \mathbb{E} \left[e^{i\omega \ln\left(\frac{S_0}{Kt} A_t^\nu\right)} \right] = \left(\frac{S_0}{Kt} \right)^{i\omega} \cdot \Phi_{\ln(A_t^\nu)}(\omega). \quad (6.41)$$

The characteristic function of Y_t is a multiplication of the constant $\left(\frac{S_0}{Kt}\right)^{i\omega}$ with the characteristic function of $\ln(A_t^\nu)$ which we have computed in Sections 4 and 5. We can substitute (6.41) in equation (6.32) to compute the price of Asian options at time $t = t_0$.

All that is left to do is define a new truncation range for the COS method based on the variable $Y_t = \frac{X_t}{K}$.

6.3.1.1 Truncation Range

In section 5.4.2 we determined the truncation range for the COS method for the density recovery of $\ln(A_t^\nu)$ via the COS method, which was given by

$$[A, B] = [\ln(\mathbb{E}[(A_t^\nu)]) - |\ln(\mathbb{E}[A_t^\nu]) - \ln(b)|, \quad \ln(b)], \quad (6.42)$$

with b given in (5.66), based on the cumulants of A_t^ν . For the option pricing, we use the CF and density function of

$$Y_T \stackrel{law}{=} \ln \left(\frac{S_0}{Kt} A_t^\nu \right) = \ln \left(\frac{S_0}{Kt} \right) + \ln(A_t^\nu), \quad (6.43)$$

which means the truncation range for the option pricing for the COS method is shifted regarding the truncation range for $\ln(A_t^\nu)$. The truncation range for the option pricing will therefore be

$$[A, B]_{opt} = \left[\ln(\mathbb{E}[(A_t^\nu)]) - |\ln(\mathbb{E}[A_t^\nu]) - \ln(b)| + \ln \left(\frac{S_0}{Kt} \right), \quad \ln(b) + \ln \left(\frac{S_0}{Kt} \right) \right]. \quad (6.44)$$

For now we set $L = 8$ and $c_6 = 0$.

We have defined our new variable of interest Y_t , and updated the truncation range for the COS method. Hence we have all the tools to price the options.

In Section 6.4, we first give an overview of all the errors in our computation of the options and compute the magnitude of the operational complexity.

6.4 Errors and Computational Complexity

In this section we give an overview of the errors which influence the computation of Asian options with Arithmetic mean using the COS method, based on Bougerol's identity. We also give the operational complexity using our method.

6.4.1 Errors

The errors in the computation follow from the performed numerical integration, the truncated integrals to compute the separate characteristic functions (tolerance levels) and the use of the COS method. They are listed below.

1. Error in the computation of $g(\omega)$. We use a level of tolerance used for the numerical integration of $g(\omega)$, hence we will create an error of TOL_g when we $g(\omega)$ is computed with Clenshaw-Curtis quadrature. We will also encounter a numerical error using the integration ϵ_1 .
Using the Gamma function, this level of tolerance is not needed, but we still encounter an error using the Gamma function in Python. We call ϵ_2 the error for the numerical computation of $g(\omega)$. Hence the error in computing $g(\omega)$ is $\epsilon_g \in \{TOL_g + \epsilon_1, \epsilon_2\}$
2. Error in the computation of $h(\omega)$. When we price options with zero drift, we use a tolerance level for the computation of $h(\omega)$, hence we have an error TOL_h , and we create an error due to numerical integration using Clenshaw-Curtis quadrature ϵ_3 . The error for the computation of $h(\omega)$ is $\epsilon_h = TOL_h + \epsilon_3$
3. Error in the computation of $k(\omega)$. We use either Clenshaw-Curtis quadrature with a tolerance level TOL_k and numerical integration error ϵ_{k_1} , or Chebyshev-Gauss quadrature, resulting in an error of ϵ_{k_2} . The error occurring for the computation of $k(\omega)$ is $\epsilon_k \in \{TOL_k + \epsilon_{k_1}, \epsilon_{k_2}\}$.
4. Error in computing $l(\omega)$. Here we use 2-dimensional numerical integration, which result in $\epsilon_{l_1} + \epsilon_{l_2}$, both with tolerance level TOL_l . The error computing $l(\omega)$ is therefore $\epsilon_l = 2TOL_l + \epsilon_{l_1} + \epsilon_{l_2}$.
5. Error by using cosine series expansion. The error for the COS method consists of three parts. Let $f_X(x)$ be the density function of $\ln(A_t^v)$.

- In (4.3) we have a truncation of the cosine series, i.e. we create a series truncation error c_1 , which is given by

$$c_1 = \sum_{k=N}^{\infty} F_k \cos\left(k\pi \frac{x - a_t}{b_t - a_t}\right). \quad (6.45)$$

- Approximating F_k as in (4.5), which creates an error c_2 by truncation of the characteristic function:

$$c_2 = \int_{\mathbb{R} \setminus [a_t, b_t]} \exp\left(ik\pi \frac{x - a_t}{b_t - a_t}\right) f_X(x) dx. \quad (6.46)$$

- We truncate the integration range for the option price in (6.32) resulting in an error c_3 :

$$c_3 = \int_{\mathbb{R} \setminus [a_T, b_T]} V(T, y) f_X(y) dy. \quad (6.47)$$

We focus on option pricing with drift. Let G, K and L denote the exact value of $h(\omega)$, $k(\omega)$ and $l(\omega)$, the error in the approximation of the characteristic function of $\ln(A_t^v)$ is then

$$\epsilon_{cf} = \frac{LK}{G} - \frac{(L - \epsilon_l)(K - \epsilon_k)}{(G - \epsilon_g)} = \frac{LK}{G} - \frac{(L - 2TOL_l + \epsilon_{l_1} + \epsilon_{l_2})(K - \max\{TOL_k + \epsilon_{k_1}, \epsilon_{k_2}\})}{(G - \epsilon_1 - TOL_g)}. \quad (6.48)$$

The local error in our computation of the option price is therefore a combination of c_1, c_2, c_3 , and ϵ_{cf} . We will not analyse the error convergence due to different tolerance levels. We use a least squared method to determine which tolerance levels result in the lowest error based on 8 reference prices in Section 6.5. We will analyze the following.

- Setting the truncation range large enough with a sufficient amount of quadrature points based on the CDF error analysis in Section 5.5 for each numerical integration technique, the error will be dominated by c_1 and exponential convergence should occur.
- Setting the truncation range large enough and using a sufficient number of cosine expansion terms, the error is dominated by ϵ_{cf} . After an experiment on different tolerance levels, the error should come from the numerical integration, i.e. the number of quadrature points.

6.4.2 Computational Complexity

We define the computational complexity for pricing options using our method, again for $\nu \neq 0$. For each $k \leq N$, we use 4 numerical integration techniques (2 for $l(\omega)$). Note that for $g(\omega)$ and $l(\omega)$ we use Clenshaw-Curtis quadrature, which takes $(J \log(J) + J)$ operations. For $k(\omega)$ we use both Clenshaw-Curtis quadrature and Chebyshev-Gauss quadrature, and the latter takes $O(J)$ operations. The computational complexity using cosine series expansion for our method based on Bougerol's extended identity is then

$$OC \in \{O(N((2J_l \log(J_l) + J_l) + (J_k \log(J_k) + J_k) + (J_g \log(J_g) + J_g))), \\ O(N((2J_l \log(J_l) + J_l) + J_k + (J_g \log(J_g) + J_g)))\}. \quad (6.49)$$

We have defined the numerical methods, the truncation range and gave an overview of the errors. In Section 6.5, we price the options based on all the results obtained in this research so far.

6.5 Option Pricing Results

In this section we will use the results from Sections 4 and 5 to price the options.

We will use Monte Carlo simulation and reference prices from literature as benchmark for our computations. Monte Carlo simulation will be used for $\nu = 0$. We make use the Antithetic Variates method as in [15] to reduce the variance of our simulation for a better accuracy, and we simulate $4 \cdot 10^{-6}$ Monte Carlo paths.

First we analyze $\nu = 0$ with two experiments. Afterwards, we price the options for $\nu \neq 0$.

We start with an important remark on reference prices.

Remark 6.1. There is no exact solution available for Asian options with Arithmetic mean. In most of the literature, prices are presented using different computational methods. The prices in these papers vary as well. We will therefore make use of prices where in the reference, most digits behind the comma are the same, which is a maximum of 3 mostly, sometimes 4. If we have convergence with an error of 10^{-4} , that does not necessarily mean we have a less accurate pricing method than the reference. Furthermore, we round up the errors to a significant number. When convergence stops in our Tables, this means convergence occurs for decimals we do not display. We will use a lot of significant numbers if necessary of course, to show convergence.

Setting the truncation range large enough with a decent amount of cosine expansion terms, the errors come from numerical integration in our computation of $\ln(A_t^r)$. Therefore, we can draw good conclusion about the quadrature rules and the parameter $\sigma^2 T$, when errors are larger than 10^{-4} .

6.5.1 Option Pricing with Zero Drift

We begin with pricing the options where $\nu = 0$. Note that by the scaling property, we then have $\mu = \frac{1}{2}\sigma^2$. No literature has been found as benchmark, hence we will use Monte Carlo simulation. As stated earlier, we will use the Antithetic Variate method to reduce the variance of our simulation [15].

The characteristic function of interest was given by

$$\Phi_{\ln(A_t)}(\omega) = \frac{h(\omega)}{g(\omega)}, \quad (6.50)$$

In section 4.3 we have done the error analysis with a very wide truncation range. Now we will use the truncation range proposed as in 5.4.2. Note that the use of Γ will not be suitable to use anymore if we want to see the error convergence due to cosine expansion terms N due to the fast decay of the Gamma function. We have shown that the computation of $g(\omega)$ using Clenshaw-Curtis quadrature also works well, which was confirmed by the error analysis for $\nu \neq 0$.

We have also confirmed that the errors come due to the computation of $h(\omega)$. We have tried multiple ways to compute $h(\omega)$ using Clenshaw-Curtis quadrature (all with other boundaries, computed based on TOL_h).

1. In section 4.3 we computed $h(\omega)$ as

$$h(\omega) = \frac{1}{\sqrt{2\pi t}} \int_{-\infty}^{\infty} e^{i\omega y} \exp \left[-\frac{1}{2t} \left[\ln \left(\sqrt{e^y} + \sqrt{e^y + 1} \right) \right]^2 \right] \sqrt{\frac{e^y}{e^y + 1}} dy. \quad (6.51)$$

2. We have tried

$$h(\omega) = \frac{1}{2\pi t} \int_{-\infty}^{\infty} e^{\ln[\sinh^2(x)] e^{-\frac{1}{2t} x^2}} dx \quad (6.52)$$

This integration led to very large errors.

3. We took out t , as the normal distribution has a variance of \sqrt{t} , creating a very narrow peak in the density function:

$$h(\omega) = \frac{1}{2\pi} \int_{-\infty}^{\infty} e^{i\omega[\ln(\sinh^2(\sqrt{t}x))]^2} e^{-\frac{1}{2}x^2} dx \quad (6.53)$$

4. We applied a change of variable to the *log* domain:

$$h(\omega) = \frac{1}{2\pi} \int_0^{\infty} e^{i\omega[\ln(\sinh^2(\sqrt{t}e^x))]^2} e^{-\frac{1}{2}e^{2x}} e^x dx \quad (6.54)$$

It appeared that no improvements were made using another method than method 1.

We will perform two experiments. In the first, we set a very wide truncation range and look at the error convergence in N for different strike prices. We compare a call option and a put option.

In the second experiment, we look at the increase or decrease of the errors for different maturity times T for a call option.

In Section 4.3 we concluded that $J_h = 800$ quadrature points would be sufficient for the computation of $h(\omega)$, this is what we will use.

In Section 5.5, there was confirmed that the computation of $g(\omega)$ did not lead to a decrease in errors using $J_g = 500$. We use therefore $J_g = 500$.

We have done testing on the tolerance level for both distributions, the maximum level of tolerance seemed to be most efficient, i.e. $TOL_g = TOL_h = 10^{-15}$ for the values for which convergence occurs with respect to Monte Carlo simulation.

A complete error analysis for multiple tolerance and quadrature points will be done for $\nu \neq 0$, we leave that for now. We are interested in the importance of the parameter t .

We show the convergence of the error in the option price compared with Monte Carlo simulation. We use $4 \cdot 10^6$ Monte Carlo paths. We may assume this gives the correct amount of precision, using a variance reduction technique as well.

For the truncation range we use $L = 12$, hence the error should come from the cosine series expansion and numerical integration. We perform two experiments.

6.5.1.1 Experiment: Call and Put option

We compute a call option and a put option using the COS method for $\nu = 0$. We set $T = 1$, and vary σ in both experiments. We should observe convergence in N , using a wide truncation range. We set $S_0 = 100$ and $\sigma = 0.2$, resulting in $t = 0.01$. The results are shown in Table 9.

N	$K = 70$	$K = 80$
8	0.413	0.670
16	0.293	0.185
32	0.295	1.41
64	2.12	1.32
128	2.05	1.31
256	2.04	1.30
512	2.04	1.30
1024	2.03	1.30

Table 9: Errors in Asian call option with $S_0 = 100$, $\sigma = 0.2$.

We observe convergence in N for $N \leq 64$ for both $K = 70$ and for $K = 80$ up to $N = 32$. The errors are quite large, which we expected for $t = 0.01$. The truncation is set too wide. We can decrease the errors by reducing the truncation range. We set $L = 9$ and $c_6 = 0$. The results are shown in Table 10.

N	$K = 70$	$K = 80$
8	0.126	0.305
16	0.125	0.304
32	0.118	0.246
64	0.073	0.105
128	0.045	0.064
256	0.072	0.079
512	0.045	0.054
1024	0.035	0.037

Table 10: Errors in Asian call option with $S_0 = 100$, $K = 70$ and $\sigma = 0.2$.

We see that the error has been reduced with an order of 10^{-2} compared to Table 9. In the next experiment, we compute two *put* option prices via the COS method using our method. We increase σ , to observe already a difference due to the parameter t . We set $\sigma = 0.4$, resulting in $t = 0.04$. The results are presented in Table 11. Here is used $L = 12$, $c_6 = 0$.

N	$K = 55$	$K = 65$
8	2.921	1.018
16	$2.796 \cdot 10^{-1}$	$1.382 \cdot 10^{-1}$
32	$2.057 \cdot 10^{-2}$	$1.277 \cdot 10^{-2}$
64	$2.285 \cdot 10^{-2}$	$5.382 \cdot 10^{-3}$
128	$2.284 \cdot 10^{-2}$	$5.390 \cdot 10^{-3}$
256	$1.811 \cdot 10^{-2}$	$1.385 \cdot 10^{-3}$
512	$2.331 \cdot 10^{-2}$	$1.629 \cdot 10^{-3}$

Table 11: Errors in Asian put option with $S_0 = 50$, $\sigma = 0.4$.

The errors are reduced compared to the call option price. As expected, as t increases, the error decreases. We see a clear convergence up to $N = 256$. The Out-Of-The-Money option shows a more accurate result compared to Monte Carlo simulation, with a precision of 10^{-3} , which is an accurate result. Next, we look at the error due the magnitude of t .

6.5.1.2 Experiment 2

In this experiment, we study the increase or decrease in the errors of the option price regarding the parameter t . We set $\sigma = 0.2$, and vary $T \in \{2, 4, 6, 8, 10\}$, resulting in $t \in \{0.03, 0.04, 0.06, 0.08, 0.1\}$. Still using a wide truncation range with $L = 12$ and c_6 , we set the number of cosine expansion terms at $N = 512$. We focus here on a Call option, with $K = 40$, $S_0 = 50$ and simulate $4 \cdot 10^6$ Monte Carlo paths. The results are shown in Figure 23.

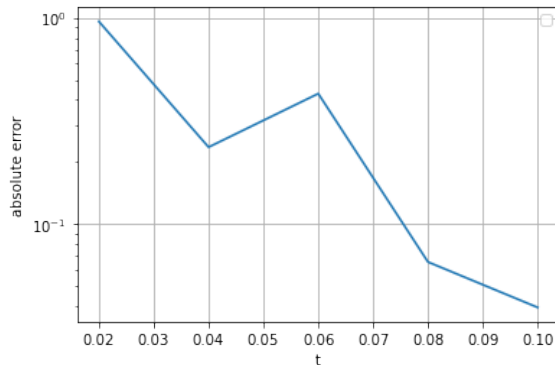


Figure 23: Errors due to an increase in t for an Asian call option with $S_0 = 50$, $K = 40$.

The results are as expected. As t increases, our computation of the characteristic function leads to an overall decrease in error. Only for $t = 0.06$, there is a slight increase. We compare Figure 23 with a new plot. Here, we set $L = 8$ and $c_6 = 0$. The results are shown in Figure

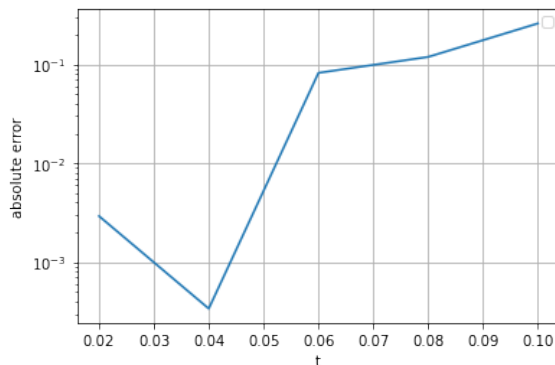


Figure 24: Errors due to an increase in t for an Asian call option with $S_0 = 50$, $K = 40$.

We see that we have massively increased the accuracy for small t . We confirm that the truncation range was set too wide in experiment 1. We could actually reach an accuracy of 10^{-3} for $t = 0.02$.

On the other hand, as t increases, the error in the truncation range dominates.

Therefore we conclude the following. When using a larger truncation range in the COS method, one would need more cosine terms N to reach the same level of accuracy. The peak in our density for such values of t is very narrow. In our computations, even with $N = 1024$ accuracy is not reached. Therefore, the truncation range should not be set this wide.

From these experiments, we conclude that option pricing for $\nu = 0$ should be handled with some care. For put options, we have very accurate results. We also observe that for call options, the errors do decrease overall as t increases. For high volatilities and large maturity times, the COS method based on Bougerol's identity is a valid way to price options when $\nu = 0$. For small t , the truncation range should be defined properly to reach a better level of accuracy.

We continue with $\nu \neq 0$, which is often observed in the market.

6.5.2 Option Pricing with Drift

We focus on the option pricing for $\nu \neq 0$. We will mostly make use of the paper by Chen [3]. This is because a very wide range of volatilities is used, comparing six numerical option pricing methods with a precision of 10^{-7} . Hence this is a good reference for our research. For the annual

risk free rate, mostly $\mu = 0.09$ is chosen, this is not accurate for this time anymore. But as we have mentioned before, the parameter μ has very little influence on the distribution of $\ln(A_t^r)$ for small values of t .

The computational time will also be included in several experiments. The computations in this research are performed on a standard laptop, 2.2GHz and 8GB memory.

In the error analysis we have used $L = 8$ and $c_6 = 0$ for the truncation range, which seemed suitable for small values of $\sigma^2 T$. We will verify which truncation range actually works best using our method.

We also need to verify which tolerance levels to use. We do this regarding the prices given in [3], and perform a least squared method. Then all the parameters are set correctly for the COS method.

In the following subsections, we focus on three components. We will perform several experiments, based on the convergence in N . Afterwards, the convergence of errors in J_k will be examined using two numerical integration methods for the computation of $k(\omega)$. At the end of this section, we examine the parameter $\sigma^2 T$ more closely.

To start the numerical tests, we check the error convergence due to the number cosine terms N , setting a wide truncation range and using the number of quadrature points we concluded from section 5.5 for both quadrature rules for $k(\omega)$.

Then the convergence of errors is examined due to the number of quadrature points J . We will do this for the distribution of $k(\omega)$, in combination with computational time.

To conclude, we look at the parameter $\sigma^2 T$ and will verify if we can price the options for extremely small values of this parameter. Throughout our experiments, a wide range of parameters is used, from which we can draw good conclusions at the end.

We first perform one experiment, which uses the risk free rate which is compatible with the current risk free rates.

6.5.2.1 Low return rates

We start with an experiment. We look at the error convergence of the option prices regarding multiple cosine expansion terms N . In this experiment, we use three times Clenshaw-Curtis quadrature. The parameters are set as $(J_l, J_k, J_g) = (700, 600, 600)$. The tolerance levels are set as $TOL_g = 10^{-9}, TOL_k = 10^{-7}, TOL_x = 10^{-15}, TOL_y = 10^{-12}$ and $L = 8, c_6 = 0$. The reference prices in this experiment uses values of the risk free rate μ which coincide with the current rates [8]. The results are shown in Table 12.

μ	σ	T	Ref. value	N	Value	CPU (sec)
0.18	0.3	1	0.219	16	0.218	1.67
				32	0.218	1.76
				64	0.218	3.42
				128	0.218	6.77
0.02	0.1	1	0.0624	16	0.0659	1.61
				32	0.0659	1.63
				64	0.0659	3.30
				128	0.0659	6.10
0.0125	0.25	2	0.172	16	0.172	1.61
				32	0.172	1.67
				64	0.172	3.28
				128	0.172	6.64

Table 12: At-The-Money Asian Call Option for $K = 2$ and $S_0 = 2$.

An error occurs for $\mu = 0.18$ and $\mu = 0.02$ both of order 10^{-3} . Using 3 digits behind the comma as the reference price, we also see no error convergence in using $N \geq 16$. Hence, the errors are either dominated by the numerical integration and the truncation range, or convergence still occurs but for more digits behind the comma. But we can already see that we developed an efficient

way for pricing Asian options with Arithmetic mean. And no error occurred in this experiment, for values which take less than two seconds to compute. Important to note is that the error for $\sigma^2 T = 0.01$, is only 0.0035.

Now we seek the optimal levels of tolerance for the numerical integration of each characteristic function for our computation of $\Phi_{\ln(A_t^\nu)}(\omega)$.

6.5.2.2 Test for tolerance level

We wish to have optimal results for our option pricing, and the convergence tests regarding N and J . Therefore we optimize the tolerance levels for our 4 numerical integration methods. As we observed in Section 5.2 for $\nu = 0$, a higher tolerance level does not necessarily mean a decrease in errors. Therefore we perform a least squared method to find the optimal levels of tolerance. Varying $\sigma \in \{0.1, 0.2, 0.3, 0.4, 0.5, 0.6, 0.8\}$ and $T = 1$, we use as reference Table 5 from [3] with In-The-Money options, i.e. $K = S_0 = 100$.

We use three times Clenshaw-Curtis quadrature, with $(J_g, J_k, J_l) = (600, 500, 500)$ based on the error analysis. We set $L = 12$ for the truncation range and use $N = 128$ cosine expansion terms with $c_6 = 0$. Starting each tolerance level with $TOL = 10^{-15}$, the tolerance levels are then varied for values which are possible for numerical integration with $M \geq 9$. The order of the analysis is $TOL_g, TOL_k, TOL_x, TOL_y$. We continue with each optimal value. The results are shown in Table 13.

M	TOL_g	TOL_k	TOL_x	TOL_y
5	-	0.73	-	-
6	-	0.67	-	-
7	-	0.56	-	-
8	-	-	-	-
9	1.04	-	0.569	1.69
10	0.74	-	0.565	1.15
11	0.56	-	0.562	0.58
12	0.94	-	0.565	0.56
13	1.34	-	0.564	-
14	1.31	-	0.584	-
15	1.32	-	0.562	-

Table 13: $\|\cdot\|_2$ -norm errors for various tolerance levels 10^{-M} .

We conclude to further use in this section the following tolerance levels: $(TOL_g, TOL_k, TOL_x, TOL_y) = (10^{-11}, 10^{-7}, 10^{-11}, 10^{-12})$. In the next subsection we seek for a truncation range we can use for a wide variety of (μ, σ, T) .

6.5.2.3 Test for truncation range

We have already seen that our method has been proven to give very accurate results for $\nu \neq 0$. The choice of truncation range plays a great part in this, especially for small values of $\sigma^2 T$, as we have also seen for $\nu = 0$. For further research, we need to define one truncation range for the COS method, hence we do another error experiment. We choose $c_6 = 0$ and vary $L \in [6, 12]$.

Furthermore we use $T = 1$, and vary $\sigma \in \{0.1, 0.3, 0.5, 0.8\}$. We use the same reference prices as in the last experiment, i.e. $S_0 = K = 100$. The tolerance levels are as we concluded from the previous experiment, and $(J_g, J_k, J_l) = (600, 500, 500)$. Using $N = 128$ cosine expansion terms, the results are shown in Table 14.

L	$\sigma = 0.1$	$\sigma = 0.3$	$\sigma = 0.5$	$\sigma = 0.8$
6	0.15	$7.5 \cdot 10^{-3}$	$4.1 \cdot 10^{-4}$	$6.7 \cdot 10^{-3}$
7	0.28	$5.2 \cdot 10^{-3}$	$8.3 \cdot 10^{-5}$	$2.8 \cdot 10^{-3}$
8	0.38	$3.3 \cdot 10^{-3}$	$1.3 \cdot 10^{-4}$	$1.3 \cdot 10^{-3}$
9	0.51	$6.9 \cdot 10^{-3}$	$6.6 \cdot 10^{-5}$	$6.9 \cdot 10^{-4}$
10	0.64	$3.6 \cdot 10^{-3}$	$5.3 \cdot 10^{-5}$	$3.2 \cdot 10^{-3}$
11	1.57	$4.6 \cdot 10^{-3}$	$7.3 \cdot 10^{-5}$	$2.2 \cdot 10^{-4}$
12	0.021	$2.2 \cdot 10^{-3}$	$1.5 \cdot 10^{-4}$	$9.8 \cdot 10^{-5}$

Table 14: Errors due to different truncation ranges.

The errors for $\sigma = 0.1$ are quite high compared to the other values as expected. For $\sigma = 0.1, 0.3$ and $\sigma = 0.8$, $L = 12$ seems to be most sufficient. Overall we can conclude from Table 14 that $L = 12$ defines a suitable truncation range for a wide variety of $\sigma^2 T$. Based on [6], this is already a wide truncation range. However, it will be shown that this is also dependent on different strike prices. But we will elaborate more on this later.

Now we perform multiple numerical test regarding the convergence in N and in J .

6.5.3 Convergence Experiments

We will analyze the convergence of the error in the option prices in the number of quadrature points J , and the cosine expansion terms N . We use the tolerance levels we have determined above for our numerical experiments. We start by analyzing convergence in N , setting a wide truncation range.

6.5.3.1 Convergence in N

We perform two experiments. In the first experiment, we check the error convergence in N for three different values of σ with $T = 1$. We look at the error convergence regarding N using three times Clenshaw-Curtis quadrature.

In the second experiment, we analyze $\sigma^2 T = 0.01$, using two numerical integration methods for $k(\omega)$.

6.5.3.2 Three values of σ

We look at the error convergence due to N for $\sigma \in \{0.2, 0.5, 0.8\}$, and $T = 1$. Using $K = 95$, $S_0 = 100$. Therefore, we set a wide truncation range, with $L = 12$, and c_6 included. We use three times Clenshaw-Curtis quadrature with $(J_g, J_k, J_l) = (600, 500, 500)$. We use 4 significant numbers. As reference, Table 5 is used in [3], with the values from the PDE method of Zhang [21] for $\sigma = 0.2, 0.5$. As reference for $\sigma = 0.8$, the Binomial Tree method is used, developed by Hsu [10], which is known to be accurate for high volatilities. The results are presented in Table 16.

N	$\sigma = 0.2$	$\sigma = 0.5$	$\sigma = 0.8$
8	272.0	66.93	15.32
16	61.87	4.633	0.2543
32	9.19	$2.180 \cdot 10^{-2}$	$4.199 \cdot 10^{-4}$
64	1.097	$1.340 \cdot 10^{-3}$	$2.144 \cdot 10^{-4}$
128	1.097	$1.340 \cdot 10^{-3}$	$2.144 \cdot 10^{-4}$
256	1.097	$1.340 \cdot 10^{-3}$	$2.144 \cdot 10^{-4}$
512	1.097	$1.340 \cdot 10^{-3}$	$2.144 \cdot 10^{-4}$
1024	1.097	$1.340 \cdot 10^{-3}$	$1.101 \cdot 10^{-4}$

Table 15: Convergence in N for various values of σ .

A clear exponential convergence is observed for $N \leq 64$. Afterwards, the errors converge only with a precision outside our range of significance. For $\sigma = 0.2$, accuracy is not reached and we need to reduce the truncation range. For $\sigma = 0.8$, the truncation range is actually well defined and we get a very low error and convergence still occurs for $N = 1024$. Keeping in mind that the reference values also vary of order 10^{-4} , we can already conclude that for $\sigma^2 T > 0.5$ the method we developed in this research is very accurate. For $\sigma = 0.2$, our computation is far from accurate. Therefore, in the next experiment, we look at a small value of $\sigma^2 T$ using two integration methods for $k(\omega)$.

6.5.3.3 Small σ

In this next experiment, we look at $\sigma^2 T = 0.01$. Two numerical integration methods for $k(\omega)$, the Arcsine distribution in the nominator of the characteristic function, are compared, still observing the error convergence regarding N . By using both numerical methods of $k(\omega)$, we can draw a conclusion for small values of $\sigma^2 T$. In Section 5.5, the errors using Chebyshev-Gauss quadrature were lower for $\sigma^2 T = 0.05$.

When $\sigma = 0.05$ and $T = 1$, it turns out there is a numerical error for computing the characteristic function of $Y \sim \chi_2^2$. We need to lower the tolerance level to avoid computation of $\ln(0)$ in the integrand. We leave this for now and come back to this later. Therefore, we use $\sigma = 0.1$. As reference, the PDE method by Zhang [21] is used.

In Section 5.5, we concluded for $\sigma^2 T$, we needed 500 quadrature points for Clenshaw-Curtis quadrature for $k(\omega)$, and $J_k = 1000$ for Chebyshev-Gauss quadrature. Therefore, we set $J_k = 1000$ for both methods in this experiment. By doing so, we can also confirm whether Chebyshev-Gauss is indeed a faster numerical integration method than Clenshaw-Curtis quadrature.

The truncation range is still set with $L = 12$ and c_6 . The error of the cosine series truncation and numerical integration must dominate. The computational time is included for each method. We use $K = 105$, $S_0 = 100$, $\mu = 0.09$. We use 6 significant digits to present the convergence up to $N = 1024$.

N	Cheb-Gauss		Clenshaw-Curtis	
	abs. error	CPU (sec)	abs.error	CPU (sec)
8	616.342	0.81	612.606	0.92
16	159.676	0.84	158.851	1.09
32	37.1607	1.64	35.0001	1.92
64	7.80040	3.57	5.40060	3.67
128	0.159823	6.23	1.84695	6.78
256	0.159823	12.46	1.84695	13.68
512	0.159817	24.68	1.84695	26.73
1024	0.159816	50.42	1.84695	55.54

Table 16: Asian call option errors regarding N for $\sigma^2 T = 0.01$ using two quadrature rules for $k(\omega)$ with $J_k = 1000$.

First we observe that Chebyshev-Gauss quadrature is indeed a faster computational method, when the same number of quadrature points is used. For $\sigma^2 T = 0.01$, it is also the more accurate integration method for $k(\omega)$, looking at the error in the option price for $N \geq 128$. For small values of $\sigma^2 T$, this looks to be the better fit for the computation of the characteristic function of $\ln(A_t^i)$.

Furthermore, exponential convergence is observed for $N \leq 128$, and we have an error in the options price smaller than 0.16, within 6.23 seconds.

Important to note is that in Table 14, we used $L = 12$, $c_6 = 0$ and for $\sigma = 0.1$, we had an error of 0.059 using Clenshaw-Curtis quadrature. The truncation range is thus chosen such wide, that the $N = 1024$ cosine terms does not reach this level of accuracy for another strike price K . We need a smaller truncation range for this parameter setting.

In this experiment we have shown that with the truncation range wide, comparing both methods of $k(\omega)$, Chebyshev-Gauss is a more accurate pricing method for $\sigma^2 T = 0.01$.

Based on the two experiments, We can confirm that for a wide range of volatilities, exponential convergence occurs in N . We can also already conclude that For $\sigma^2 T = 0.01$, Chebyshev-Gauss quadrature seems to be more accurate than Clenshaw-Curtis quadrature.

In the following experiment, we explore the error convergence due to J , especially for $k(\omega)$, since we then can compare two different methods as well.

6.5.3.4 Convergence in J_k

We perform an experiment due to the error convergence in J . We set the truncation range as found by Table 14, and compare the two integration methods of $k(\omega)$ for two values of σ , to get good comparison between the methods for $\sigma^2 T$. We can also verify whether the defined truncation range leads indeed to low errors for two values different values of σ .

6.5.3.5 Experiment: CC vs Cheb-Gauss

From the error analysis in Section 5.5, we could conclude that we need $J_k \geq 1000$ for Chebyshev-Gauss quadrature, and $J_k = 500$ for Clenshaw-Curtis quadrature for the computation of $k(\omega)$ (this was actually tested for $\sigma > 0.21$).

So far we have had already a very low error for $N = 128$ in each experiment, and the errors did not decrease much after that. Looking at Table 3, the difference in computational time for $N \leq 128$ is not that large, and we set $J_k = 1000$. For smaller values of J_k , this difference should even be smaller.

Therefore, we need to verify the accuracy of both methods more precisely regarding $\sigma^2 T$. We do not wish to compare the two for each value of $\sigma^2 T$, $\sigma \in \{0.1, \dots, 0.8\}$.

Based on the previous experiment, for $\sigma^2 T = 0.01$, one should use Chebyshev-Gauss quadrature. In Table 16, the results for $\sigma = 0.2$, $T = 1$, were very poor using Clenshaw-Curtis quadrature. Recall that in both experiments, we had a wide truncation range. And for $\sigma > 0.5$, the results with Clenshaw-Curtis quadrature were very accurate in Table 16.

In Section 5.5, the errors for Chebyshev-Gauss quadrature were only lower for $\sigma \approx 0.21$. We therefore compare $\sigma = 0.3$ and $\sigma = 0.4$ to observe the difference between the two methods.

We also use the truncation range we determined using our experiment, i.e. $L = 12$, $c_6 = 0$, to verify whether this was chosen sufficiently. We look at the convergence of error in J_k , also measuring the computational time for $\sigma = 0.3$. Since we use the same amount of quadrature points for $\sigma = 0.4$, it is not needed to measure again.

We set $N = 128$, $J_l = 600$, $J_g = 500$. For $\sigma = 0.3$, we set $K = 90$, $S_0 = 100$ and $r = 0.05$, and use again the reference from Zhang's PDE method [21]. For $\sigma = 0.4$, we set $K = 105$, $S_0 = 100$, $\mu = 0.09$, also the reference price is from the method from Zhang. The results are shown in Table

	$\sigma = 0.3$				$\sigma = 0.4$	
	CG		CC		CG	CC
J_k	abs.err	CPU	abs.err	CPU	abs.err	abs.err
100	2.81	9.88	3.06	11.23	0.627	3.757
200	4.16	11.92	0.24	10.88	0.973	0.141
300	0.173	11.79	0.0390	11.31	1.090	$1.362 \cdot 10^{-2}$
400	1.06	11.34	$7.955 \cdot 10^{-3}$	11.70	0.151	$1.028 \cdot 10^{-5}$
500	0.248	11.55	$3.865 \cdot 10^{-3}$	12.37	1.51	$3.980 \cdot 10^{-5}$
600	0.387	11.88	$6.204 \cdot 10^{-3}$	12.99	1.52	$1.840 \cdot 10^{-5}$
700	0.093	12.07	$5.958 \cdot 10^{-3}$	13.08	0.683	$2.990 \cdot 10^{-5}$

Table 17: Errors for $\sigma \in \{0.3, 0.4\}$ using two quadrature rules for $k(\omega)$.

We observe that for both values of σ , Clenshaw-Curtis quadrature is favourable, getting an error of order 10^{-3} for $J_k = 400$ quadrature points.

Based on the error analysis in Section 5.5 and the experiments performed in this Section, for values of $\sigma^2 T > 0.05$, one should use Clenshaw-Curtis quadrature for the computation of $k(\omega)$.

We also observe that for $J_k = 500$, the error is slightly lower for $\sigma = 0.3$ than $J_k = 600, 700$. For $\sigma = 0.4$, our method works perfectly for $J_k > 400$, leading to an error of order 10^{-5} .

Therefore, we also conclude that for $\sigma^2 T \geq 0.09$, we have developed a very accurate method using Clenshaw-Curtis quadrature for each separate characteristic function, where the parameters should be set as $(J_k, J_l, J_g) = (500, 600, 500)$. Option pricing for $\sigma^2 T > 0.09$ leads so far to an accuracy of order 10^{-3} , for $N = 128$ which led to a computational time of 6.78 seconds in the previous experiment. Note that we may reduce this by decreasing the truncation range properly.

In the following experiment, we focus on small values of $\sigma^2 T$, as we have shown our method is efficient for $\sigma^2 T \geq 0.09$.

6.5.3.6 Small values of $\sigma^2 T$

We have shown the exponential convergence of the option prices in N . In each experiment, convergence stopped at $N = 128$, and the results for $\sigma^2 T > 0.09$ are very accurate. We have also shown the convergence in J_k , based on two different integration methods for $k(\omega)$.

In this experiment we are looking at very small values of the parameter $\sigma^2 T$. As we have already seen, using a very wide truncation range, we cannot reach the proper accuracy of the option pricing. Chebyshev-Gauss seemed to be preferable for small values of $\sigma^2 T$, but the truncation range was set very large.

In this experiment, we set $c_0 = 0$, and we varied the parameter L between $[6, 12]$, and $L = 8$ seemed to most accurate for small values of $\sigma^2 T$.

The option price for two values of $\sigma^2 T < 10^{-3}$ are computed. As a good comparison, we also include larger values of $\sigma^2 T$, to verify whether the chosen truncation range is still sufficient, or that the error is dominated by the truncation range. We show two Tables, one with Chebyshev-Gauss quadrature using $J_k = 1000$, the other with Clenshaw-Curtis quadrature with $J_k = 500$. We can draw our final conclusions afterwards.

In these Tables, different strike prices, risk free rates, maturity times and volatilities are used. Each value of $\sigma^2 T$ has its own reference value. The last 4 columns are from [3], the first two columns are from [2]. The results are shown in Table 18.

N	$\sigma^2 T = 10^{-6}$	$\sigma^2 T = 2.5 \cdot 10^{-5}$	$\sigma^2 T = 2.5 \cdot 10^{-3}$	$\sigma^2 T = 0.09$	$\sigma^2 T = 0.25$
4	$1.334 \cdot 10^{-2}$	$2.173 \cdot 10^{-2}$	$7.51347 \cdot 10^{-2}$	2.2029	4.6752
8	$1.339 \cdot 10^{-2}$	$2.196 \cdot 10^{-2}$	$7.51370 \cdot 10^{-2}$	0.3238	0.3581
16	$1.324 \cdot 10^{-2}$	$2.194 \cdot 10^{-2}$	$7.51061 \cdot 10^{-2}$	0.1942	0.2666
32	$1.325 \cdot 10^{-2}$	$2.194 \cdot 10^{-2}$	$7.51770 \cdot 10^{-2}$	0.1942	0.2660
64	$1.324 \cdot 10^{-2}$	$2.194 \cdot 10^{-2}$	$7.51770 \cdot 10^{-2}$	0.1942	0.2660

Table 18: Errors for various values of $\sigma^2 T$ in N using $L = 8$. with Chebyshev-Gauss quadrature for $k(\omega)$.

And using Clenshaw-Curtis quadrature, we have the following values.

N	$\sigma^2 T = 10^{-6}$	$\sigma^2 T = 2.5 \cdot 10^{-5}$	$\sigma^2 T = 2.5 \cdot 10^{-3}$	$\sigma^2 T = 0.09$	$\sigma^2 T = 0.25$
4	$1.334 \cdot 10^{-2}$	$2.172 \cdot 10^{-2}$	$8.3572 \cdot 10^{-2}$	2.2029	4.4174
8	$1.299 \cdot 10^{-2}$	$2.180 \cdot 10^{-2}$	$8.3572 \cdot 10^{-2}$	0.1426	0.8181
16	$1.292 \cdot 10^{-2}$	$2.183 \cdot 10^{-2}$	$8.3678 \cdot 10^{-2}$	$2.101 \cdot 10^{-2}$	$1.544 \cdot 10^{-2}$
32	$1.293 \cdot 10^{-2}$	$2.185 \cdot 10^{-2}$	$8.3661 \cdot 10^{-2}$	$2.101 \cdot 10^{-2}$	$1.603 \cdot 10^{-2}$
64	$1.291 \cdot 10^{-2}$	$2.185 \cdot 10^{-2}$	$8.3661 \cdot 10^{-2}$	$2.101 \cdot 10^{-2}$	$1.603 \cdot 10^{-2}$

Table 19: Errors for various values of $\sigma^2 T$ in N using $L = 8$. with Clenshaw-Curtis quadrature for $k(\omega)$.

We finalize this section by drawing the following conclusions from all the experiments, combined with Table 18 and Table 19 for the pricing of Arithmetic averaged Asian options with $\nu \neq 0$.

- Using a wide truncation range, convergence in N has been showed for multiple values of σ^2T , for different strike prices, values of the underlying at $t = 0$, risk free rates and volatilities.
- We have showed convergence in the option prices in J_k . We have compared two numerical methods for the computation of $k(\omega)$; Clenshaw-Curtis quadrature and Chebyshev-Gauss quadrature. When the truncation range was wide, Chebyshev-Gauss seemed more accurate for small values of σ^2T , but after reducing the truncation range, this was not valid anymore. For very small values of σ^2T , one method is not more accurate than the other. For larger values, i.e. $\sigma^2T \geq 0.05$, Clenshaw-Curtis quadrature leads to more accurate prices solutions than Chebyshev-Gauss quadrature for the computation of the Arcine distribution in our computation of the characteristic function of $\ln(A_t^\nu)$.
- The truncation range is crucial for the option pricing, and varies for different parameters. For small values of σ^2T , the truncation range needs to be reduced. Setting a wide truncation range, and compensating using many cosine expansion terms N , the same level of accuracy may only be reached when one would use extremely many cosine expansion terms. The peak in the density is too narrow.
- Option pricing can be done using our method for values of σ^2T of order 10^{-6} with a precision of order 10^{-2} . This is not very accurate, but other numerical methods do not lead to a solution at all.
- Our method has proven to be very accurate for $\sigma^2T \geq 0.09$, where a precision of 10^{-5} can be reached, which is the same compared to literature values.

We have performed many experiments based on the convergence in N , convergence in J_k and we have zoomed in on the parameter σ^2T at the end. For $\sigma^2T \geq 0.09$, throughout earlier experiments, we already obtained very accurate results regarding the error compared to reference prices from the literature.

Lastly, we present one Table, including different strike prices, volatilities, risk-free rates and maturity times. We set $L = 10$ and $c_6 = 0$ and use $N = 128$ cosine expansion terms. The reference prices are from [3].

K	μ	σ	T	ref.value	abs.error
95	0.09	0.1	3	15.2137661	$7.92 \cdot 10^{-3}$
100				11.6376573	$5.49 \cdot 10^{-3}$
105				8.3911498	$9.72 \cdot 10^{-3}$
90	0.05	0.3	1	13.9538233	$3.34 \cdot 10^{-3}$
100				7.9456288	$7.41 \cdot 10^{-3}$
110				4.0717442	$4.98 \cdot 10^{-3}$
95	0.09	0.5	3	24.5718705	$5.80 \cdot 10^{-4}$
100				22.6307858	$5.82 \cdot 10^{-4}$
105				20.8431853	$5.89 \cdot 10^{-4}$

Table 20: Multiple Asian call options with $S_0 = 100$.

From Table 20, in which the errors are of order 10^{-3} , and we conclude to have developed a very accurate pricing method. It is just very depending on the truncation range and parameters, especially when the distribution of IGBM gets smaller.

6.6 Conclusion

In this section, we have been able to price continuous Arithmetic averaged Asian options using the COS method, based on Bougerol's extended identity.

We started with the financial background of Asian options. Then we showed that for the Geometric averaged options, an analytical solution can be found.

In the following section, the COS method was presented regarding option pricing in general, and we applied this to our variable of interest. Based on Bougerol's identity we could derive the characteristic function of $\ln(A_t^\nu)$ in Section 5, and by and the scaling property of IGBM, we could compute the characteristic function of our variable of interest, and use this for the pricing of the options.

We have observed that for $\nu = 0$, a wide truncation range was not sufficient. After reducing the truncation range, the accuracy of the option was of order 10^{-2} for a Call option. For Put options, a larger value of t was used, and we had an error in the option price of order 10^{-3} based on Monte Carlo simulation. The accuracy increases as t increases, as long as we increase the truncation range with it.

In the final section, we used $\nu \neq 0$. We have seen that we have developed an efficient method for $\sigma^2 T > 0.09$ with an error of 10^{-2} or smaller. However, $\sigma^2 T$ is not the only parameter leading to sufficient results, as we lost accuracy in Table 19.

We explored smaller values of $\sigma^2 T$ afterwards. A reduction of truncation range was necessary to reach a certain level of precision. However, the accuracy of the option price was of order 10^{-2} for extremely low values of $\sigma^2 T$.

We conclude that we have developed an accurate new method for the pricing of continuous Arithmetic averaged Asian options. Using Clenshaw-Curtis quadrature for each method gives very accurate prices of the option. The accuracy is however very dependent on the truncation range which is used, and on certain parameters.

In all the experiments, a wide variety of parameters has been used, and comparisons between numerical methods have been done to verify which is more suitable. For a wide variety of parameters, our new proposed method is sufficient for pricing. However, when the distribution of IGBM gets very small, the errors do increase, and a precision of 10^{-2} is reached.

7 Conclusion & Further Research

In this research we have developed a new method for pricing continuous Arithmetic averaged Asian options, where the underlying is assumed to be Geometric Brownian motion. For this type of option, the underlying follows Integrated Geometric Brownian Motion (IGBM). No analytical solutions are available to price this type of option and as new numerical method we have proposed the COS method.

In Section 3 we have given insight on the distribution of IGBM in general and we introduced Bougerol's identity, which is a particular relation between two independent Brownian motions. Using this identity, we could derive the characteristic function of the *log* of IGBM, which was the input needed for the COS method.

The derivation for the characteristic function for Bougerol's identity with drift term $\nu = 0$ has been showed in Section 4, which is the ratio between two independent characteristic functions. Two computational methods were compared for the computation of the denominator. Afterwards, an error analysis on the CDF, recovered by the COS method, was conducted based on Monte Carlo simulation.

In Section 5, the characteristic function for $\nu \neq 0$ was derived, which consists of three separate characteristic functions. For both cases, $\nu = 0$ and $\nu \neq 0$, we showed the importance of parameter settings regarding numerical integration, as the combination of using multiple characteristic functions for the computation of the characteristic function of $\ln(A_t^\nu)$ leads to numerical errors quickly. A change of variable had to be made for two distributions. Furthermore, a parameter study was performed on the influence of (μ, σ, T) on the distribution of A_t^ν and an error analysis was conducted, comparing different numerical integration methods.

In Section 6, we presented the analytic solution for the pricing of continuous Geometric averaged Asian option, afterwards the COS method was used to price the Arithmetic averaged.

The results were very sufficient, but were highly dependent on the parameters. As the distribution of $\ln(A_t^\nu)$ would decrease, so would the accuracy in our computation. We applied a proper truncation range, but the diameter parameter L was of great influence for the results as well, mostly for lower values of $\sigma^2 T$.

However, once this parameter L was properly adjusted, for small values of $\sigma^2 T$, i.e. t , we could reach an accuracy of order 10^{-2} . Overall, as $\sigma^2 T$ increased, the accuracy of our method would improve, and we have shown to be able to price the options with an error of order 10^{-5} , which coincides with the comparison between existing numerical methods. However, $\sigma^2 T$ is not the only parameter from which conclusions can be drawn, as the accuracy is not the same using different strike prices, volatilities and risk-free rates. It remains very parameter dependent.

From these results, we conclude that we have found a new sufficient way to price continuous Arithmetic Averaged Asian options. But improvements still have to be made.

As we stated above, the errors occur mostly when the distribution is small. For further research, one could try to improve the numerical integration for each distribution, or make use of incredibly many cosine expansion terms.

The dependency on the truncation range, which was not allowed to be wide for small values of $\sigma^2 T$, is a flaw in our method as well. There is not found one definitive truncation range for a wide range of parameters. One could investigate better on the influence of the parameters to the truncation range, since this was already determined by the moments of A_t^ν , and we have to deal with very narrow density functions.

We have also established that the numerical integration is highly dependent on the tolerance level used, as well as the number of quadrature points. This is due to the fact that we use multiple separate characteristic functions, each computed numerically. The number of quadrature points needs to be quite large as well.

For the purpose of using the COS method, one could also try to derive the characteristic function of $\ln(A_t^\nu)$ in a different way, which is not dependent on a ratio, which consists of three separate distributions. The sensitivity to parameters was hereby very high, and the computation of the characteristic function was therefore not very stable.

References

- [1] Bénédicte Alziary, Jean-Paul Décamps, and Pierre-François Koehl. A pde approach to asian options: analytical and numerical evidence. *Journal of Banking & Finance*, 21(5):613–640, 1997.
- [2] Ning Cai and Steven Kou. Pricing asian options under a hyper-exponential jump diffusion model. *Operations Research*, 60(1):64–77, 2012.
- [3] Kuan-Wen Chen and Yuh-Dauh Lyuu. Accurate pricing formulas for asian options. *Applied Mathematics and Computation*, 188(2):1711–1724, 2007.
- [4] Catherine Donati-Martin, Raouf Ghomrasni, and Marc Yor. On certain markov processes attached to exponential functionals of brownian motion; application to asian options. *Revista Matematica Iberoamericana*, 17(1):179–193, 2001.
- [5] Daniel Dufresne. *Bessel processes and a functional of Brownian motion*. Centre for Actuarial Studies, Department of Economics, University of Melbourne, 2004.
- [6] Fang Fang and Cornelis W Oosterlee. A novel pricing method for european options based on fourier-cosine series expansions. *SIAM Journal on Scientific Computing*, 31(2):826–848, 2009.
- [7] Fang Fang and Cornelis W Oosterlee. A fourier-based valuation method for bermudan and barrier options under heston’s model. *SIAM Journal on Financial Mathematics*, 2(1):439–463, 2011.
- [8] Michael C Fu, Dilip B Madan, and Tong Wang. Pricing continuous asian options: a comparison of monte carlo and laplace transform inversion methods. *Journal of Computational Finance*, 2(2):49–74, 1999.
- [9] Yuu Hariya and Yohei Matsumura. On two-dimensional extensions of bougerol’s identity in law. *Electronic Communications in Probability*, 28:1–7, 2023.
- [10] William Wei-Yuan Hsu and Yuh-Dauh Lyuu. A convergent quadratic-time lattice algorithm for pricing european-style asian options. *Applied mathematics and computation*, 189(2):1099–1123, 2007.
- [11] Angélien GZ Kemna and Antonius CF Vorst. A pricing method for options based on average asset values. *Journal of Banking & Finance*, 14(1):113–129, 1990.
- [12] Gregory F Lawler. *Introduction to stochastic processes*. Chapman and Hall/CRC, 2018.
- [13] Daniel Revuz and Marc Yor. *Continuous martingales and Brownian motion*, volume 293. Springer Science & Business Media, 2013.
- [14] M Schröder. On the valuation of arithmetic-average asian options: Integral representations. *Preprint, University of Mannheim*, 1999.
- [15] Karl Sigman. Introduction to reducing variance in monte carlo simulations. *Department of Industrial Engineering and Operations Research*, 2007.
- [16] Peter JC Spreij. Stochastic integration. *Lecture notes accompanying the course “Stochastic Integration” taught at the University of Amsterdam*, 2011.
- [17] Stavros Vakeroudis. Bougerol’s identity in law and extensions. 2012.
- [18] Marc Yor. On some exponential functionals of brownian motion. *Advances in applied probability*, 24(3):509–531, 1992.
- [19] Bowen Zhang and Cornelis W Oosterlee. Efficient pricing of european-style asian options under exponential lévy processes based on fourier cosine expansions. *SIAM Journal on Financial Mathematics*, 4(1):399–426, 2013.

- [20] Hongbin Zhang. *Pricing Asian Options using Monte Carlo Methods*. 2009.
- [21] Jin E Zhang. A semi-analytical method for pricing and hedging continuously sampled arithmetic average rate options. *Journal of Computational Finance*, 5(1):59–80, 2001.